"Characterization of Damage Evolution on Metallic Components using Ultrasonic Non-Destructive Methods"

"Thesis submitted in partial fulfillment of the requirement for the PhD Degree issued by the Universitat Politècnica de Catalunya, in its Electronic Engineering Program"

Juan Fernando Piñal Moctezuma

Director: *PhD. José Luis Romeral Martínez*

Co-Director: *PhD. Miguel Delgado Prieto*

Terrassa, Barcelona. September 2019

Abstract

When fatigue is considered, it is expected that structures and machinery eventually fail. Still, when this damage is unexpected, besides of the negative economic impact that it produces, life of people could be potentially at risk. Thus, nowadays it is imperative that the infrastructure managers, ought to program regular inspection and maintenance for their assets; in addition, designers and materials manufacturers, can access to appropriate diagnostic tools in order to build superior and more reliable materials. In this regard, and for a number of applications, non-destructive evaluation techniques have proven to be an efficient and helpful alternative to traditional destructive assays of materials. Particularly, for the design area of materials, in recent times researchers have exploited the Acoustic Emission (AE) phenomenon as an additional assessing tool with which characterize the mechanical properties of specimens. Nevertheless, several challenges arise when treat said phenomenon, since its intensity, duration and arrival behavior is essentially stochastic for traditional signal processing means, leading to inaccuracies for the outcome assessment.

In this dissertation, efforts are focused on assisting in the characterization of the mechanical properties of advanced high strength steels during under uniaxial tensile tests. Particularly of interest, is being able to detect the nucleation and growth of a crack throughout said test. Therefore, the resulting AE waves generated by the specimen during the test are assessed with the aim of characterize their evolution.

For this, on the introduction, a brief review about non-destructive methods emphasizing the AE phenomenon is introduced. Next is presented, an exhaustive analysis with regard to the challenge and deficiencies of detecting and segmenting each AE event over a continuous data-stream with the traditional threshold detection method, and additionally, with current state of the art methods. Following, a novel AE event detection method is proposed, with the aim of overcome the aforementioned limitations. Evidence showed that the proposed method (which is based on the short-time features of the waveform of the AE signal), excels the detection capabilities of current state of the art methods, when onset and endtime precision, as well as when quality of detection and computational speed are also considered. Finally, a methodology aimed to analyze the frequency spectrum evolution of the AE phenomenon during the tensile test, is proposed. Results indicate that it is feasible to correlate nucleation and growth of a crack with the frequency content evolution of AE events.

Keywords

Acoustic emission
Material testing
Quality of detection
Dimensionality reduction
Material testing
AE thresholding method
Short-time analysis
Support vector machines
Metallic components
Performance analysis
Frequency analysis

Acknowledgements

To the Mexican Consejo Nacional de Ciencia y Tecnología, for having given me the opportunity to accomplish my Doctoral studies through the scholarship No. 411711. As well as the Ministry of Economy and Competitiveness of Spain for the research project grant TRA2016-80472-R.

To the staff of the Department of Materials Technology from Eurecat Centre Tecnològic de Catalunya, particularly to Dr. Daniel Casellas i Padró and Dr. Begoña Casas Aguirregomezcorta, for their expertise and allowing me access to their human and material resources.

To the Universitat Politècnica de Catalunya, especially to Dr. Luis Romeral and Dr. Miguel Delgado Prieto for their guidance and support during these years.

TABLE OF CONTENTS

LIST OF TABLES

LIST OF FIGURES

ACRONYMS AND DEFINITIONS

AE	Acoustic Emission
AET	Acoustic Emission Testing
AHSS	Advanced High Strength Steels
AI	Artificial Intelligence
AIC	Akaike Information Criterion
ASTM	American Society of the International Association for Testing and Materials
CF	Characteristic Function
CM	Condition Monitoring
CWT	Continuous Wavelet Transform
EEE	Electrical, Electronic and Electromechanical
DAQ	Data Acquisition
DE	Destructive Evaluation
DIC	Digital Image Correlation
DPA	Destructive Physical Analysis
DSP	Digital Signal Processing
DT	Destructive Testing
DM	Damage Prognosis
FFT	Fast Fourier Transform
GW	Guided Wave
IA	Instantaneous Amplitude
MAE	Modal Acoustic Emission
NDC	Non-Destructive Characterization
NDE	Non-Destructive Evaluation
NDI	Non-Destructive Inspection
NDT	Non-Destructive Testing
POD	Probability of Detection
SEM	Scanning Electron Microscope
SHM	Structural Health Monitoring
SPM	Statistical Process Control
SSWT	Synchrosqueezed Wavelet Transform
STFT	Short Time Fourier Transform
STA/LTA	Short-Time Average to Long-Time Average ratio
STA	Short-Time analysis
STE	Short-Time Energy
UT	Ultrasonic Testing
WT	Wavelet Transform
ZCR	Zero-Crossing Rate

Chapter 1. INTRODUCTION

1.1 Research topic

In general terms, damage can be defined as changes introduced into a system, either intentionally or unintentionally, that adversely affect the current or future performance of that system [1]. In this sense, evaluation of damage is relevant to all engineering fields. Nowadays is carried out in conjunction with six multidisciplinary areas, for which monitoring and assessing damage are the principal concerns:

1) Structural Health Monitoring
2) Condition Monitoring
3) Non-Destructive Evaluation
4) Destructive Testing
5) Statistical Process Control
6) Damage Prognosis

All these areas use transducers in order to know the status of structures, machinery, processes or materials by detecting faults, damages or defects, taking advantage of the physical properties of matter and its response to the different forms of energy exerted on it in order to survey the integrity of such elements. However, in order to introduce the research topic of this thesis proposal, the definition of each of these damage evaluation approaches is presented.

The process of implementing a damage identification strategy for aerospace, civil and mechanical engineering infrastructure is referred as *Structural Health Monitoring*. Here, damage is defined as changes to the material and/or geometric properties of these systems, including changes to the boundary conditions and system connectivity, which adversely affect the system's performance [2]. SHM implicates the online supervision of a system which evolves through time, measuring with a defined periodicity, extracting critical damage features, executing a statistical evaluation of these features in order to establish the actual health condition of the system, and lastly the data generation regarding to the ability of the structure to continue performing its intended function with the inevitable aging and damage accumulation.

Condition Monitoring of machinery is the measurement of various parameters related to the mechanical condition of rotating and reciprocating machinery (such as vibration, bearing temperature, oil pressure, oil debris, and performance), which makes it possible to determine whether the machinery is in good or bad mechanical condition [3].

According to the American Society of the International Association for Testing and Materials (ASTM), in the guideline of Standard Terminology for *Non-Destructive Examinations*, Non-Destructive Evaluations or Non-Destructive Testing [4], is defined as the development and application of technical methods to examine materials or components in ways that do not impair future usefulness and serviceability in order to detect, locate, measure and evaluate flaws; to assess integrity, properties and composition; and to measure geometrical characteristics. NDE is critical and necessary in order to determine the safety and reliability of a system. Usually it is an offline process and performs in sectored fashion. Main aims of NDE are damage characterization and severity check measurement (if previously exists indication of damage).

Destructive Testing is a set of methods to testing a material that degrades the sample under investigation [5], generating on it a permanent variation of its chemical structure or its dimensional geometry. These methods are usually easier to implement, provides more data, and are more affordable to interpret than NDE. DT fits better, for objects that will be produced on mass, for example: on EEE (electrical, electronic and electromechanical) production devices -under the name of Destructive Physical Analysis-, in the designing of bituminous materials to paving roads, in software designing area to force a program to collapse in an uncontrolled routine and so test its robustness, or in the Automotive field when an automobile is crashed to assess the safety.

Statistical Process Control is a set of tools for managing processes, and determining and monitoring the quality of the outputs of an organization. It is also a strategy for reducing variation in production, deliveries, processes, materials, attitudes and equipment [6]. These statistical strategies have been used to recollect and analyze changes in measured time series [2], in order to detect and reduce variability by using a variety of sensors to monitor changes in the process.

When damage is confirmed, *Damage Prognosis* (DP) is used to predict the remaining life of a system [2]. DP is defined as the estimated remaining useful life of engineered systems [7], projecting the operation of the system through damage evaluation of these, reporting the

likely loading scenario for that system, and forecasting its remaining useful life by means of simulation and prior events. The effective advancement of a DP capacity will demand additional development and the composing of multiple technology disciplines including telemetry hardware and a collection of deterministic and probabilistic predictive modeling potentials, beside of competences to quantify the uncertainty of these forecasts [8].

In recent years these strategies have been implemented and have proven their effectiveness. It has been seen that for complex structural and material systems, the ability to diagnose and predict structural failures through embedded sensing, actuation and data management can reduce operating costs [9] [10], while increasing safety [11]. The essential commercialization motivations for the technology are life cycle cost, prevention of catastrophic failure and evaluation of hard to reach places. Early detection of damage and appropriate retrofitting will aid in preventing failure of structures and equipment and will save money spent on maintenance and ensure that structure will operate safe and efficiently during its whole intended life. For instance, as civil infrastructures get older, monitoring their structural integrity and devising and improving monitoring methods are both gaining priority for owners, engineers and researches. In this area, bridges constitute one class of aging infrastructure that require effective damage detection, especially due to their economic significance (high building costs) as well as their direct effects on public safety. Many bridges in use today were built decades ago and are now subjected to increased loads or changes in loads patterns that originally designed for, that will cause deterioration and aging with a probably result of structural failure [12]. In Australia, there are about 33,500 bridges with a replacement value about 16.4 billion dollars and annual maintenance expenditure of about a $100 million dollars [13]. In the United States on 2003, out of a total 597,377 bridges, 164,971 that is around 27.6 percent, were identified as being either structurally deficient of functionally obsolete, as reported by the Federal Highway Administration, in year 2004 the Highway Bridge Replacement and Rehabilitation Program (HBRRP) had to invest more than $3.5 billion of dollars in order to replace or rehabilitate deficient bridges [14], with a proper strategy of monitoring and preventive maintenance it is possible to earn substantial economical savings on life-cycle costs [15], and most important to avoid fatalities. However, there is a prior stage to that of "in-service" monitoring, which implies the characterization of the materials that will be used during the asset manufacturing. Indeed, from industrial point of view, tensile tests are widely used by manufacturers of sheet metal and metal forming companies, such as those associated with the automotive sector, which ensures the required levels of quality material.

1.2 Research problem

Technological and Scientific Advances in Non-Destructive Evaluation of materials, made over the last twenty years in this field, have contributed to the recognition of these techniques as a powerful, proven and very well-suited set of tools on diverse engineering disciplines.

Nevertheless, these techniques have not been fully exploited and there is still progress to do, particularly, a problem found for this thesis work is that many laboratory assays make use of specialized equipment, however these, are starting to lack of enough data resolution of the phenomena being characterized. Specifically, for the Essential Work Fracture test, most of the machinery commercially available only make use of a strain sensor to characterize the stress-strain behavior of the material under examination [16] [17].

Certainly these equipment have proved to perform effectively their propose for the last forty years in this given application (EWF) [18], but with the progress of Materials engineering and the advent of new developments, the measurement methods of these machinery it is beginning to be insufficient.

A few research of applying acoustic emission on EWF has been done [19] [20] [21] [22][23], most of these work has been done with aim to validate the AE technique on certain type of material. Nevertheless, for some ultrasonic technique (AU, GW, UI) there are not reported work.

Some possible reasons might be that:

- Particularly in metallic components, the AE signals exhibit faster time-varying behavior due to multiple mode and multipath propagation [24], so the available hardware technology to capture entirely the phenomenon was limited, due the demanded specifications (several channels to be captured, high frequencies conversion, deep resolution conversion, manipulation of data converted, lack of standardized instrumentation).
- Lack of calibration methodology (selection of transductors, location of these on specimens, etc.) to make a proper acquisition of the test.
- Absence of bases of knowledge with available recorded data, there is have been a slow development of DSP and AI techniques on this area.
- Studying of the state of the art of fracture characterization of metals by acoustic emission test.

It is worth mentioning that, despite of modern studies of Acoustic Emission phenomena were born through the use of destructive evaluation machinery (viz., Pendulum Impact Testing) [25], and there had been many disciplines of engineering with successful applications of NDT, nowadays exists an absence of these methods on the laboratory environment.

Detection and identification of these phenomena may allow advanced mechanical design tests and a detailed characterization of the behavior of the material. In this sense, noise emissions are a variable source of mechanical pattern detection capability stages of incipient cracks in materials. However, considering the current state of technology, specific research is necessary to determine the specific patterns contained in the AE associated with the different stages of fracture in these types of applications.

In conclusion, **there is a need to improve the phenomenon characterization of metal fracture on laboratory updating the strategy to capture and analyze said phenomenon.** The actual methods to examine it need to be reinforced by solid framework of analysis and processing in order to tackle these issues and strive towards a better understanding of damage in materials.

1.3 Hypotheses

In order to tackle the presented research problems, the following hypotheses were formulated as a starting point for this research work:

1. The use of the Acoustic emission phenomenon will provide an improvement on the resolution of the measurements obtained in the Tensile tests on metals, transcending the tolerance allowed by the current metrology standards of laboratories of 0.2% in the stress-strain relationships.
2. Based on the State of the Art of Acoustic emission applied to Tensile tests, will be possible to correlate the stages of damage on the metallic specimen under evaluation, through the frequency content of the digitized signals.
3. Using suitable frequency DSP techniques will allow not only suppressing noise of the obtained signals, but enhancing the relevant information within these
4. The adequate selection and processing of statistical extracted features of each AE event, will allow to apply automatic patterns recognition with the aim of diagnose the nucleation and growth of cracks in the assayed specimen.

1.4 Aim and objectives

In order to solve the research problem and validate the research hypothesis, the aim of this thesis is to work in the state-of-the-art **development of characterization of damage on metals. For this, stages of damage of the materials under test will have to be identified and analyzed, making emphasis at early stages by means of the use of the AE phenomenon,** attempting to adapt them to this particular application by a proper calibration of instruments and DSP techniques.

To successfully achieve this purpose, the following specific objectives are identified:

- The generation of an AE knowledge base, derived from metallic component assays; by proposing and implementing an ad-hoc digital acquisition system for capturing the entire tests, as well as the proper choice of cabling, amplification stages and transductors.
- The research, proposal and performance analysis of a suitable technique with the aim of detecting AE events within a continuously collected data stream.
- The research, proposal and validation of a methodology capable to assess the spectral frequency content of the AE events with the aim of detect the nucleation and growth of cracks during tensile tests.
- The research, proposal and validation of a set of extracted statistical features derived from the AE events, with the aim of identify by means of a basic artificial intelligence technique the nucleation and growth of cracks during tensile tests.

1.5 Outline of the chapters

With the aim of cover the exposed objectives, this dissertation is divided into five different sections, ordered as it follows:

Chapter 2 makes a brief review of the NDT, the tensile test and finishes with a summarized description of the AE phenomenon.

In **Chapter 3** an exhaustive analysis of the limitations of the classical AE threshold approach is presented. Additionally, the performance's detection of advanced AE event detection methods representing to the current state-of-the-art are evaluated.

Chapter 4 presents a highly precise and yet very efficient AE event detector method, which is based on the short-term analysis of the energy and the zero-crossing rate belonging to the AE waveform.

In **Chapter 5** a methodology to assess the evolution of the frequency spectrum with regard to the collected AE events manifested during the tensile tests with the aim of identify the nucleation and the growth of a crack is presented.

Finally, in **Chapter 6** discussion and general conclusions are presented. Additionally, this chapter also offers the contributions resulting from this dissertation.

Chapter 2. ON THE MEASURING OF THE TENSILE TEST

2.1 Tensile testing for metallic components

Also known as tension test, tensile test is one of the most fundamental and common types of mechanical testing [26]. In production and laboratory test is the preferred testing choice due to the elastic properties derived from test. The **ductility and strength** (measured by a tensile test), **related hardness properties** and **fracture toughness** (or impact resistance) are the three most frequently obtained characteristic properties. A secondary batch can include properties related to torsion, shear, bending and fatigue (although usually on components rather than raw materials) with additional measurements of creep behavior required for elevated temperature service. Tensile tests are usually carried out on wire, strip or machined samples with either circular or rectangular cross section. Test specimens are screwed into or gripped in jaws and stretched by moving the grips apart at a constant rate while measuring the load and the grip separation (see **Figure 2-1**).

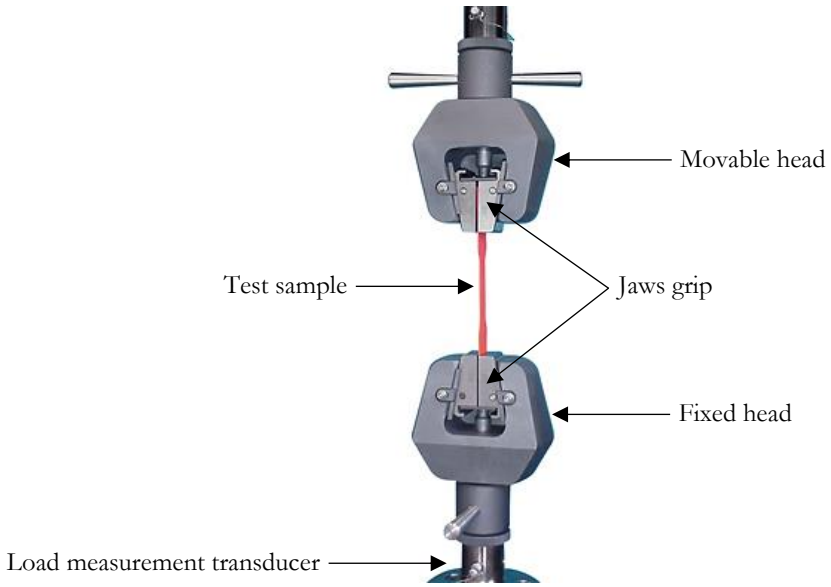

Figure 2-1. Mounting apparatus for a tensile testing machine.

The characterized data is plotted as load vs extension and then converted to engineering stress (load/original area) vs engineering strain, i.e., fractional change in length over the test section assuming the deformation is uniform [27] (see **Figure 2-2**).

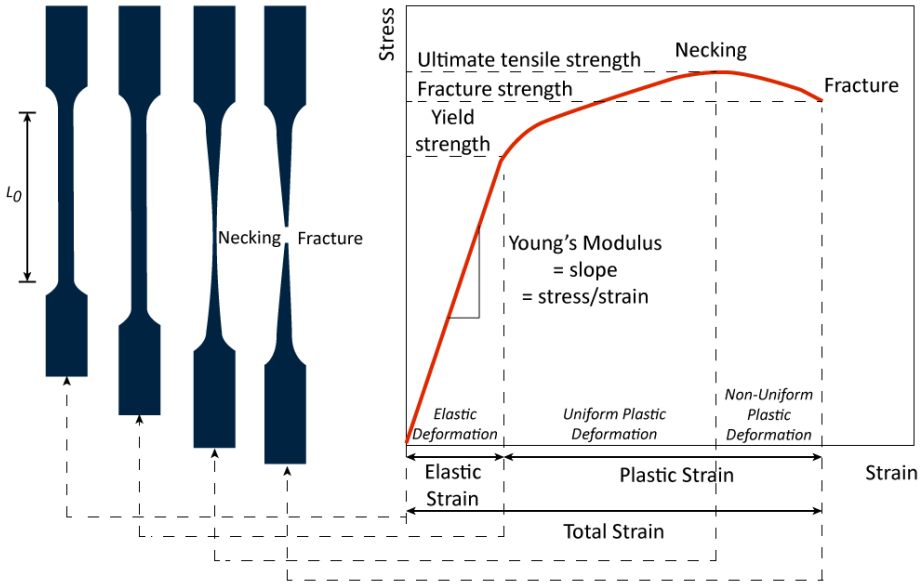

Figure 2-2. Change of shape of a specimen during tensile test, and its correlation to the strain-stress curve.

In special circumstances, the actual stress and strain may be calculated if the true cross section is measured during the test. International standards set out the requirements for sample size, test methods and equipment and includes examples of the representative shapes of stress vs strain plots which may be expected when tensile tests are performed. Typically, strain is described by means of an extensometer with the aim of measure the change of specimen's length during the assay (see **Figure 2-3**). Modern tensile machines make use of video-extensometer by capturing continuous images of the specimen during test [28,29]; nonetheless, and despite achieving displacement measures up to 1μm, these video-systems are unable to measure the material's internal changes during assay.

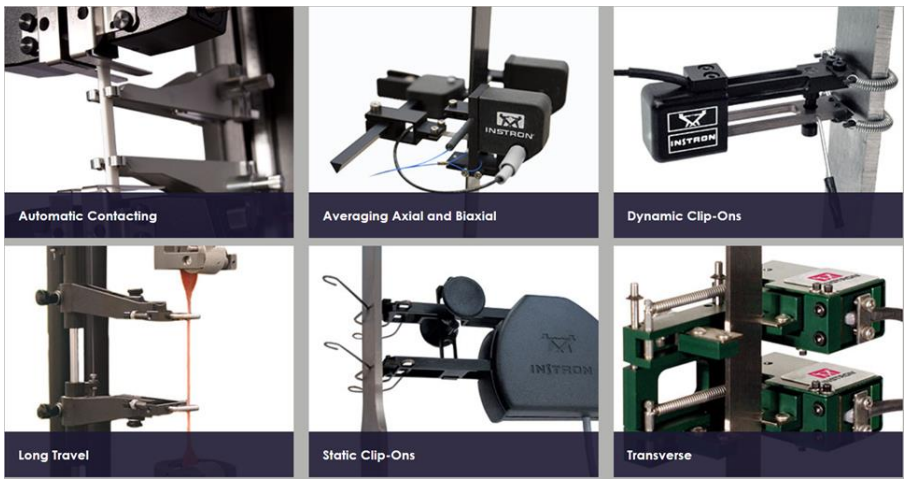

Figure 2-3. Six different extensometers technologies for different applications (image courtesy of Instron® corporation).

Typically, mechanical parameters measured from tensile test are the yield stress at 0.2% deformation (estimated by using a rule parallel to the initial linear portion of the load/elongation plot and offsetting the measurement by 0.2% displacement), the maximum stress, Rm or the ultimate tensile stress (UTS), i.e. the maximum applied stress and the ductility which is measured by percent reduction in area of the fracture face or the percentage change in gauge length. If the sample necks significantly, the (high strain) final part of the curve will dip below the UTS. Brittle materials will only deform by a small amount before fracture. The slope of the linear portion approximates the elastic modulus (or Young's modulus) while the area under the entire, non-linear portion of the curve gives the energy absorbed during deformation, and is thus an indication of toughness.

2.2 Non-Destructive Testing

Regardless of the chosen strategy (i.e., NDE, SHM, CM, etc.) for a given particular application (e.g., industrial, aerospace, civil, medical, geophysical, etc.), with the aim of monitoring damage, it is important to understand that non-destructive detection is feasible due to the underlying phenomena that occur in particles, materials and objects, since all of these are governed by physical rules, in consequence they all eventually will respond to external stimulus of a source of energy on a specific manner. This response can be captured by the use of a sensor and translated conveniently into an electrical signal, which can be manipulated in order to store, transform, and/or process it.

2.2.1 Methods of NDE

Nowadays, an ample variety of techniques are used in order to detect defects, using for this several forms of energy (depending of the selected technique), with the purpose to excite particles, materials, or objects, and thus being capable to measure variability on these. **Table 2-1** summarizes the most applied methods on the field of nondestructive damage detection.

Table 2-1. Non-destructive methods and their relevant features (emphasizing ultrasonic technologies)

Method	Physical Principle	Techniques	Detectable Defects	Advantages	Limitations
Dye Penetrant	Capillary Action	Solvent Removable Water-Washable Post-emulsifiable	Admitted to detect cracks, pores and other defects that break the surface of the material	Large surfaces can be rapidly inspected Cheaper than other methods Objects with difficult geometry are easily inspected	Not suitable on porous materials Surface preparation is crucial Required post-cleaning for chemical removal Required chemical handling directions
Magnetic Particle	Magnetic Permeability	Yokes Prodes Coils Central Conductor	Used to survey for flaws on the surface and subsurface of materials	Large surfaces can be rapidly inspected Affordable equipment Easy surface preparation	Only works on ferromagnetic materials Large electrical currents required Crucial alignment of magnetic field and flaw Required post-demagnetization

Electromagnetic	Focault currents	Eddy Current Alternating Current Field Remote Field	Used to survey for flaws on the surface and subsurface of materials	Test probe does not require to be in contact with the material Minimal surface preparation Used to characterize materials	Can only be used on conductive materials Ferromagnetic materials need a pre-treatment to add magnetic permeability Finite depth penetration Surface's finish and roughness may add noise to readings
Radiographic	Radiation	Film Radiography Computed Radiography Computed Tomography Digital Radiography	Used to achieve images of objects in function of their density and thickness	Nearly all materials can be inspected Easiness to inspect complex shapes and multi-layered structures Minimum part preparation	Deep skills and training required Availability to both sides of the structure Expensive instrumentation Hazardous radiation exposure
Ultrasonic Inspection	Body (Compressional/Shear) mechanical waves	Straight Beam (Pulse-Echo) Angle Beam Immersion testing Through transmission Phased Array Time of Flight Diffraction	Used to survey flaws on the surface and subsurface on a variety of materials, including metals, plastics and wood	Superior depth capabilities than other methods Only one side of the material is required to make the inspection Distance of the flaw is provided Used to characterize materials	Imperative use of coupling media Considerable training and skills required Reference standards must be followed Parallel linear defects could be unnoticed Expensive instrumentation

Guided Wave Ultrasonic Test	Superficial mechanical waves	Transmission – Reflection Through transmission	Used to survey for flaws on metallic pipes	Superior range distance capabilities than other methods Possibility to inspect hard-to-reach elements Distance of the flaw is provided	The method cannot differentiate between external-internal flaws Difficult to detect small size flaws Not very effective at survey areas near of accessories (valves, gates, etc.) Considerable training and skills required Expensive instrumentation
Acoustic Emission	Stress waves	Passive detection	Used to detect early stages of damage on materials	Materials can be inspected on service Materials can be monitored during their entire history service	Only suitable to detect creation of new flaws Particular tests are not perfectly replicable Expensive instrumentation Provides only qualitative damage information (unless there exists a model of the surveyed object). For quantitative damage estimation it is necessary to combine with another method

Understanding the underlying phenomena regarding to these NDE methods, will enable to interested people (i.e., technicians, engineers, instructors,) of being capable to implement, design, certificate, standardize, measure, and most important, to choose the proper method for a given particular application, in order to obtain quality information about damage in materials. Needless to say that there is not a better method than another, each one has its own particularities, advantages and disadvantages, however it is possible to combine some methods for evaluating a single parameter in order to increase confidence, and assessing the quality of structures, machinery or materials [30].

2.3 Ultrasonic Technologies for NDE

Ultrasound, is the known phenomenon of sound with a pitch excessively high (frequencies greater than 20kHz) like to being perceived by humans. *Ultrasonics* is the field of study and application of ultrasounds (see **Figure 2-4**).

Nevertheless, aside of this definition, for NDE ultrasonic discipline, ultrasound techniques, make use of mechanical elastic waves, either on an active or passive manner (i.e., inducing or only detecting waves on the inspected specimen). That is, ultrasonic methods do not use sound as intuitively is known by humans (like perturbed air), but actually they use periodical mechanical stresses (mechanical stress waves) applied on the object to evaluate. This stress waves can be "injected" on the material in order to stimulate it and analyze its response (e.g., Ultrasonic Inspection, Guided Wave Testing and Picosecond Laser Ultrasonic), or only continuously monitoring, so that a detection system identifies physical changes on materials (e.g., Acoustic Emission technique).

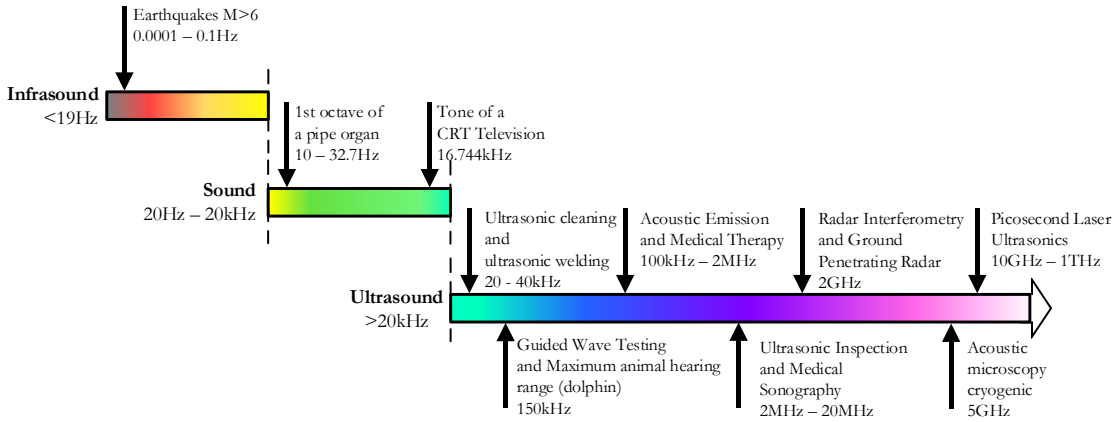

Figure 2-4. Examples of applications of sound phenomenon. It can be identified three main regions: Infrasound, Sound and Ultrasound. The use of the ultrasonic waves fits in a large field of applications, over an extended gamut of frequencies and intensities, including cutting, cleaning and welding at lower boundary, going through NDE and Medical applications, and at the upper end Acoustic Microscopy and Picosecond Laser Ultrasonic. Some authors conventionally name the frequencies above 1GHz as Hypersonic region [31].

2.3.1 Ultrasonic Inspection

Ultrasonic testing is a method to control materials with low or moderate acoustical attenuation as metals, ceramics or polymers. Inner and outer lack of homogeneities may be found. If the time of flight can be measured, it is also possible to determine velocities or the thickness of objects or coatings. The usual frequency range lies between 0.5 MHz to 20 MHz

[32]. In solids, sound waves can propagate in four principle modes that are based on the manner that particles oscillate. Sound can propagate as longitudinal waves, transverse or shear waves, surface waves and in thin materials as plate waves. Longitudinal and shear waves are the two modes of propagation most widely used in ultrasonic testing.

In longitudinal waves, the oscillations occur in the longitudinal direction or the direction of wave propagation. Since compressional and dilatational forces are active in these waves, they are also called pressure or compressional waves. They are also sometimes called density waves because their particle density fluctuates as they move. Compression waves can be generated in gases and liquids, as well as solids because the energy travels through the atomic structure by a series of compression and expansion movements [11].

In the transverse or shear wave, the particles oscillate transverse to the direction of propagation. Shear waves require an acoustically solid material for effective propagation and, therefore, are not effectively propagated in materials such as gases or most liquids. Shear waves are usually generated in materials using the mode conversion from longitudinal waves.

The basic technique of ultrasonic inspection is simple: a transducer transforms a voltage pulse into an ultrasonic pulse (wave). One places the transducer onto a specimen and transmits the pulse into the test object. The pulse travels through the object, responding to its geometry and mechanical properties. The signal is then either transmitted to another transducer (pitch–catch method) or reflected back to the original transducer (pulse–echo method) [33]. Either way, the signal is transformed back into an electrical pulse, which is observed on an oscilloscope. The observed signal can give a detailed account of the specimen under investigation. Using either method, it can be determined:

- The ultrasonic wave velocity in or thickness of the specimen.
- The presence of a flaw, defect, or delamination, and its size, shape, position, and composition.
- Material properties, such as density and elastic constants (Young's Modulus, Poisson's ratio, etc.)
- Part geometry or the nature of layered media.
- Finally, a transducer can be scanned across a surface to create a 2-D or even a 3-D image of a specimen.

2.3.2 Guided Wave Testing

Guided Wave testing (GWT) is one of latest methods in the field of non-destructive evaluation. The method employs mechanical stress waves that propagate along an elongated structure while guided by its boundaries. This allows the waves to travel a long distance with little loss in energy. Nowadays, GWT is widely used to inspect and screen many engineering structures, particularly for the inspection of metallic pipelines around the world. In some cases, hundreds of meters can be inspected from a single location. There are also some applications for inspecting rail tracks, rods and metal plate structures [34].

Although Guided wave testing is also commonly known as Guided Wave Ultrasonic Testing (GWUT) or Ultrasonic Guided Waves (UGWs) or Long-Range Ultrasonic Testing (LRUT), it is fundamentally very different from conventional ultrasonic testing. Guided wave testing uses very low ultrasonic frequencies compared to those used in conventional UT, typically between 10~100kHz. Higher frequencies can be used in some cases, but detection range is significantly reduced. In addition, the underlying physics of guided waves is more complex than bulk waves.

2.3.3 Acousto Ultrasonic Inspection

Acousto-Ultrasonics is a new method for non-destructive testing and evaluation of the plates, which was proposed by American scientists at the end of the 1970 [35]. The term of Acousto-Ultrasonics may be taken as a contraction of acoustic emission simulation with ultrasonic sources. In acousto-ultrasonic approach, the sender and receiver probes are usually coupled to the same surface of the tested object. This satisfies the need of testing on one side in many cases. In order to excite the stress waves, which propagate parallel to the surface of the tested plate, the sender is coupled directly to a surface with fluid (coupling). These stress waves are taken as the simulation of acoustic emission. But in this technique loading is not needed which is necessary in the acoustic emission detect. The transducer receives these stress waves at certain distance from the transmitting transducer. So, the acousto-ultrasonic method is also an ultrasonic testing in nature.

In acousto-ultrasonics, a stress wave factor (SWF) is used to characterize acousto-ultrasonic waves. The SWF is based directly on acoustic emission practice such as energy, peak voltage or ring-down. It indicates the energy of the received signal in the given time domain or frequency domain. The modes of the ultrasonic waves in the plate are complicated because of the arrangement of the transducers in the acousto-ultrasonic approach. It may be thought

that, in the tested plates, there are lamb waves and the waves, which are reflected many times between the two surfaces of the plate. But the SWF often used disregards the nature of the ultrasonic propagation, this greatly restricting the utilization of the acousto-ultrasonic technique.

2.4 Acoustic emission

The acoustic emission (AE) testing method is a unique nondestructive testing (NDT) method where the material under inspection generates elastic waves that warn of impending failure. These waves are produced when the material is either mechanically, thermally or chemically stressed to the point where an irreversible internal deformation occurs [36].

During plastic deformation, dislocations move through the material's crystal lattice structure [37] (see **Figure 2-5**), due to formation of intermolecular voids, and the coalescence of these voids [38].

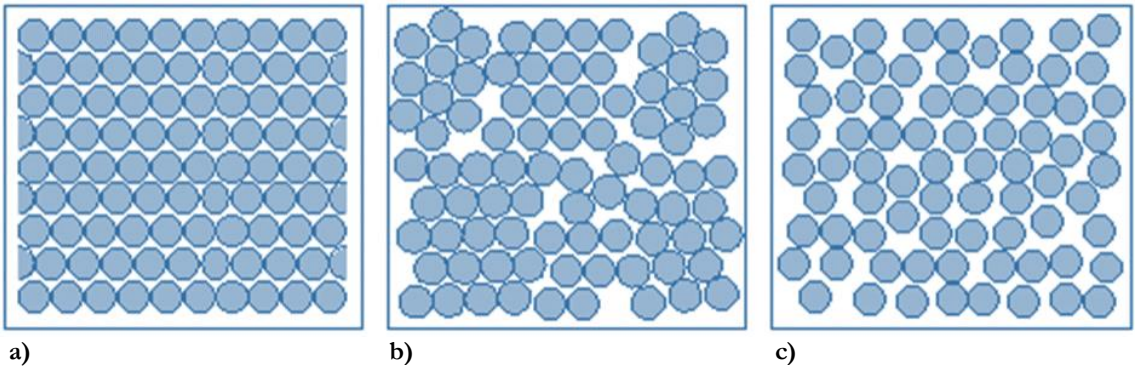

Figure 2-5. Atomic scale structure of materials. **(a)** Single crystal, periodic arrays across the whole volume. **(b)** Polycrystal, periodic across each grain. **(c)** Amorphous solid, non-periodicity.

Each intermolecular activity involved on the fracture's process (see **Figure 2-6**), will produce a low-amplitude and short duration elastic wave on the surface of the material, this phenomenon is known as acoustic emission. AE. This elastic wave propagates in all directions and cannot be stopped, similarly as a microscopic earthquake with its epicenter at the defect. On flat surfaces, the wave propagates as concentric circles around the source and multiple installed sensors can detect it.

Like a pebble thrown in water, the amplitude of the concentric waves is attenuated with increasing time and distance. Depending of the mechanical properties and geometry of the material, as well as the induced stress field that formed the AE phenomenon, the AE waves will scatter on the material in a variety of forms, i.e., body, compressional, flexural, etc. Nevertheless, nowadays the AE waves that are captured by sensors and subsequently assessed are mainly surface AE waves.

Historically, it is said that first practical use of AE occurred in about 6500 B.C. as pottery makers listened to the cracking sounds made by clay pots that had been allowed to cool too

quickly [39]. By experience the potters learned that cracked pots were structurally defective and would fail prematurely. However, the pioneer of modern AE testing was Josef Kaiser of Germany. In 1950, Kaiser published his Ph.D. thesis, which was the first comprehensive investigation of acoustic emissions [25].

He made two important discoveries, first was that a material emits low intensity pulses of elastic energy when placed under stress. His second discovery stated that once a given load was applied and the acoustic emission from that noise had ceased, no further emission would occur until the previous stress level was exceeded, even if the load was removed and later reapplied. This so-called "Kaiser effect" can be time dependent for materials with elastic aging. The principle is used in present-day AE proof testing of fiberglass and metallic pressure vessels.

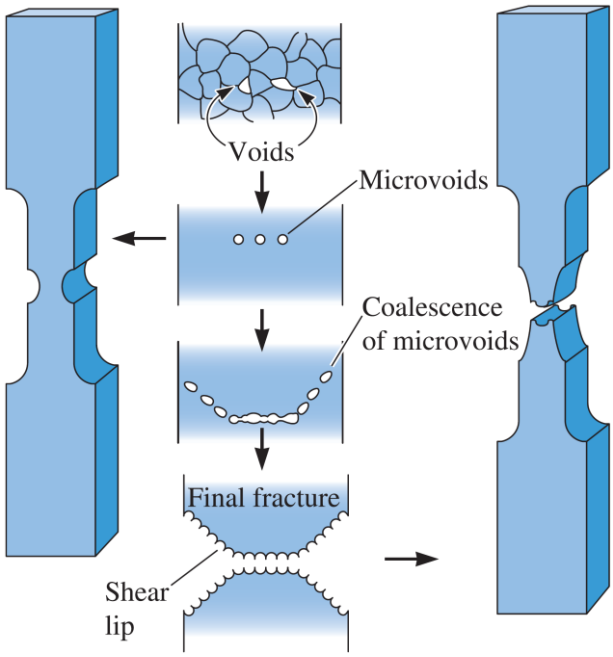

Figure 2-6. Mechanic evolution of fracture for a tensile test.

AE as NDE method can detect, locate, identify and display flaw data for the stressed object the moment the flaw is created. Therefore, flaws cannot be retested by the AE method; contrasting to ultrasonic testing, that characterizes flaws after have been created. Practically, all solid materials produce acoustic emissions when they are stressed beyond their structural stress limits [40] (see **Figure 2-7**).

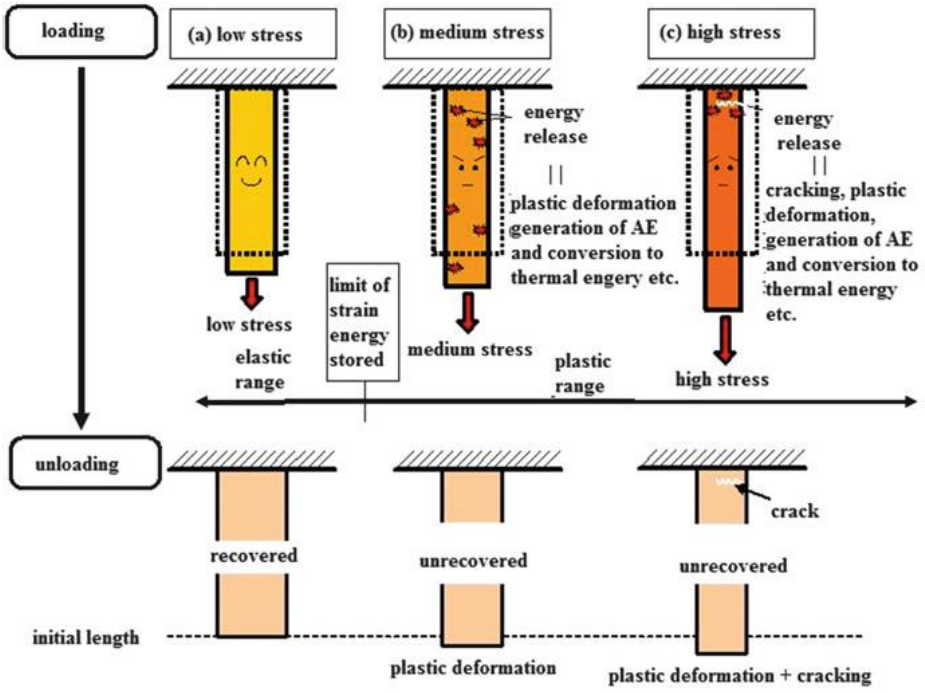

Figure 2-7. Generation of AE due to strain energy release under uniaxial tensile stress [41].

2.4.1 Advantages and disadvantages of AET

Compared to alternative NDT, AET does not require the direct inspection of the specimen under analysis, that is, materials can be monitored on service; that is, without dismounting and avoiding service interruptions.

Ultrasonic inspection as instance, require the injection of artificial waves, may interfering the normal operative conditions on the inspected material. AET conversely, may monitoring, passively, specimens and structures with only few sensors, making it very convenient to implement.

Additionally, AET takes advantage of the mechanical responses of materials, that is, AE phenomenon is only manifested when the material experiences irreversible changes (beyond of its elastic limit). Therefore, when signals are properly processed, AET only will inform about damage related events.

A disadvantage of AET lies in not to be identically reproducible, this, due to the nature of the material's damage, since heavily depending on the geometry, anisotropies, as well as the exerted force over it, different and randomly located damage sources can be generated.

Furthermore, comparatively to UT, the mechanical waves of AE phenomenon are characterized by very low amplitudes, very short durations and being largely attenuated. Thus, requiring in order to be captured, more sensitive sensors as well as higher amplification stages. However, these strategies may induce significant noise floor to the acquired signal, diminishing the resultant SNR, which increases the processing complexity.

2.4.2 AE signals

In order to either monitoring, locating or assessing damage by means of the AE phenomenon, after an AE wave have been generated and propagated through the material of interest, it must be properly acquired, detected and conditioned [42], (see **Figure 2-8**).

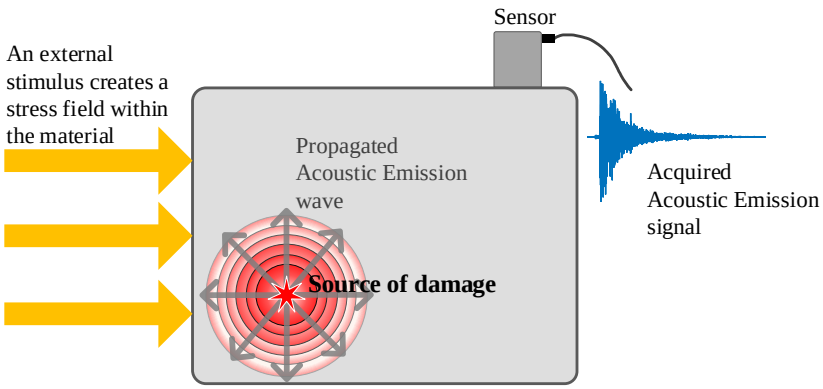

Figure 2-8. Generation, transmission and acquisition process of the AE phenomenon.

The first step in the AE processing chain, consists of the transduction of the elastic material displacement generated by the energy of the AE wave into a tractable (from the signal processing point of view), electrical signal. This is achieved by means of an AE transducer, which ideally should provide a wide and flat frequency spectral response; without adding noise-floor and presenting an input mechanical impedance as large as possible.

Nowadays, there exists a variety of technologically available AE sensors, which ought to be properly selected given the oriented field of application. These include strain gages, accelerometers, piezoelectric sensors, electromagnetic acoustic transducers (EMAT) and optical or fiber-optic interferometers. As aforementioned, AE waves exhibit low amplitude (rarely exceeding 1Å, i.e., 10^{-10}m) and short durations (averaging tens of microseconds), hence, choosing an AE sensor (like measuring any other physical phenomenon), implies compromises and tradeoff to be considered in order to determining the appropriate

transducer for the required application, e.g., sensitivity, SNR, dynamic range and frequency band response.

After acquiring the transduced AE wave, typical AE electrical signals will display very low voltage amplitudes (in the order of microvolts). Thus, in order to transmit and process these waves, an amplifying stage is required. Nowadays, typical gain values range from 10-80dB.

The last stage in the processing chain, consists of the recording and/or transmission of the AE electrical signals. Hence, ideal electronic systems would be capable of continuously recording signals from several AE sensors and for undefined time tests. Nevertheless, due to requirements of the ADC sampling rates, storage memory and data-bus transfer specifications in order to process the AE phenomenon; the commercially available AE electronic equipment, regularly will present a tradeoff between high sampling rates data and the capability of storing continuous large tests.

2.5 Discussion and conclusions

In this chapter, it was pointed out the relevance of the tensile test in the materials design discipline. This procedure, aids in the characterization of several essential mechanical properties regarding to the inspected material. Yet, traditional extensometers systems used to measure the displacements experienced by the specimen during the assay are useful to a certain extent, since they are not capable to obtain information about the internal changes suffered by said specimen.

Additionally, it was highlighted that despite that efforts made in order to overcome these drawbacks, implementing additional technologies to the assay (as is the case of DIC systems, which incorporates high-resolution cameras), and regardless of adding resolution to the test, these, still entail the same restriction of only being capable of analysing the surface of the material, without contributing supplementary information about internal evolution of the specimen.

In this sense, it was outlined that non-destructive technologies are placed as an attractive alternative with the aim of analysing to the tensile test from a different physical context. Particularly, ultrasonic elastic waves have demonstrated to significantly add complementary information to the test, either by inspecting the specimen under an offline monitoring approach with the aim of searching by flaws by means of ultrasonic inspection technologies; or also, during the assay under an online monitoring approach by means of the acoustic emission phenomenon.

Finally, it was briefly revised the physical production of the AE phenomenon, the characteristics of its resulting elastic waves, as well as the faced challenges in order to these be digitally processed. In this regard, it was pointed out the development necessity of novel methods that can manage the AE signals with higher accuracy with the aim of achieve better results from assessments.

Chapter 3. DETECTION OF ACOUSTIC EMISSIONS

3.1 Introduction

Nowadays, AE phenomenon is an active field of research [43], nevertheless, in order to conduct such an analysis, proper detection and capture of every AE event is highly desirable. In order to automatically detect the AE events, also known as hits, the most frequently used technique is to compare the obtained electrical signal against a predefined voltage threshold level; whenever the signal rises above this threshold, a hit has been detected.

This technique was used in the first applications of AE as an evaluation tool and emerged due to the lack of digital hardware capable of handling the payload from the large data stream required for proper digital processing of the near-baseband signal [44].

With the advent of fully digital platforms, and given the relative efficiency and ease of implementation, nearly all the established standards for AE [45,46], as well as the commercially available instrumentation (and, as a result, most field work), use the threshold voltage technique as the default for AE activity detection.

However, although it has not been exhaustively analysed in the literature, the threshold method has critical drawbacks and limitations that could impair performance in the case of an irregular AE waveform.

Typically, once a set of AE hits has been detected, different features of each hit are extracted in order to locate or assess damage to the specimen. As might be expected, the more accurate and precise the detection, the better the quality of the subsequent evaluation [47]. Indeed, in recent years, significant efforts have been made to develop advanced signal processing approaches for better AE hit detection outcomes [48,49].

Due to similarities in the origination of AE emission and earthquakes, some of the most widely used alternatives are inspired by geophysics.

Four main approaches are outlined in the literature: the instantaneous amplitude (IA) threshold method [50], the short-term average to long-term average (STA/LTA) ratio [41], the Akaike information criterion (AIC) [51] and time-frequency distributions based on the continuous wavelet transform (CWT) [52].

Nevertheless, although these methods perform relatively well for determining the onset time of transient AE signals, their performance for determining the signal endpoint and their efficiency in the case of a burst of AE events, remain unconcerned. Due to the lack of a common frame benchmarking, there are significant constraints on the widespread application of the four methods in non-destructive testing procedures, particularly fracture mechanism tests that could potentially be used to improve the methods.

3.2 Limitations and drawbacks of the traditional AE threshold detection method

Although widely applied in many industrial applications, the thresholding approach used to detect and extract hits from an AE waveform presents some important shortcomings that must be identified in order to assess its suitability for high-performance applications. The main weaknesses of this method when dealing with AE signals, and their impact on the resulting AE hit detection, are presented and discussed below. The signals presented in this section were captured during unidirectional tensile tests (with a load rate of 1 mm/min). Each image corresponds to a different advanced high strength steel specimen, all of which have the same dimensions; height (h) = 240 mm, width (w) = 55 mm, and thickness (t) of 2 mm.

3.2.1 Inability to detect bipolar activity

Only the positive part of the resulting electrical signal (or negative, according to the configuration) is considered for onset detection, as shown in **Figure 3-1**, where it is shown the actual onset time arrival (vertical dotted green line) and the automatic detection time arrival (vertical dash-dot orange line), of two p-waves showing opposite arrival polarities for two different AE signals (solid line) evaluated under a positive detection threshold of 50mV (horizontal dashed line), and obtained from the same tensile test on a Complex Phase (CP) steel sample.

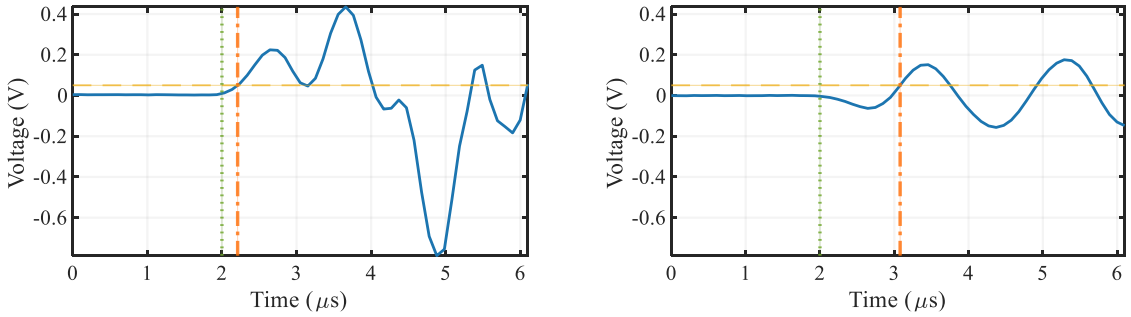

Figure 3-1. Onset determination by means of the traditional threshold technique. **(a)** Compressional wave. **(b)** Dilatational wave.

In **Figure 3-1 (a)**, a compressional wave (first movement up) detected with a low time detection error Δt_{error} (i.e., detected onset time minus true onset time). **Figure 3-1 (b)** shows a dilatational wave (first movement down), due the mismatch of the positive polarity of threshold and the falling edge start event of the signal, accuracy of the onset detection

measurement is affected, furthermore, under this approach is not possible to use some evaluation techniques based on polarity information of p-waves.

The first motion direction (i.e., up or down) of an AE wave cannot be predicted deterministically, so depending on the chosen configuration for the threshold detector (i.e., rising or falling edge triggering), the onset times of a significant number of hits will be inaccurate. This is particularly relevant in damage location techniques where an accurate time of arrival or time of flight (i.e., relative measurement time between elements of a sensor array) is crucial [53]. Alternatively, in the case of damage assessment methods (like those based on moment tensor inversion), information about the direction of the primary wave (i.e., *p*-wave) is essential [54,55].

This problem can be lessened with the use of: *a)* secondary thresholds (i.e., positive and negative thresholds detecting in parallel); *b)* pre-trigger buffering, which considers a certain number of data samples before a detection at the cost of an inaccurate measure of the actual onset time, as well as adding the risk that the detection will overlap with a previous hit, and *c)* signal transformation towards a characteristic function (CF), where it is common to use hardware to work with a rectified voltage or by means of software to work with a simple absolute value function.

3.2.2 Varying background noise inaccuracies

Varying background noise may cause: *(i)* false detection, due to increasing noise, *(ii)* incomplete detection, due to increasing noise, and *(iii)* insufficient sensitivity to trigger a detection, due to decreasing noise. Acoustic emission waves are highly susceptible to noise and are therefore likely to exhibit dynamic behavior during surveys, reducing detection quality due to the fixed threshold level.

Despite extensive research into noise treatment strategies for AE signals [56,57], which can be applied before or after hit detection, the problem of varying noise during discrimination of AE activity remains inherent to the method when a fixed threshold value is used. Traditionally [58], and in recent studies [59,60], this issue has been addressed by using a floating threshold (also known as an automatic, adaptive or smart threshold) whose value is continuously adapted to noise. To obtain a floating threshold, a simple moving-average filtered version of the raw signal acquired from the AE-sensor is typically used, and as in the case of the fixed threshold approach, a hit is detected when the raw signal rises above the new floating threshold level.

Ultimately, however, this technique does not solve the problem, since there is a trade-off between detection sensitivity and the capacity to avoid noise, according to the time segment value of the moving-average function. In the case of the use of extreme values, for a very short time frame, the new threshold will behave as an envelope of the raw signal, avoiding all transient noises however inhibiting detection; if, however, it is too long, the floating threshold behaves as a fixed threshold. Consequently, this approach is best suited to applications in which background noise varies gradually; nevertheless, in applications prone to sudden mechanical noises (e.g., friction or slip) or with high AE activity it is difficult to find an optimum time response value [61,62].

This fact is depicted in **Figure 3-2**, for a 140 ms data frame containing four AE events, located at 18.8, 46.5, 55.2 and 90.0 ms, respectively (shaded green areas). First, it can be seen that a fixed threshold (horizontal red line), which is calibrated at 3.5 mV (just above the background noise level at the beginning of the signal frame) is not suitable in this instance, since after 8 ms a highly variable noise floor affects the signal, leading to a saturation detection error (except at around 80 and 110 ms, where the background noise returns to similar levels to the beginning of the data frame).

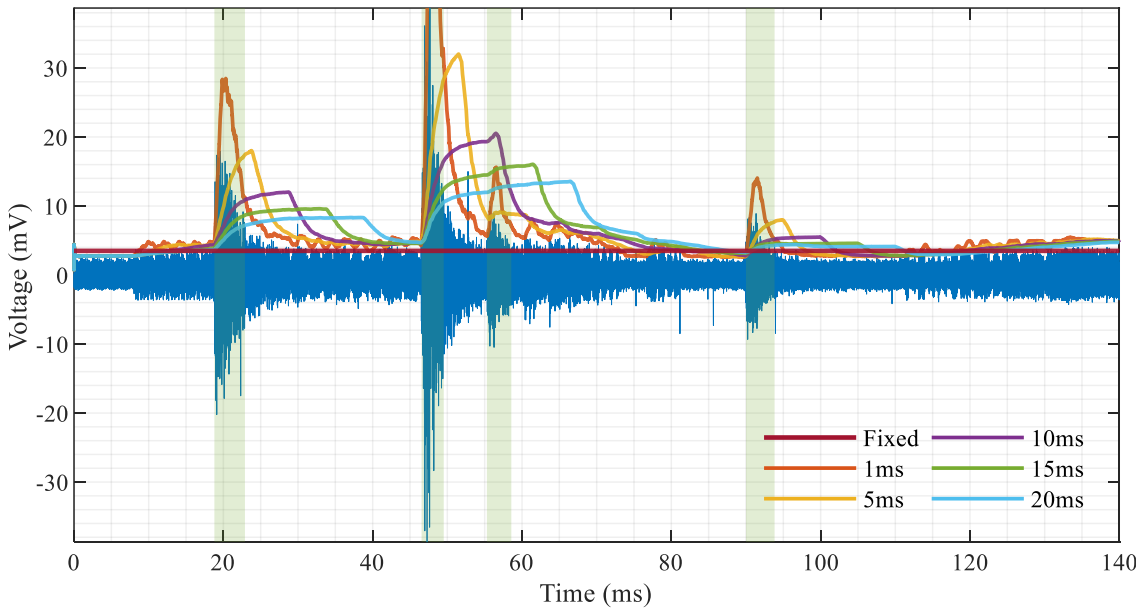

Figure 3-2. Five different floating threshold configurations on a highly noise-tainted data frame.

Additionally, five floating thresholds are implemented using a simple boxcar filter (zero-lag correction) for frame time configurations of 1 ms (orange curve), 5 ms (yellow curve), 10 ms (magenta curve), 15 ms (green curve) and 20 ms (cyan-blue curve) respectively.

In this instance, although floating thresholds clearly perform better than the fixed threshold, none of them completely solves the problem, since each one leads to its own detection errors.

This trade-off is evident in the case of the 1 and 5 ms configurations, where there is a choice between responding rapidly to non-transient background noise (achieved at 8.5 and 112 ms, respectively) and detecting more AE events than the slower configurations (third AE event located at 55 ms), but losing accuracy for determining the durations of all hits. By contrast, for longer time values, as in the case of the 10, 15 and 20 ms configurations, the determined durations are closer to the actual values (hits 1, 2 and 4). These configurations can also avoid some highly energetic transient noises by being far from the noise floor (as at 30 and 75 ms), but at the cost of requiring too much time to respond to the variation in background noise (as can be observed for the time ranges 8.5–10 ms and 112–130 ms). Finally, none of the configurations is capable of avoiding transient mechanical noises when the floating threshold value is close to the noise floor (as at 8.2, 76 and 111 ms).

3.2.3 Random on the incidence and duration of events

The appearance and duration of AE events seem to behave stochastically during surveys. To address this, the fixed threshold technique is extended to include two time-driven parameters, hit definition time (HDT) and hit lockout time (HLT), which aim to prevent error detection, establishing a mechanism that determines the end of the event. However, and as in the above case of the floating threshold technique, these additional parameters imply a trade-off between detection sensitivity and robustness against errors.

Hit definition time, also known as duration discrimination time (DDT), uses a fixed timer to establish the end of a hit. Once a hit is detected, the system that implements the threshold technique will trigger the HDT timer with the condition that it restarts whenever the raw AE signal crosses the threshold level again before the time is complete.

However, the use of this timer also entails a latent risk in the quality of detection of AE activity, since it is impossible for a pre-set value to consider the variety of durations (i.e., lifetime or lifespan of an AE wave) that the different hits will exhibit during a survey. In other words, a short preset duration will cause most of the identified hits to be truncated after detection and possibly split into two (or more) different events, whereas a long preset duration risks poses the risk of splicing the identification of two or more hits into a single event (sometimes misinterpreted as a cascaded hit).

Hit lockout time, also known as rearm time (RAT), aims to avoid the splicing of a detected hit with its own reflection, which is achieved by triggering the timer once the HDT reaches the end of its count. While HLT is active, the detector will not accept any further activity on the raw AE signal (whatever the nature is) until the HLT timer reaches the end of its count. The drawback of its implementation is that a short pre-set time will result in false-positive hit detection due to reflections or a split hit, while a long pre-set time will lead to the truncation or, in the worst case, the misdetection of a hit due to the risk that a hit will emerge during the HLT timing process [63].

Precise selection of the DHT and HLT timer values will obviously increase the detection accuracy of the threshold technique during a survey. However, even if instrumentation is carefully calibrated according to the characterisation of the material under inspection (e.g., attenuation, speed of sound, etc.), the implementation of pre-set times will eventually induce errors as consequence of applying a fixed parameter to a stochastic phenomenon.

This trade-off is depicted in **Figure 3-3**, where two different AE event detection outputs are compared by maintain the same threshold level value of 3.25mv and slightly varying the HDT and HLT parameters for a 920 μs data frame. Shaded green areas indicate the actual durations of each of the hits found at 43.4, 471.5 and 527.3 μs, respectively. Vertical dotted lilac lines and vertical dash-dot pink lines, respectively, indicate the automatic onset and endpoint detections made by the conventional threshold technique.

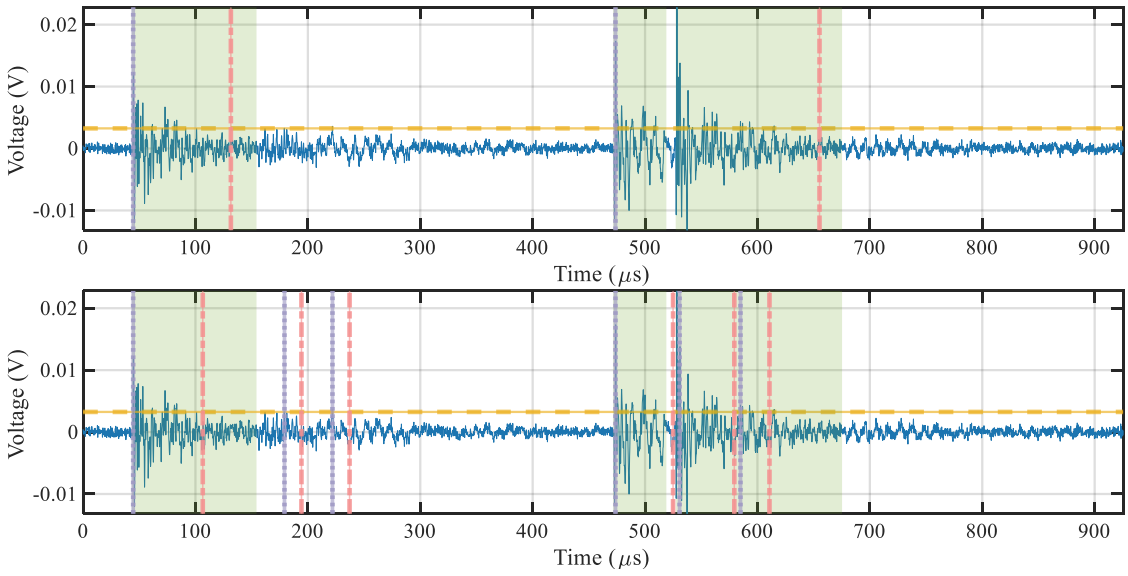

Figure 3-3. Two different output determinations for the same AE frame signal using slightly different preset times. **(a)** Greater time. **(b)** Smaller time.

The calibration shown in **Figure 3-3 (a)** (HDT = 40 μs, HLT = 100 μs) is intended to achieve the best approximation for the durations of each hit, using higher timer values in order to reject detection errors caused by reflections of the hit. As can be observed, the selected values meet the objective, but at the cost of truncating the first hit (located at 43.4 μs and automatically detected after 1.2 μs), as well as splicing the second and third hits (471.5 and 527.3 μs, respectively) into a single event.

By contrast, the aim of the calibration shown in **Figure 3-3 (b)** (HDT = 15 μs, HLT = 5 μs) is the timely detection of each hit. Thus, the highest timer values are used in order to identify the minimum required time difference in the values of the HDT and HLT parameters between calibrations. As can be observed, the onset of every hit is properly detected, but reflections of the hits are mistakenly detected as independent AE events. Moreover, the reflections of hits one and three are miss-detected as AE events.

3.2.4 High dynamic signal range

The amplitudes of the AE waves will exhibit highly diverse scales, ranging from the order of picometres, giving rise to a transduced electrical signal that covers a range from millivolts to volts. To address this issue, it is a common practice to use a CF based on the logarithmic absolute value of the raw AE signal. This approach seeks to improve the calibration of the instrumentation by enhancing the visual deployment of the signal to process, so that the level of the fixed threshold can be adjusted. By using this approach, the threshold level is typically given in decibels. **Figure 3-4** illustrates this approach, showing the same 200ms data frame for a linear scale **(a),** and a logarithmic scale **(b)**, and containing sixty-six different AE events.

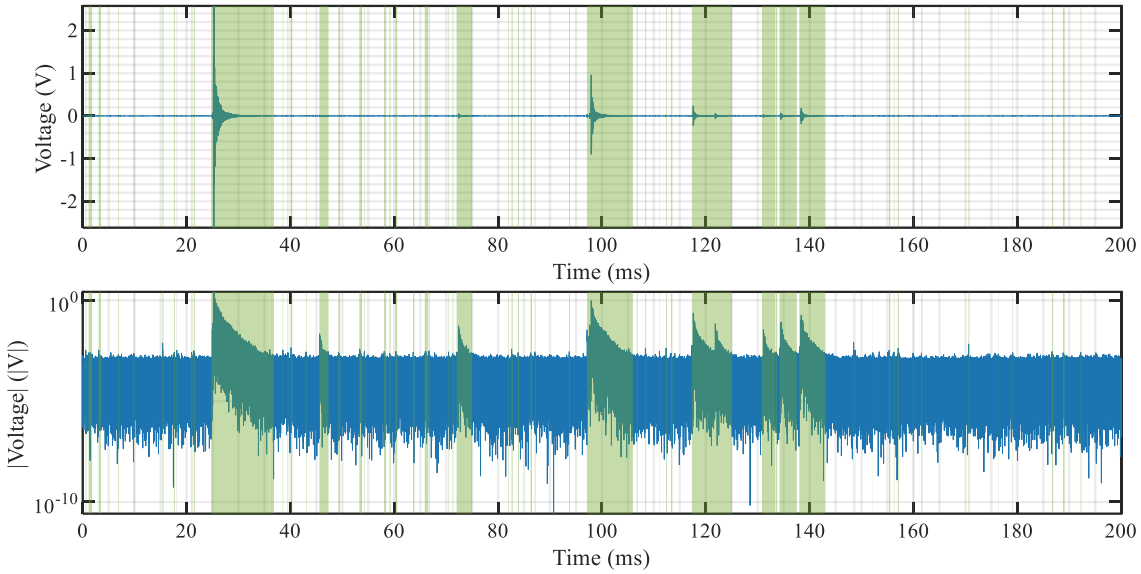

Figure 3-4. Amplitude variance of AE waves for the same datastream. **(a)** Linear scale. **(a)** Logarithmic scale.

As can be observed, there is a significant difference between peak amplitudes for the different AE events, ranging from a minimum of 2.8 mV at 176.3 ms to a maximum of 2.6V at 25.3 ms. **Figure 3-4 (a)** shows that in a linear representation of the raw signal, only the most energetic events are discernible. In **Figure 3-4 (b)**, having depicted the data frame on a logarithmic scale, it is less difficult to distinguish the different AE events.

Nevertheless, the use of this alternative approach still poses a risk to detection quality, as a fixed threshold is applied despite the large variance in the amplitudes of the AE events. This aspect leads to an additional trade-off when selecting the threshold value, forcing a choice between detection sensitivity and robustness to detection errors.

While it is true that increasing the threshold value, reduces detection errors due to transient background noises, it also reduces detection sensitivity due to the loss of detection of the less energetic events and leads to inaccurate onset determination due to the misdetection of *p*-waves. Conversely, reducing the threshold value increases detection sensitivity (since more AE events can be identified) as well as improving the accuracy of onset detection. Nevertheless, these improvements also raise susceptibility to false-positive detection errors (due to transient background noises, particularly those of a mechanical nature), as well as increasing the likelihood of splicing two or more hits into a single event.

This trade-off is illustrated in **Figure 3-5**, which compares two different output determinations of AE events by using two different threshold levels for the same 33 ms data frame.

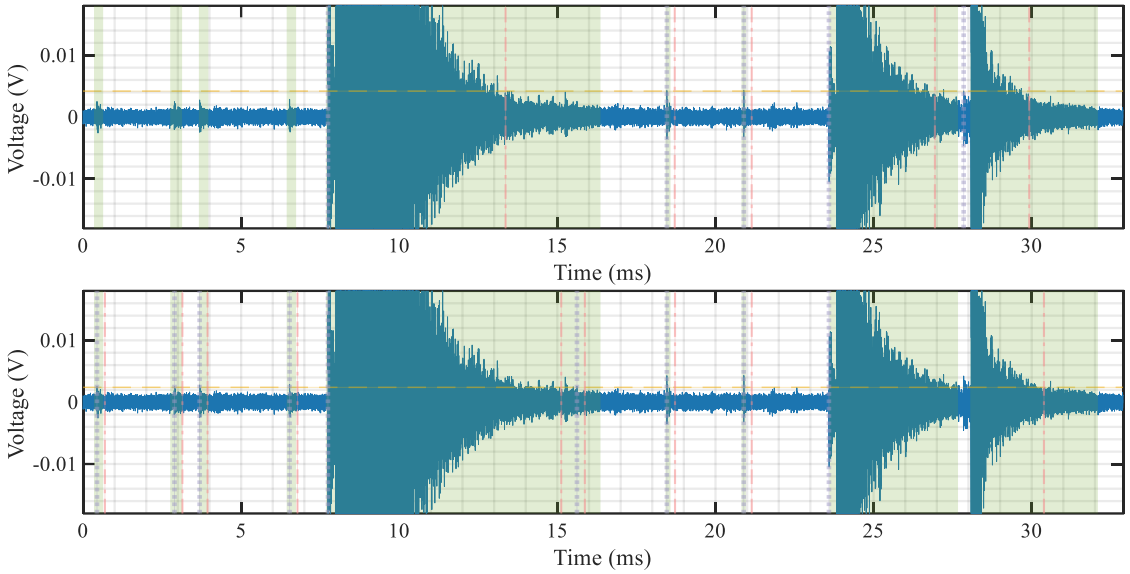

Figure 3-5. Two different outcomes for slightly different threshold levels. **(a)** Higher value. **(b)** Lower value.

Shaded green areas indicate the actual durations for each of the nine hits found at 0.38, 2.75, 3.66, 6.44, 7.68, 18.42, 20.82, 23.59 and 28.06 ms, respectively, ranging from 2.795 mV (at 2.75 ms) to 2.5 V (at 7.65 ms).

Vertical dotted lilac lines and vertical dash-dot pink lines, respectively, represent automatic onset and endpoint detections. Both calibrations are set with the same HDT and HLT values of 250 μs and 400 μs, respectively. Automatically determined durations are also indicated by the upper horizontal solid black guidelines.

In **Figure 3-5 (a)**, the threshold level value is set at 4.2 mV, the aim of the calibration being to accurately determine the duration of the AE events while avoiding any false-positive detection. To achieve this, the threshold level is lowered to its minimum value before any error detection is generated. Although the approach achieves duration determinations close to the actual values, the number of AE events effectively detected is reduced considerably, with only five of the nine hits detected.

In **Figure 3-5 (b)**, this trade-off is highlighted by lowering the threshold level to the largest value that is required for detecting the nine existing AE events. As can be observed, each hit is detected effectively, but several transient noise events are mistakenly detected as hits, resulting in three false-positive events at 16.91, 21.86 and 22.57 ms. Moreover, events number eight and nine are spliced and detected as if they were a single event.

3.3 Advanced detection methods of AE activity

In order to overcome the limitations described above for AE hit detection based on the classical thresholding approach, some alternative CFs are implemented with the aim of avoiding the application of the threshold level to the raw signal, as is the case of the envelope of the signal by means of the absolute value function, as well as by the instantaneous energy of the signal [41,64]. Nevertheless, due to similarities in the origination of AE and earthquake phenomena, some of the most widely used methods are inspired by geophysics discipline (where these tools are known as phase pickers).

For this study, four advanced methodologies representative of the current literature were considered: IA, STA/LTA, AIC and time-frequency distribution methods.

One current trend is to build the CF by means of the Hilbert transform [41,50,65]. The aim of this approach is to obtain by means of the analytic signal of the captured data (preserving only the positive side of its frequency spectrum) a decomposition of the AE signal into two different time-variant components: instantaneous amplitude (IA) and instantaneous phase (IP). Instantaneous amplitude is of particular interest as it enables the construction of a CF that geometrically depicts the envelope of the AE wave with greater accuracy (in comparison to the conventional absolute value function). Once the CF has been obtained, the classic threshold scheme is applied. However, although under this scheme, uncertainties associated with the inability to detect bipolar onset activity are overcome; those related to background noise, randomness of the phenomenon and high dynamic range remain unaddressed.

The STA/LTA ratio picking method was proposed by Allen [66] for determining the onset time of earthquake events, with the aim of reducing false-positive alarms in seismic monitoring. First, a CF is obtained from the raw AE signal (typically an absolute value or its instantaneous energy), then each of the STA and LTA contributions derived from the CF is calculated by means of a moving average filter, with two different response times for each one. The short-term against long-term contributions of the CF are compared through the STA/LTA ratio, and then a fixed threshold level is applied directly to the ratio to detect AE hits. This reduces the influence of rapid events such as mechanical background noises, while maintaining a reasonably good response of the ratio in relation to the original signal. The drawback of this technique is the delay induced by the LTA contribution, which affects the precision of onset detection measurement, in particular losing detail for primary wave detection.

The AIC is a tool for statistically modelling time series, developed for automatic control applications by Akaike [67], first proposed by Maeda for seismic data [68], later implemented by Kurz [69] in the field of AE, and broadly revised by several authors of the AE discipline [53,70–73]. It works by modelling the time series data of the raw AE signal under an autoregressive scheme (of low order). By estimating two locally stationary parametric components of the framed original signal (noise and AE activity); to later compare the entropy of each point of the modelled data, with the aim of find a critical point (the minimum). Thus, this critical point will indicate the arrival time instant of the AE wave.

Based on non-parametric signal processing methods, the time-frequency distribution analysis is a more accurate tool for detecting the onset time of AE waves. Using the short-time Fourier transform, Unnthorson proposed a fully automatic hit detector method [61,74]. However, most current research focuses on the use of the wavelet transform (WT) [52,75–78], which improves the resolution of the energy localisation of the AE event in the time-frequency plane, increasing the accuracy of onset determination.

The AIC and CWT techniques clearly provide a more accurate onset determination of AE events than the classical threshold method, however, in a fully automatic AE hit detector application, typically they only serve to refine a coarsely detected hit (i.e., their use implies prior detection of the AE wave of interest). Clearly, this adds a degree of uncertainty to the outcome of these methods, since they will necessarily require an early thresholding detection framework.

Finally, it should be considered that although these advanced methods improve the detection accuracy for AE waves, the high data rates required to process the phenomenon make them computationally expensive, so they are usually implemented in an offline framework (first capturing the data of a survey, later extracting the AE events). Nevertheless, efforts have also been made to implement hardware architectures that can work in an online approach [79–81].

3.4 Performance evaluation of advanced detection methods of AE

As stated above, the most significant methods require to be compared within a common analytical framework in order to establish a quantitative assessment of their performance. Consequently, based on the current literature, in this dissertation are considered four AE detection methods: *a)* a classical threshold technique enhanced by the instantaneous amplitude component [50]; *b)* a typical STA/LTA detector [82]; *c)* a two-step AIC picker [51], and *d)* a CWT-Otsu detector over binary image mapping [52], which like *c)*, uses the same function derived from Allen's formula as CF for the threshold-based preliminary detection.

Performance of methods is evaluated using two different datasets. First, to measure the precision of onset and endpoint detection, a collection of one-hundred different AE waves derived from a standardized Hsu-Nielsen test are processed by each method; then for each resulting outcome, the absolute detection errors are measured. The second test bench measures the quality of event detection (i.e., accuracy, precision, false-positive rate, etc.) of each method using a data frame derived from a tensile test of a metallic component, which contains a wide variety (in terms of duration, amplitude and incidence) of AE waves.

For both experimental test benches, only one sensor, WSα from Physical Acoustics® manufacturer (see **Figure 3-6**), with a band frequency response of 100-1000kHz, was attached to the surface of each metallic component; using a glycerol-based couplant Sonagel-W from Sonatest® manufacturer. The transduced electrical signals are amplified by a Mistras® preamplifier 2/4/6, with a 20dB gain over a band frequency response of 10–2500kHz.

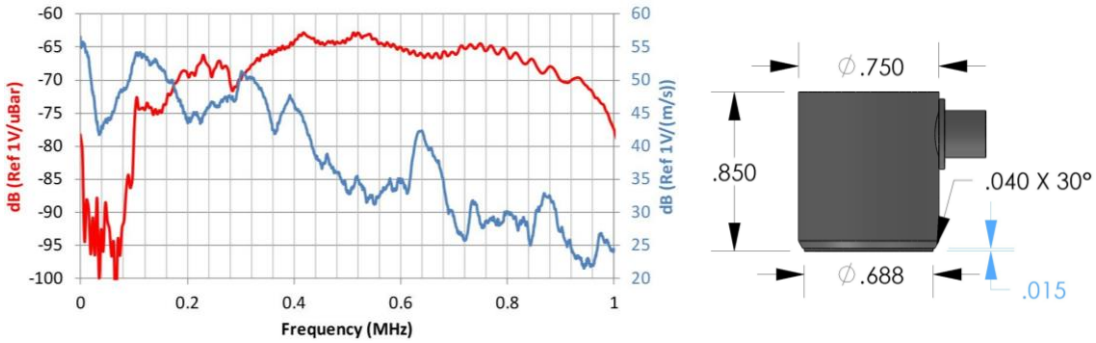

Figure 3-6. WSα sensor. **(a)** Frequency response. **(b)** Physical dimensions.

Then, the amplified electrical signals are recorded under a free-running sampling scheme using a CSE4444 digitizer from GaGe® manufacturer (see **Figure 3-7**), with a sampling frequency of 5 MHz for the Hsu-Nielsen data and 10 MHz for the tensile test data (both

samplings with 16-bit depth of vertical resolution and SNR of 75.2dB). Before processing the test bench, raw signals are band-pass filtered, using a FIR equiripple implementation (10–2200 kHz); this, with the aim of discard spurious frequencies outside from the pre-amplifier's bandwidth work.

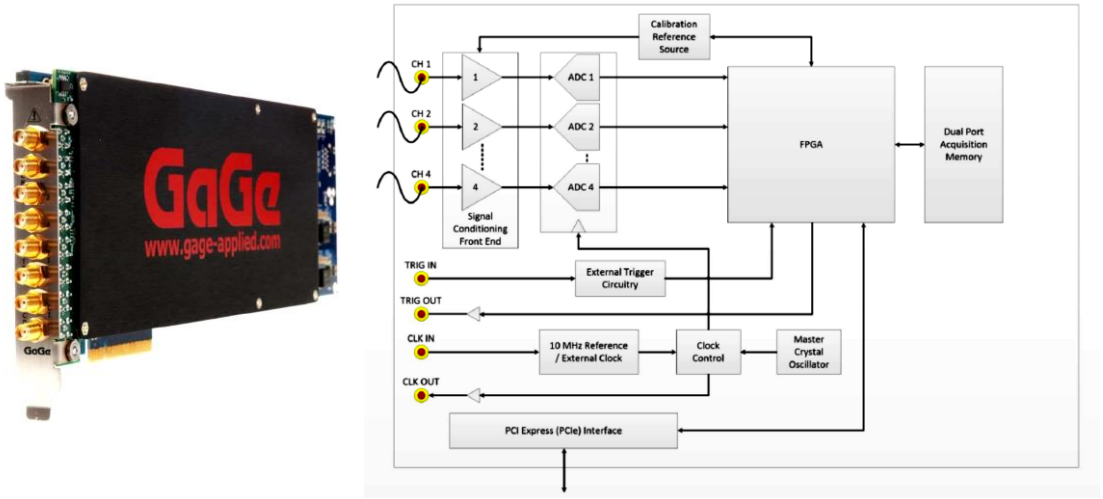

Figure 3-7. Digitizer used to collect the AE sensor channel. **(a)** PCIe card. **(b)** Functional diagram block.

For each method, the most suitable calibration parameters for the test bench are set following the recommendations in the literature [51,83–87] and in line with current standards [45,46,88–92]. Prior to performing the corresponding test benches, the onset and endpoint times of each of the AE waves were manually picked supported by time-voltage plots and a high-resolution time-frequency distribution [93].

3.4.1 Hsu-Nielsen data test bench

For the pencil-lead break test bench, for each of the one-hundred iterations, a graphite lead of ⌀ 0.5 mm and 2.5 mm tip-length with a contact angle to the surface of 30° is used. A distance of 12 cm between source and sensor is maintained (see **Figure 3-8**).

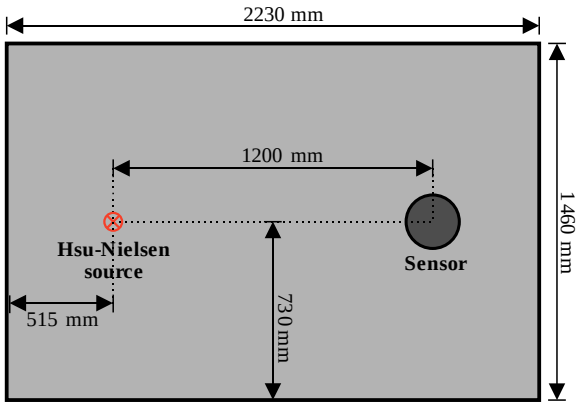

Figure 3-8. Setup for the standardized Hsu-Nielsen test-bench over a Press-Hardening 1500 steel plate specimen. Schematic diagram indicating the dimensions of the specimen and the locations of the source and sensor.

For repeatability purposes, each synthetic AE wave is edited so that its peak value is centred on 5 ms and its length extends an additional 40 ms; a typical waveform obtained from this procedure is shown in **Figure 3-9.**

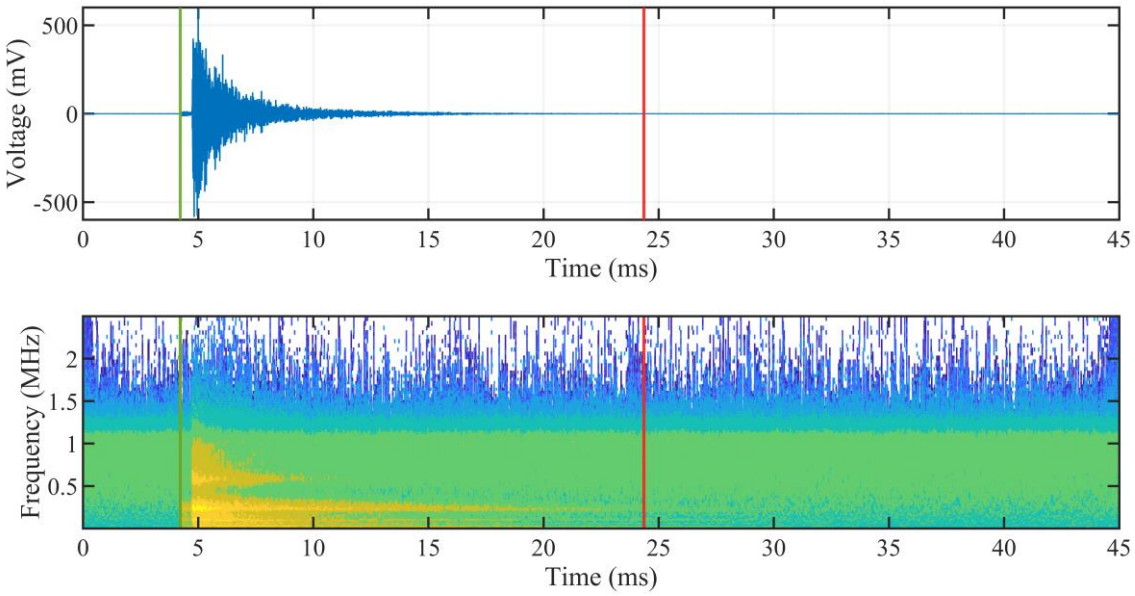

Figure 3-9. Typical AE waveform analysed in the synthetic data test bench. **(a)** Time-voltage domain. **(b)** Synchrosqueezed wavelet transform used to assist in the manual determination of the onset and endpoint pick locations of the AE wave (green and red vertical lines, respectively).

The objective of this test bench is to quantify the accuracy of each method in the measurement of onset, endpoint and duration times, by means of the absolute error of each measure. To assure accuracy, a strategy is used to calibrate the parameter values for each method, lowering the fixed threshold value to just above the background noise level for each characteristic function (see **Table 3-1**).

Table 3-1. Calibration parameter values for the Hsu-Nielsen test bench.

Parameter	Method			
	1A	*STA LTA*	*AIC*	*CWT Otsu*
Fixed threshold level	3e-3	5e-4	2e-1	2e-1
Hit definition time [µs]	1e3		100	100
Hit lockout time [µs]	10e3		10e3	10e3
De-trigger threshold		9e-3		
STA window time [µs]		75		
LTA window time [µs]		1e6		
Pre-event time [µs]		15		
Post-event time [µs]		10e3		
Weighting-R constant			4	4
End delay time window 1 [µs]			25	25
End delay time window 2 [µs]			10	
Start delay time window 1 [µs]				1.5e3
Start delay time window 2 [µs]			100	
CWT scales				101
Greyscale image bit-depth				16
Median filter pixel neighbours				50

Since each method involves different signal-processing strategies, different CFs are obtained (except in the case of AIC and CWT-Otsu, and only for early detection). Thus, specific calibrations (i.e., threshold levels and timing values) are required for the selected technique (as reflected in Table 1). Once each of the methods has been applied to each synthetic AE wave, the accuracy of the onset, endpoint and duration times are quantified using the absolute error from the outcomes of the methods with respect to the manually selected time locations (see **Table 3-2**).

Table 3-2. Absolute error and standard deviation for onset, endpoint and duration detections in the Hsu-Nielsen test bench

Method	Onset time error (μs)	Endpoint time error (μs)	Duration time error (μs)
LA	-21.83 ± 8.26	2454 ± 1120	2476 ± 1120
STA/LTA	-19.82 ± 7.92	3828 ± 1159	3848 ± 1161
AIC	-13.34 ± 7.00	16338 ± 1045	16352 ± 1045
CWT-Otsu	-1.19 ± 97.88	17795 ± 1047	17796 ± 1039

Table 3-2 shows that despite dealing with a challenging signal, by having to detect the AE onset when the p-wave arrives (which clearly has less amplitude than secondary waves), all methods perform relatively well for this detection stage, where in general terms the error is less than 20 μs for all cases. However, by executing a refinement of this onset examination, the AIC and CWT-Otsu methods present the lowest errors and can be considered to perform better.

Nevertheless, while the CWT-Otsu technique gives the lowest absolute error, it also shows the greatest dispersion values. The high accuracy and low precision can be attributed to the fact that the grayscale image derived from the CWT analysis of the signal (with which Otsu's method operates), when it contains a strong presence of either s-waves or noise regarding p-waves, tends to reduce the quality of the bimodal distribution of the image histogram, leading to segmentation errors. In the case of AIC, the inherent separation between noise and signal components, by means of finding the minimum in the calculated entropy of the raw signal, gives greater precision for the onset detection but at the cost of less accurate detections (i.e., lower dispersion error values but higher error detection values).

For the endpoint detection stage, all methods show poorer performance than for onset determination, which also has a direct effect on the estimation of the duration time. AIC and CWT-Otsu give nearly the same error values because they use the Allen's formula derivative

as CF. However, IA and STA/LTA are the best options, reducing the average error of the AIC and CWT-Otsu methods by 80%.

As can be observed, the endpoint determination has not yet been satisfactorily resolved, since the absolute error is approximately 2–18ms. This problem derives from the fact that instead of using a measure based on a tangible indicator extracted from the signal, in all of the methods endpoint determination is based on the combination of a fixed threshold and a fixed timer. Despite this drawback, the results also illustrate the advantage of obtaining a better representation of the signal through a more accurate CF, since although IA and STA/LTA also give significant endpoint determination errors, they can be considered to perform better thanks to lower absolute error values. In the case of IA this is achieved by a more responsive waveform, while in the case of STA/LTA, it is due to the consideration of future values of the signal with respect to current values.

3.4.2 Field data test bench

The objective of the second test bench is to quantify the quality of event detection for each method using field data. This is carried out by means of a tensile test of a metallic component (see **Figure 3-10**).

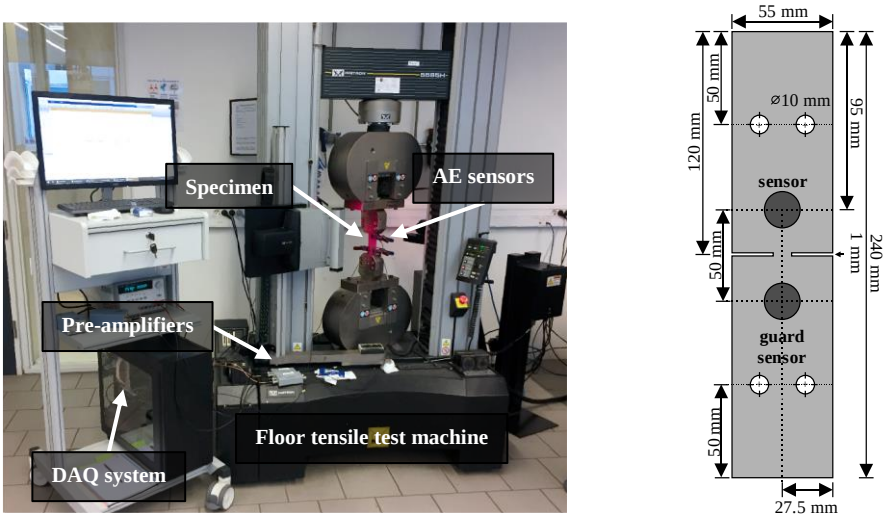

Figure 3-10. Standardized tensile test setup for a ferrite-pearlite annealing steel specimen (load rate of test 1mm/min).

The AE signal produced by the tensile test is recorded. For the field data test bench derived from this assay, a frame of 500 ms in length, containing 380 AE events (corresponding to an early damage stage of the specimen), is used as the input for each detection method (see **Figure 3-11**).

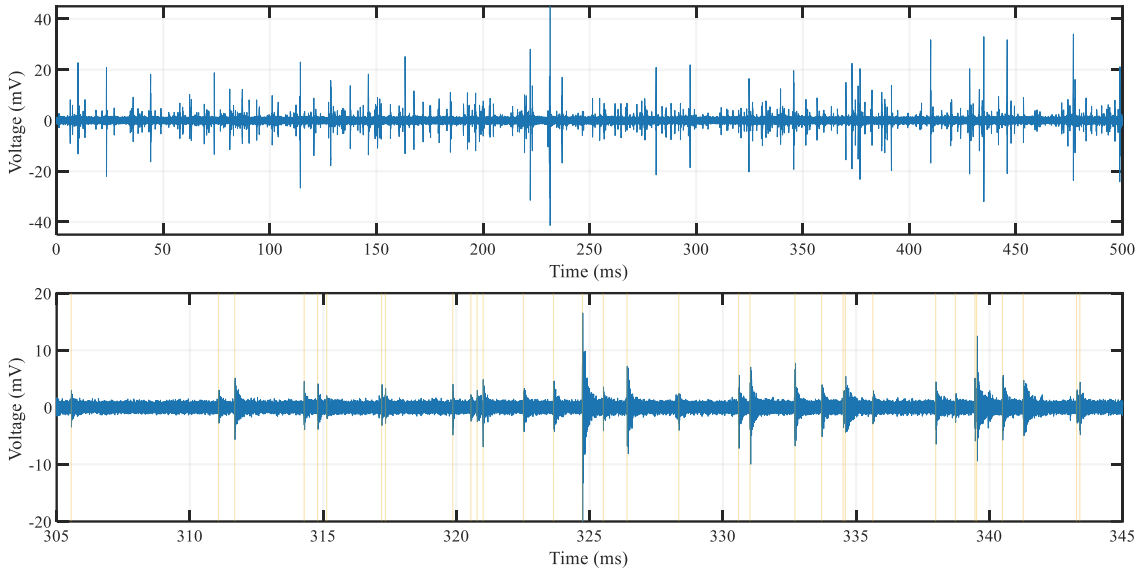

Figure 3-11. Signal used for the field data test bench. **(a)** Full dataframe. **(b)** Zoom of 40ms, showing the variety in the incidence, duration and amplitudes of the AE waves present in the test bench (manual onsets indicated by vertical lines).

For this test bench, each of the AE events (as well as their onset and endpoint locations) is picked using the waveform of the frame and supported by its time-frequency distribution.

In comparison with the artificial AE events produced by the standardized Hsu-Nielsen procedure, real AE waves typically exhibit smaller amplitudes and shorter durations (depending, of course, on the damage stage of the specimen). Therefore, for the calibration used for this test bench (see ***Table 3-3.*** *Calibration parameter values for the field data test bench***Table 3-3**), the time-driven parameters and the threshold level have been shortened to increase the sensitivity of the methods (with regard to temporal and amplitude detection capabilities).

Table 3-3. Calibration parameter values for the field data test bench

Parameter	**Method**			
	IA	*STA LTA*	*AIC*	*CWT Otsu*
Fixed threshold level	2.25e-3	4e-3	6e-3	6e-3
Hit definition time [µs]	100		100	100
Hit lockout time [µs]	15		15	15
De-trigger threshold		3e-3		
STA window time [µs]		25		
LTA window time [µs]		10e3		
Pre-event time [µs]		1		
Post-event time [µs]		0.5		
Weighting-R constant			4	4
End delay window 1 [µs]			10	10
End delay window 2 [µs]			5	
Start delay window 1 [µs]				75
Start delay window 2 [µs]			20	
CWT scales				101
Greyscale image bit-depth				16
Median filter pixel neighbours				50

Once all of the methods have processed the field data frame, the quality of event detection is quantified in two steps. The first consists in quantifying the total number of detected events that each method concludes against the true locations of the 380 AE events. This step also inspects the sum of correctly detected events (true positive), the sum of undetected events (false negative) and the sum of the incorrectly detected events (false positive); see **Table 3-4**.

Table 3-4. Detected events with respect to 380 AE waves

Count	Method			
	IA	*STA/LTA*	*AIC*	*CWT Otsu*
Detected	373	380	372	372
True-positive	322	324	299	299
False-negative	58	56	81	81
False-positive	51	56	73	73

For this field data test bench, and only considering the total number of true positive events, the absolute errors for the onset, endpoint and duration are calculated (see **Table 3-5**).

Table 3-5. Absolute error and standard deviation for the onset, endpoint and duration detections with the field data test bench

Method	Onset time error (μs)	Endpoint time error (μs)	Duration time error (μs)
IA	-9.69 ± 7.56	38.39 ± 101.27	48.09 ± 102.13
STA/LTA	-2.49 ± 8.63	12.07 ± 83.65	14.56 ± 84.85
AIC	-6.15 ± 10.44	19.57 ± 543.74	50.4 ± 692.6
CWT-Otsu	2.53 ± 29.45	-92.36 ± 97.4	89.82 ± 97.74

Similar results are observed in the experimental scenario to those exhibited in the Hsu-Nielsen test bench. For the onset detection measure, all methods perform relatively well, showing in all cases error values of less than 10 μs, and with a difference among them of less than 7 μs.

For the endpoint detection measure, the results are also consistent with the Hsu-Nielsen test bench, with all methods showing poorer performance than for onset detection. Nevertheless, STA/LTA seems to be the most balanced technique, particularly when dispersion error values are also considered, yielding values that are approximately 25–85% lower than the dispersion generated by IA and AIC, respectively. As can be seen, this endpoint error value also directly affects the absolute duration time error.

The second step in this field data test bench consists in quantifying the quality of event detection achieved by each method. Using the number of detected events shown in Table 4, the following statistical metrics are calculated: (a) accuracy (the ratio of true positive events to all detected and undetected events), (b) precision (the ratio of true positive events to the

number of true and false positive events), (c) sensitivity (the ratio of true positive events to the sum of true positive and false negative detections, (d) f1-score (the harmonic average of precision and sensitivity), (e) false discovery rate (the ratio of false positive detections to all detected events), (f) false negative rate (the ratio of false negative detections to the sum of false negative and true positive events).

With regard to the statistical metrics, **Table 3-4** and **Figure 3-12** show that although, on average, all of the methods quantitatively detect nearly 99% of the total detection target (i.e., 380 AE events), the quality with which these detections are performed still differs from the target.

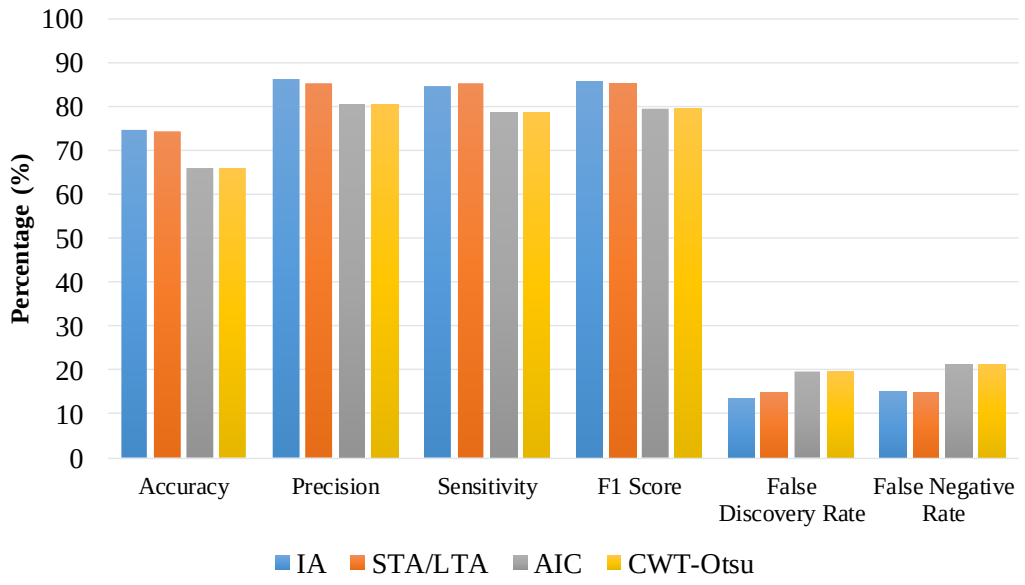

Figure 3-12. Statistical metrics corresponding to the quality of event detection in the data field test-bench.

Looking at the accuracy of the methods (i.e., the ratio of correctly detected events), although all of them perform reasonably well, with a lowest value of 66%, none achieves a value greater than 75%. STA/LTA and IA achieve accuracies nearly 10% greater than those of AIC and CWT-Otsu. This superior performance is consistent with the results obtained for the absolute endpoint error, since better determination of the event conclusion eventually raises the overall detection accuracy.

For the precision indicator (i.e., the ratio of correct positive detections) all methods perform better than for accuracy, achieving an average value of 83%. This improvement performance is due to the nature of the assay, in which there is a low proportion of false AE events (most of them derived from high-energy reflections and mechanical noises) relative to the number of true AE events in the analyzed data frame. Again, STA/STL and IA perform

approximately 5% better than the AIC and CWT-Otsu methods, since they do not detect the false positive events for more cases in the test bench.

With regard to the sensitivity metric (i.e., the ratio of correctly detected positive events), all methods show similar behavior to that observed for the precision metric, achieving nearly the same values. However, with the exception of STA/STL, performance decreases by about 2%, with a propensity for false negative detections, caused by low energy AE events and, predominantly, by misdetection of spliced AE waves.

For the F1 score, all methods achieved satisfactory results, due to the fact that only minor deviations were obtained between the sensitivity and precision metrics.

For the false discovery rate metric (i.e., the ratio of false alarm detections), all methods show reasonably low values, completing the ratios observed for the precision metric, with the lowest value of 20% obtained by the AIC and CWT-Otsu techniques.

For the false negative rate (i.e., the proportion of actual events which do not produce detections), all methods show tolerable values consistent with the results for the sensitivity metrics, with the lowest value of 22% scored by the AIC and CWT-Otsu techniques.

3.5 Discussion and conclusions

In this chapter it was observed that four critical characteristics influence the detection of AE events under the classical thresholding approach: bipolar onset activity, varying background noise, high dynamic signal range, and randomness in the incidence and duration of the events. The drawbacks and impacts of these characteristics have been discussed and analysed.

Also, four advanced AE detection methods representing the current state of the art were presented, and their performance quantified with AE data generated from standardised Hsu-Nielsen tests and for a standardised tensile test.

In general, all methods showed suitable capabilities for accurate onset detection, achieving absolute errors of less than 20 μs for the Hsu-Nielsen test and less than 10 μs for the tensile test.

By contrast, all methods exhibited low and nondeterministic performance for endpoint determination, yielding absolute errors of 2–18 ms for the Hsu-Nielsen test and 10–100 μs for the field data test bench. This lack of accuracy is due to the fact that all methods define the end of an event by means of the combination of a fixed threshold and a fixed timer instead of using an indicator extracted from the signal, which also critically increases the event duration error.

With regard to detection quality, none of the methods achieved an accuracy of more than 75%, with IA and STA/STL achieving scores approximately 10% higher than obtained with AIC and CWT-Otsu. For the precision and sensitivity metrics, due to the low proportion of false events in the test bench, all methods scored higher than for accuracy, achieving average scores of 83%. All methods were also found to be slightly more susceptible to false negative detection errors, most of them derived from spliced detections.

In general, statistical metrics are directly affected by the lack of accuracy of endpoint determination, and by four particular characteristics of the AE signal (i.e., duration, amplitude, appearance and noise floor).

In this study, AIC and CWT-Otsu are the best methods for accurate onset measurement. In particular, despite exhibiting significant error dispersions, CWT-Otsu improves onset measurement by approximately 90–95% with respect to all methods for the Hsu-Nielsen test and by 60 and 73% relative to AIC and IA, respectively, for the tensile test. Nevertheless, since these methods were conceived for AE event location applications, in which highly

accurate event arrival times are critical, their scopes must be carefully considered to only refine this onset detection.

For this study, IA and STA/LTA can be considered the most suitable techniques for fully automatic AE event detection application, having achieved the highest scores for quality of detection analysis. This high performance is strongly related to the use of characteristic functions that are more suitable for detection purposes, which are more responsive in the case of IA and more accurate in the case of STA/LTA.

STA/LTA stands out in this study as the most balanced option between low-error accuracy for onset and endpoint determinations and the quality of detection metrics.

Finally, it should be noted that, due to the stochastic nature of the AE phenomenon, there is no overall method capable of guaranteeing reliable detection across all different applications, materials and instrumentation. Thus, careful consideration must be given to selecting the most suitable detection method for the performing environment in question.

For the further development of this topic, two branches can be defined. First, additional analysis of the performance of existing methods (such as the specificity of the threshold levels) and further experimental scenarios (such as in-service applications). Second, toward achieving meaningful and reliable AE assessing applications through the proper separation of each wave, the necessity of development of novel strategies that can determine more accurately not only the onset of an AE event but the conclusion as well

Chapter 4. HIGHLY ACCURATE DETECTION OF AE EVENTS

4.1 Introduction

As aforementioned, in AE as an assessing damage tool, the processing chain is usually composed by the transduction and acquisition of the phenomenon and in the separation and analysis of each captured AE wave. Particularly, for the separation stage of AE events, due to the inherent features of the phenomenon, the resulting waveform from the acquired signal implies a very challenging task in which to be able to perform a proper identification and separation of each AE event; this mainly caused by exhibiting a highly varying background noise, a large difference of amplitudes between events, and a randomness on the incidence and lifespan of these AE events.

Efforts have been made in order to overcome the aforementioned limitations of the classical thresholding approach, and despite that the previously analyzed methods clearly represent a superior alternative to the classic thresholding technique, traditionally they have evolved in light of applications for locating AE sources, where a highly accurate onset detection is critical, so consequently, the issues related to the endpoint determination have been disregarded. Methodologically, this has implied that instead of considering, some intrinsic feature related the phenomenon, all the AE activity detection methods only make use of the combination of a threshold level along with a fixed timer in order to determine the conclusion of the AE event. Nevertheless, due to the stochastic manifestation of said events, this methodology leads to inaccuracies on the measurement of the endpoint determination, what directly affects to the quality of detection of all methods (i.e., the amount of properly detected AE events on a survey); being a critical aspect for assessing damage applications.

Evidently, Acoustic Emission is not the only discipline related to the Signal Detection Theory (SDT). Particularly in the speech processing discipline, SDT finds its application on the Voice Activity Detection (VAD) stage [94,95]; where a randomly present speech activity from a highly noisy digitized signal aims to be extracted in order to reduce the payload from the subsequent stages given a particular application (e.g., voice telecommunications, artificial intelligence, hearing aids among others). One of the best-established automatic VAD for the speech processing area is the technique developed by Rabiner and Sambur [96]. This

parameter-based VAD was originally designed with the objective to accurately detecting the beginning and the end of an utterance, while preserving an efficient and straightforward processing scheme as well as being robust against varying background noise. This was achieved with the use of two indicators of the signal: Zero-Crossing Rate (i.e., the rate at which the waveform changes from a positive to negative voltage and back), and the Short-Term Energy. Additionally, the algorithm was intrinsically capable of executing suitably in any realistic acoustic environment in which the signal-to-noise ratio (SNR) was in the order of 30dB. Despite of the dissimilar origins between Acoustic Emission and Speech phenomenon, and as in consequence the technical requirements in order to be processed (e.g., instrumentation, bandwidth —8kHz vs. 2MHz, etc.,), behaviors of their waveforms share similar characteristics, such is the case of a high variance on the occurrence of activity, rapid varying background noise and significant dynamic range.

In this chapter, an AE activity detector inspired by the VAD developed by Rabiner and Sambur [96] is presented. The detector is revised for an application related to the recording of a single channel from a continuous AE monitoring, derived of the characterization of a metallic component by means of an axial tensile test, where the AE waves derived from this assay typically exhibit a large difference of amplitudes between events, a stochastic occurrence and duration, and a highly varying mechanical background noise due to cumulative reflections.

In order to evaluate the performance of the presented STE-ZCR method, both experimental setups presented in Chapter 3 are used with aim to quantify the accuracy of the onset and endpoint determinations as well as for assessing the robustness of the method with regard to induced background noise; additionally with the same data stream obtained from a standardized tensile test in order to quantify the quality of detection of this method.

4.2 Methodology

The idea behind of a Short-Time or Short-Term Analysis (ST-ANLYS) relies on the stationarity of a time series, with aim of creating a new sequence that can represent some varying feature of the original. This is achieved starting from the fact that some signals (such is the case of an AE signal) intrinsically will not show a stationary behavior, that is, during their lifespans there will not be a clear tendency of repeatability on them (e.g., statistical mean and covariance). However, some other signals (again, an AE signal) when are enough and equally time segmented will show a relative slow variation (compared with the original time frame) for some property between segments, so these time segments (usually known as analysis frames) relate the analysis of the signal regarding a fixed size time window.

An activity detector exploits this artificially induced stationarity by identifying the relatively higher energy and smaller number of zero crossings that are associated with a performing phenomenon, contrary to an idle activity condition. Despite of the inherent uncertainties induced by a ST-ANLYS, it has proven to be an efficient tool with the aim of identifying the regions of activity of a signal.

For this work, the STE-ZCR method (see **Figure 4-1**), is composed at first of the generation of two characteristic functions by means of the ST-ANLYS of the Energy and the Zero Crossing Rate respectively of the acquired AE signal; and second, taking as inputs these pair of CFs', the detection of AE events performed by a dedicated algorithm.

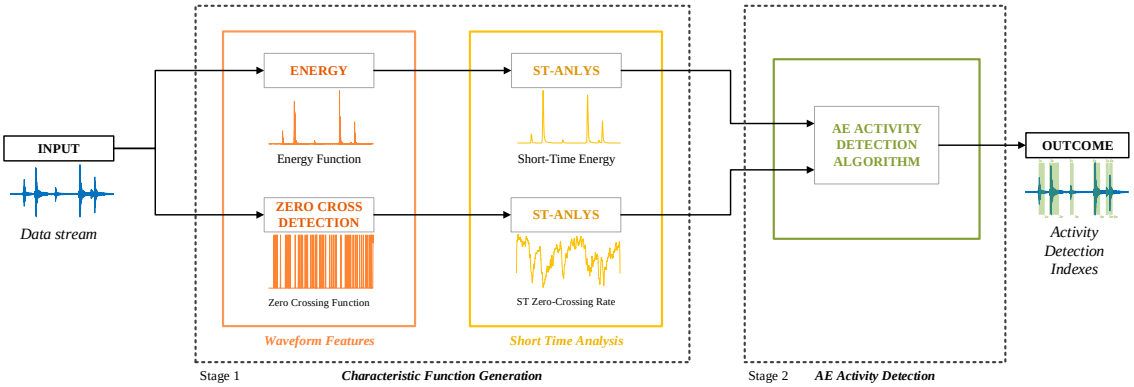

Figure 4-1. Block diagram for the STE-ZCR method. This is composed of two main stages: 1) Production of two CF by means of the ST-ANLYS framework, and an 2) Activity detection algorithm that searches for the onset and endpoint by means of the STE and the STZCR respectively. The outcome of this method is a set of a pair of indexes that mark the temporal star and end sampling points with regard to the input datastream for each detected AE event.

4.2.1 Stage 1. Generation of Characteristic Function: Short-time analysis framework

In the following sub-sections are established the required theoretical framework in order to implement the AE detector.

4.2.1.1 Short-Time Energy

As is known, the energy E of a discrete-time signal of length L from a point of view of signal processing can be expressed as $\sum_{m=0}^{L}|x(m)|^2$. For this framework, the short-time energy of the signal is defined as:

$$E_{\hat{n}} = \sum_{m=\hat{n}-N+1}^{\hat{n}} |x(m)|^2 \, w(\hat{n}-m) \qquad (1)$$

where $w(\hat{n}-m)$ is a window function of N width, centered at sample $\hat{n}$, and where $\hat{n}$ in turn indicates the overlapping factor between windows through the relation $\hat{n} = kT$, with $k = 0, 1, \ldots$, and $T < N \leq L$.

For this AE activity detection application, the association of $E_{\hat{n}}$ lies in provide a measure to separating the presence of AE waves from idle activity on the acquired sequence, since values of $E_{\hat{n}}$ for an AE wave are considerably greater than noise floor energy. It is important to note that under this scheme there are three different parameters to configure for the short time energy approach:

a) *Window function.* As is well known, this type of functions typically must meet some requirements in order to be considered suitable for the processing of the signal (i.e., smoothness, non-negative terms, compact support, square integrable resultant products). The resulting waveform from the analysis will strongly depend on the choice of the window function, and since there is not exists an optimal overall option, selection must entirely rely on the scope of the application in which the analysis will perform (e.g., spectral, statistics, etc.,) and therefore on the pursued feature to highlight. For applications related with analysis of transients (like an activity detector), where the objective is to accurately concentrate the energy of the signal in the time domain taking advantage of the low-pass filtering nature of the ST-ANLYS at expense of diminishing the bandwidth of the resulting signal, typical windows include rectangular and raised cosine categories.

b) *Window length.* Ideal response of any CF is to depict a feature of interest at a rate comparable of the original signal; the resulting signal by means of a ST-ANLYS will

inherently contain uncertainties on the temporal relocations of the analyzed feature, still, these can be significantly reduced through a proper choice on the length of the window. As in the case of the window function, the length of the window relies entirely on the application, there is not ideal generic value, thus it is necessary to take considerations about of the tradeoffs on the responsiveness in the selection of the window length with regard of the expected lifespan of an AE wave in function of the material under analysis:

i. Small length, uncertainties due to a small amount of data. Although is desirable to have a CF function that rapidly responds to abrupt changes of the signal under analysis, a too short window will not reveal any stationarity derived of the ST-ANLYS.

ii. Medium length, uncertainties due to loss of rapid transients. While a conservative value for the analysis will provide a superior depiction about of the stationarity of the signal (aside from discarding fast mechanical noises), this will not accurately resolve the rapid transitions between a pair (or more) of too near AE waves (also known as cascaded hits).

iii. Extended length, uncertainties due to significant amount of exclusions of signal changes. Even if what is sought as result of the ST-ANLYS is to obtaining a smooth CF capable to easily portrait the tendency of the analyzed signal (this achieved through increasing the length of the window size), an excessively wide window will suppress the dynamics of the signal making difficult to identify sharp changes.

c) *Window overlapping factor.* Once that the type and the length of the window have been selected, the last step of the ST-ANLYS is to slide the window over the analyzed signal in order to reveal the stationarity of the signal. For applications where the extracted ST-ANLYS between subsequent samples may not be required since the variation of the feature is relatively slow, the shift can be kept larger than one sample. Under this overlapped scheme, the computational load of the analysis can be largely reduced (this is particularly useful when long duration signals are under evaluation); typical overlapping values are in the range of 50 to 75% of the window length. Still, since overlapping implies to downsampling the resulting signal by a T factor in **(1)**, for applications where a highly temporal accuracy on redistributing a feature is required, is desirable to keep the sample shift as minimum as possible.

4.2.1.2 Short-Time Zero Crossing Rate

The zero-crossing point for an alternating electrical signal is the instantaneous time value when voltage equals to zero. Since the point of view of the discrete-time signal processing, a

zero-crossing point occurs where two adjacent sampling points on the sequence have different mathematical signs (i.e., having opposite polarities). The ratio count of zero crossings over a unit of time is a quite basic but still effective measure of approximating the spectral content of the signal. The short-time zero-crossings rate per sample in this work is defined as:

$$Z_{\hat{n}} = \frac{1}{2N} \sum_{m=\hat{n}-N+1}^{\hat{n}} |sgn(x[m]) - sgn(x[m-1])|\, w(\hat{n}-m) \quad \textbf{(2)}$$

where $w(\hat{n}-m)$ is the chosen window function, N is the length of said window centered at sample $\hat{n}$, and also indicating the overlapping factor between windows through the relation $\hat{n} = kT$, with $k = 0, 1, \ldots$, and $T < N \leq L$. Finally, sgn denotes the signum operator defined as:

$$sgn(x[n]) = \begin{cases} 1, & x[n] \geq 0 \\ -1, & x[n] < 0 \end{cases} \quad \textbf{(3)}$$

Still, is possible to express the ZCR normalized for an interval of M-samples, whence ZCR becomes:

$$Z_M = MZ_{\hat{n}} \quad \textbf{(4)}$$

and where an interval of τ seconds corresponding to M-samples is:

$$M = \tau F_s \quad \textbf{(5)}$$

As in the case of the STE, in order to obtain a proper description of the STZCR it is necessary to make the same considerations about of the type, length and the overlap shifting of the window with regard to the required application. Additionally, there are further practical considerations to make (by means of a filtering scheme) before applying the analysis, since ZCR is heavily biased by DC offset of the analog-to-digital conversion, the 50/60 Hz mains hum and low frequency mechanical background noises.

4.2.2 Stage 2. AE event detection algorithm

Once that both CF's (STE and ZCR) are obtained, the second stage of the STE-ZCR method is to find the pairs onset/endpoint for the AE events on the sequence. For this, using the fact that the waveform derived from an AE event will exhibit higher energy and lesser ZCR count, it is possible to set up the basis to implement an algorithm that can detect AE events on a straightforward but yet efficient scheme (see **Figure 4-2**).

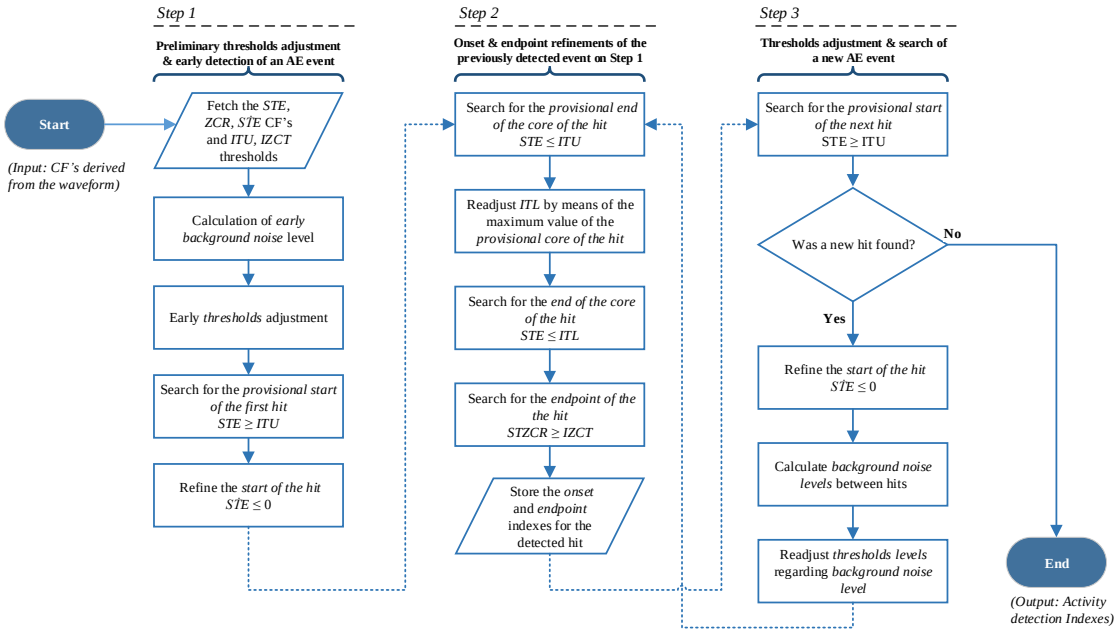

Figure 4-2. Flowchart for the activity detection algorithm composed of three main steps. *1)* Preliminary calculation of background noise for an idle state of the signal, *2)* Search job for the onset and endpoint of a hit, 3) Threshold level adaptation regarding to the updated background noise. Reader is also referred to **Figure 4-3** for a visual instance of the CF's and threshold levels used by the algorithm.

The algorithm makes use of two different fixed threshold values for its operation, the *Identification Upper Threshold* (ITU) that works on the STE signal in order to detect new AE events and the *Identification Zero Crossing Threshold* (IZCT) that works on the STZCR with the aim of determining the endpoint for a detected AE event. Thus, a previous characterization of the instrumentation with regard to the surveyed material is highly recommended to characterize the background noise level and the amplitude of the electrical waveform of the monitored AE channel, in order to carry out a proper calibration of said threshold parameters. In addition to the CF's generated by means of the ST-ANLYS, the algorithm makes use of the derivative of the STE with the aim of refining the onset determination of the AE event. Finally, with the purpose to enhance the quality detection, a basic adaptive threshold scheme is implemented by continuously taking measurements of background noise and adjusting the threshold levels between search jobs iterations.

The search work initiates with an estimation of the *STE early background noise level* for a small segment of the sequence, and belonging to the beginning of said sequence (where is assumed that there is not exists any AE hit yet). This is achieved by means of the sum of the arithmetic mean $\bar{x}_{STE}$ and the α-weighted factor for the standard deviation σ_{STE} of the STE signal, (this α factor can be estimated along with the previous calibration for the thresholds, if a heavy background noise is expected the value for this weighting value must be incremented). In

order to perform the first threshold adaptation, the *early background noise level* is added to the preset *Identification Upper Threshold* (*ITU*), expressed in levels of energy (v^2.s) $ITU_{adjust} = ITU + (\bar{x}_{STE} + \alpha * \sigma_{STE})$.

For the calculation of the *STZCR early background noise level*, the same calculations that for the STE case are performed, now over the same segment length belonging to the STZCR sequence. Thus, the resulting *adjusted Identification Zero Crossing Threshold* will be: $IZCT_{adjust} = IZCT + (\bar{x}_{STZCR} + \alpha * \sigma_{STZCR})$, expressed in normalized ST-ZCR of the signal, for a length window of M samples ($\widehat{STZCR}$). Additionally, for this parameter and for a simpler threshold presetting, it is also possible to handle the *IZCT* threshold value as a percentage of the computed *early background noise level*.

After both parameters ($IZCT_{adjust}$ and ITU_{adjust}) are computed, the next step is to find the first sample $n_{Prov-onset}$ in the *STE* sequence where: $STE[n] \geq ITU_{adjust}$. This $STE[n_{onset}]$ sample will be the *provisional onset hit*.

The last task for this first stage comprises the refinement of the onset detection of the hit by means of the first derivative of the *STE* sequence ($\dot{STE}$). The purpose on the use of this signal is to take advantage of the sensitivity to the energetic change that the STE provides, by finding the first incidence of the energetic variation of the captured AE phenomenon. Thus, it is possible to assume that in this sample the arrival of p-waves is manifested. For this is carried out a backward search from the corresponding $\dot{STE}$ sample of the *provisional onset hit* sample until finding the $n_{true-Onset}$ sample where $\dot{STE}[n_{true-onset}] \leq 0$. This sample is indexed as the *true onset hit detection*, and will be the first outcome of the onset-endpoint pair of indexes.

The first task for the second stage of the algorithm consists in finding the *core of the hit*. Since in this region most of the AE wave energy is concentrated, it is necessary to delimit it accurately with the aim of aid to find the lifespan of the hit. For this step, the first subtask requires to find the *provisional end of the core of the hit* $n_{provEoC}$, this can be picked up readily by locating the first sample from the *provisional onset hit* sample where $STE[n] < ITU$.

Next, for the search work of the *end of the core of the hit*, it is required to find the maximum value $STE_{max-core}$ regarding to the provisional core of the hit (i.e., the range between *STE*[*provisional onset hit*] and *STE*[*provisional end of the core of the hit*]), to then readjust the *Identification Lower Threshold* (*ITL*) expressed in levels of energy (v^2.s). For this, it is necessary

to start from the fact that for the Acoustic Emission discipline one of the most accepted models [65,97–103] of an electrically transduced AE wave, considers to the wave as an underdamped sinusoidal function with the form:

$$u(t) = \begin{cases} A\,exp\left(\frac{-t-T}{\gamma}\right) sin\,2\pi v_0(t-T)\,, & t \geq T \\ 0, & t < T \end{cases} \quad \textbf{(6)}$$

Where A is the amplitude and T is the arrival time of the AE wave; and γ and v_0 the decay constant and the resonant frequency both belonging to the sensor. Therefore, the envelope of the wave of **(6)** can be expressed as:

$$e(t) = Ke^{-v_0 t}, \qquad t \geq T \quad \textbf{(7)}$$

Is evident that this simple exponential decay model can be enhanced, still, for the application of this work it is only required to identify that the STE CF corresponding to an AE wave behaves as an impulse response function of a linear-time-invariant dynamical system of first order. As is well known, the time constant τ that characterizes the response of the system and its bandwidth for a system like in **(7)**, it is located at the instant of time t_τ where $e(t_\tau)$ equals to 36.8% of its maximum value. Therefore, taking advantage of this fact, it is possible to assume that the core of an AE wave will expire when the STE equals to the 36.8% of its maximum value. Hence, the value for the *ITL* threshold will be adjusted to $ITL = 0.368STE_{max-core}$ to then perform a forward search from $STE[n_{max-core}]$ until find the n_τ sample where $STE[n] \leq ITL$. This n_τ sample will be the *end of the core of the hit*. While it is true that after the *end of the core of the hit* most of the energy of the AE wave is nearly vanished, the region between of this *STE* endpoint detection and the one that will be determined through the *STZCR* CF still will comprise a relevant content of energy. Thus, the joint use of these pair of CF's will provide a more robust and precise approach for determining the end of the lifespan of an AE wave. For this, a simple search forward work over the *STZCR* sequence will be performed from the n_τ sample (related with the *end of the core of the hit*) until finding the $n_{endpoint}$ sample where $STZCR[n] \geq IZCT_{adjust}$. This sample will be indexed as the *true endpoint of the hit*. With these two indexes as outcome (*true onset hit detection* and *true endpoint of the hit*) concludes the work for the second stage of the algorithm and the third and last part of this will be executed. Searching for this a new hit over the *STE* sequence, and using the last adjusted value of the *ITU* threshold from the *true endpoint of the hit* sample. Once detected, a refinement of the onset detection will be performed.

Next, an update of the noise levels over their corresponding CF's will be performed (from the last *true endpoint of the hit* to the new *true onset hit detection*), to then readjusting of the *ITU* and *IZCT* thresholds values. However, with the purpose to avoid an overlap of AE events, if a new hit were detected before the *true endpoint of the hit* sample (obtained by means of the STZCR CF), the *true endpoint of the hit* must be readjusted to one sample before of the *true onset hit detection*. Finally, the second stage of the algorithm will be performed again and the iteration repeated until all events of the sequence under analysis are detected.

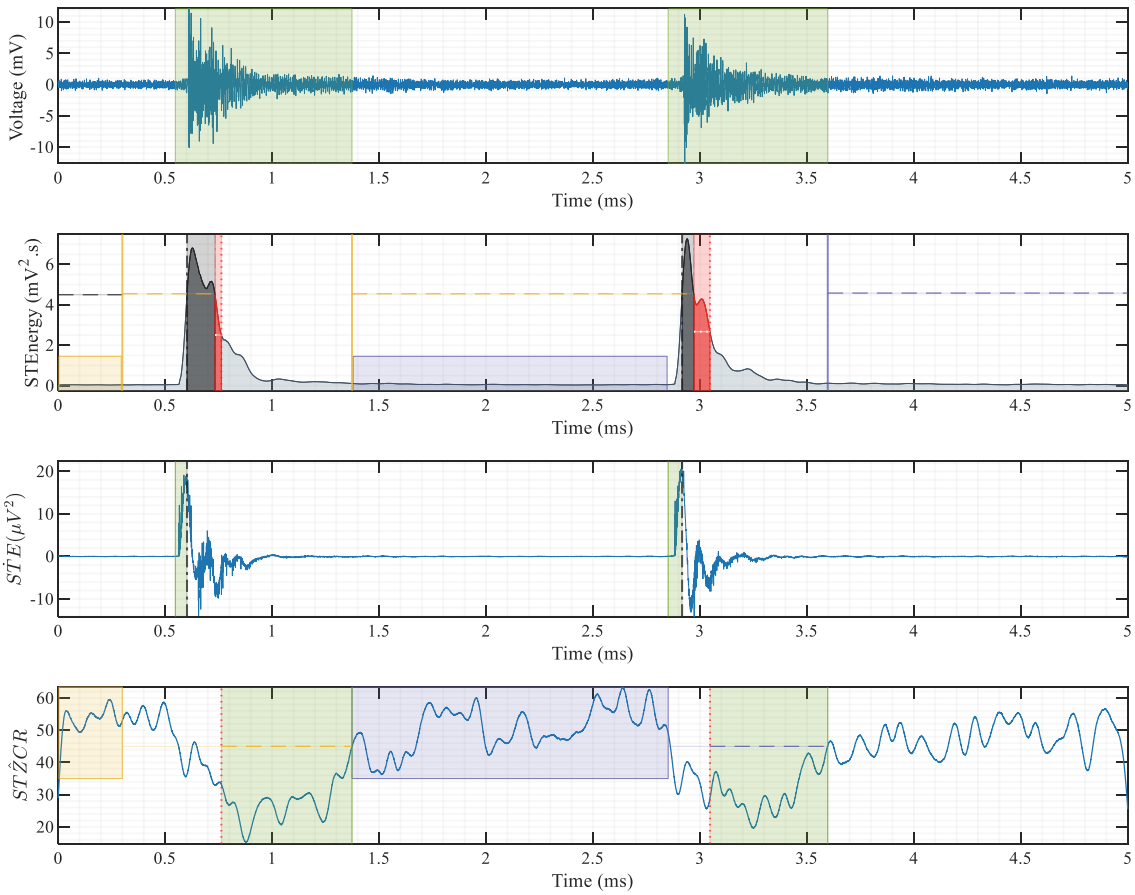

Figure 4-3. Depiction of the STE-ZCR detection method for a data 5ms frame. **(a)** Two AE events and their corresponding lifespans detected by the AE activity detector (green shaded areas). **(b)** Onset detection work. Short-time energy CF (blue-steel area under the curve), preset threshold level (horizontal dotted black line), signal segment for the early background noise calculation (yellow shaded area), first adjusted threshold (horizontal dotted yellow line) and sample of activation (vertical solid yellow line), signal segment for the second background noise calculation (lilac shaded area), second adjusted threshold (horizontal dotted lilac line) and sample of activation (vertical solid lilac line). Provisional core of the hit (gray shaded areas), Identification Lower Threshold (horizontal dotted white line), signal segment for the end of the core search job (red shaded areas). The core of the hit for each AE event is composed by the gray and red shaded areas respectively. **(c)** Refinement work for the onset detection. Backward search job from the start of the core sample (vertical dash-dotted black line) through the derivative of the STE-CF (blue solid curve). Onset time samples (vertical solid green lines). **(d)** Endpoint determination work. Short-time ZCR CF (blue solid curve), signal segment for the early background noise calculation (yellow shaded area), samples of activation end of the core of the hit (vertical dotted red lines), first adjusted threshold (horizontal dotted yellow line), signal segment for the second background noise calculation (lilac shaded area), second adjusted threshold (horizontal dotted lilac line), endpoint determination samples (vertical solid green lines).

4.3 Experimental procedures

The same experimental scenarios used to survey the performance of the advanced AE event detection methods presented in Chapter 3, are used in order to assess the performance of the proposed method.

The test benches as well as the considered methods are implemented using software scripts executed by MATLAB® R2018a in a PC with a CPU Intel Core i7-6800k (3.4GHz) and 64GB of DDR-2400 RAM.

4.3.1 Artificial source test-bench

For the Pencil-lead breakage (PLB) test-bench, and for each of the one-hundred realizations, a graphite lead of ⌀ 0.5mm, 2.5 mm tip-length and with a contact angle to the surface of the specimen of 60° is used. In addition, a distance of 12cm between source and sensor is preserved (see **Figure 4-4**).

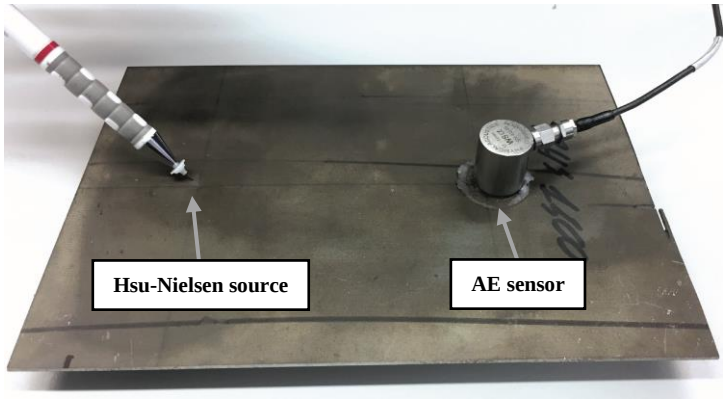

Figure 4-4. Photograph of the AE sensor, the guide-ring tube used to generate the artificial sources and the steel plate (stood over a foam base).

For a frequency range of up to 1MHz, the average phase velocity for the extensional mode is of 5194m/s and for the group velocity case is about of 4471m/s. In **Figure 4-5**, it is shown the characterization of the used sheet specimen by means of its dispersion relation of the fundamental Lamb wave modes (obtained using the Wavescope software [104]). With this information, and considering the operative frequency of the used sensor, the source-sensor layout shown in **Figure 3-8** and assuming an ideal isotropy in the material, it is possible to neglect the effect of the change of velocity for this experiment.

For repeatability purposes, each synthetic AE wave is edited so its peak value is centered on 5ms and the signal be extended during 40ms more, as a result each AE wave from the data set collection will exhibit an average lifespan of 20.86 ± 1.16ms.

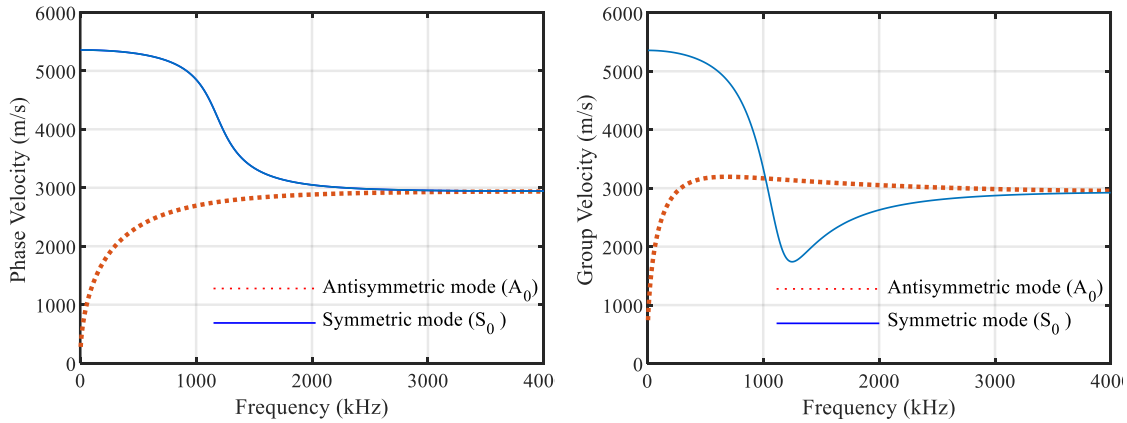

Figure 4-5. Fundamental dispersion curves of the Press-Hardening 1500 steel sheet. Thickness of 2mm, Young's modulus of 211GPa, density of 7850kg/m3, Poisson's ratio of 0.3 and shear modulus of 83GPa. **(a)** Phase velocities. **(b)** Group velocities.

4.3.1.1 Operational robustness in front of background noise

Second objective for this test-bench consists of evaluating the operational robustness of the method in front of background noise. For this, since each AE wave from the data set collection exhibits an average Signal-to-noise ratio (SNR) of 27.1 ± 1.15dB, their corresponding SNR will be decreased by means of AWG noise in three different rounds of analysis of 20, 15 and 10 dB respectively (see **Fig 7**).

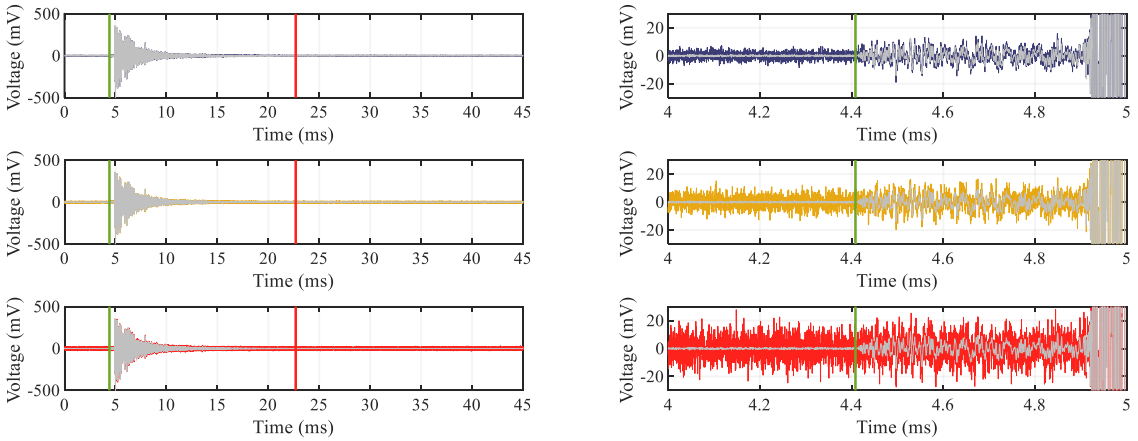

Figure 4-6. Example of an AE wave used for the evaluation of operational robustness against noise. Onset and endpoint locations (green and red lines respectively). In the test, a synthetic AE signal (gray) is tainted by AWGN in order to obtain three different signals with levels of SNR of: **(a)** 20dB (lilac), **(b)** 15dB (yellow), **(c)** 10dB (red). Images of the right column show a 1ms zoom of the corresponding data frame for the wave onset.

4.3.2 Uniaxial tensile test

The objective for the second test-bench is to quantify the quality of event detection by means of statistical indicators in front of field data. For this, a tensile test of a metallic component is carried out (see **Figure 4-7**).

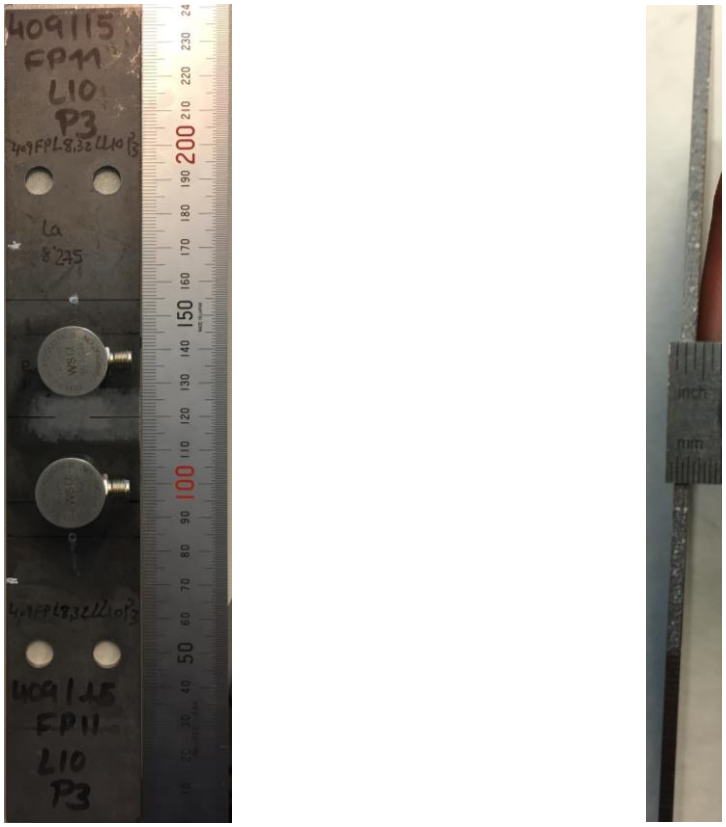

Figure 4-7. Photograph of the Ferrite-Pearlite annealing steel sheet specimen, used in the test-bench. Dimensions 55mm x 240mm x 2mm.

Even though a pair of identical sensors were attached during the assay, for this test-bench, only the signal of the main sensor will be analyzed.

As in the case of the Hsu-Nielsen experimental scenario, when is assumed an ideal isotropy in the material, the characteristic average extensional mode wave velocities (~5104m/s for the phase and ~4348m/s for the group **Fig. 9**) and considering the operative frequencies range of the sensor (and its location over the specimen, **Figure 3-10**), it is possible to neglect the effect of the change of velocity for this experiment. The AE signal produced by the tensile test was collected; and for the experimental scenario a frame length of 500ms that contains 380 AE events is used as the input for each detection method (see **Figure 3-11**). For each of said AE events, their onset and endpoint locations are manually picked supported by the frame waveform and its corresponding time-frequency distribution.

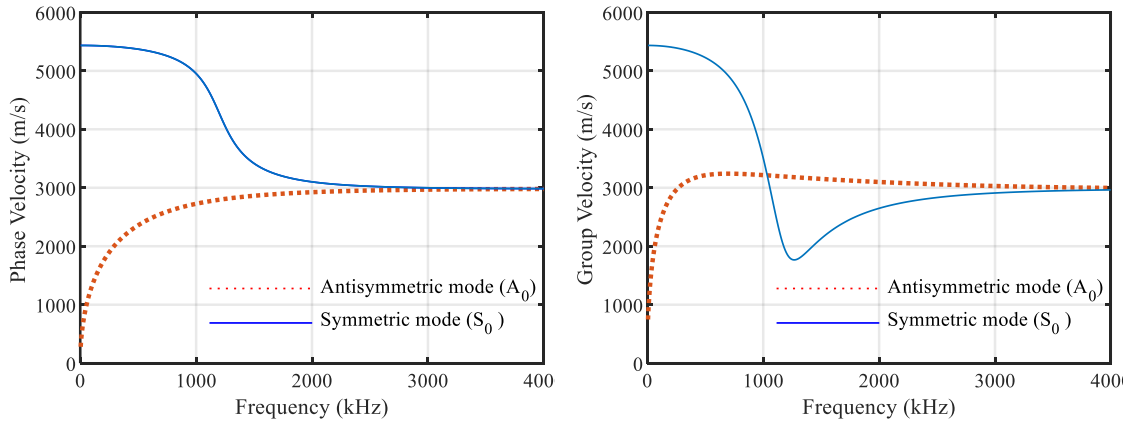

Figure 4-8. Fundamental dispersion curves of the Ferrite-Pearlite annealing steel sheet with a thickness of 2mm, Young's modulus of 205GPa, density of 7850kg/m3, Poisson's ratio of 0.3 and shear modulus of 83GPa. a) Phase velocities. b) Group velocities.

4.4 Evaluation results

The competency of the STE-ZCR method was analyzed in front of two different experimental scenarios. Additionally, its performance is compared against four different representative AE detection techniques: (a) a classical threshold detector enhanced by means of the Instantaneous Amplitude envelope [50], (b) a STA/LTA detector [82], (c) a two-step Akaike Information Criterion picker [51], (d) and an Otsu detector working over a binary map image based on the Continuous Wavelet Transform [52], (which alike (c) uses the same waveform derived from the Allen's Formula as CF for the threshold-based early coarse detection).

4.4.1 Artificial source data test-bench. Accuracy of the onset and endpoint determinations

As aforementioned, the objective for this test-bench is firstly to quantify the accuracy of the measurement for the onset, endpoint and lifespans by means of the absolute error of each measure, and secondly to evaluate the operational robustness of detection in front of background noise.

For the calibration of the STE-ZCR method with regard to the corresponding temporal window analysis (type, length and overlapping factor), after a series of exhaustive trials, it was determined that one of the window functions that accomplished higher accuracy results was the Hamming implementation (in general those belonging to the raised cosine family). For the window overlapping factor, at expense of increasing the computational load, the best accuracy was achieved by maintaining the window overlapping to one sample, (i.e., by directly convolving the instantaneous energy and the window function). Finally, the choice of the duration values of the window time, the threshold levels and the weighting factor for the noise analysis will be entirely determined by a prior calibration of the employed instrumentation as well as by the mechanical properties of the material.

The calibration values of the comparative methods (see **Table 4-1**), was carried out following the recommendations of the related literature [51,83–87] as well as the current standards [45,46,88–92]) of the AE discipline.

Table 4-1. Calibration parameters values used for each method for the artificial data test-bench.

Parameter	Method				
	IA	*STA LTA*	*AIC*	*CWT Otsu*	*STE ZCR*
Fixed threshold level	3e-3	5e-4	2e-1	2e-1	2e-4
Hit Definition Time [µs]	1e3		100	100	
Hit Lockout Time [µs]	10e3		10e3	10e3	
Threshold de-trigger		9e-5			
STA window time [µs]		75			
LTA window time [µs]		1e6			
Pre-event time [µs]		15			
Post-event time [µs]		10e3			
Weighting-R constant			4	4	
End delay time window 1 [µs]			25	25	
End delay time window 2 [µs]			10		
Start delay time window 1 [µs]				1.5e3	
Start delay time window 2 [µs]			100		
CWT scales				101	
Grayscale image bit-depth				16	
Median filter pixel neighbours				50	
STA length [µs]					20
STA window					Hamming
Overlapping window samples					1
ZCR threshold [%]					70
α-weighting STD noise					4
Early noise analysis [µs]					2e3

In **Figure 4-9** an instance of the manual onset pick procedure for an AE event is depicted. This is carried out by identifying the time instant when the bi-dimensional manifold created by means of the contour mapping of the SSWT becomes closed by connecting all the modal frequencies of the signal.

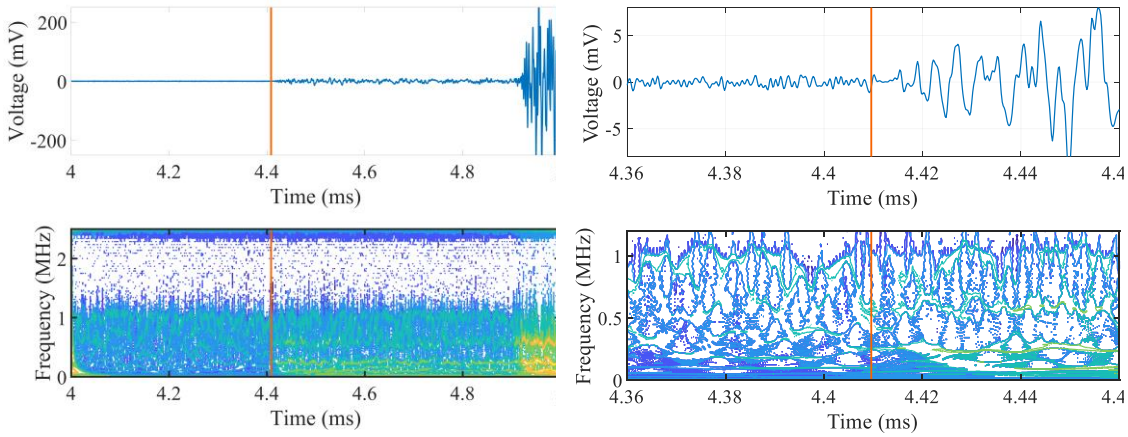

Figure 4-9. Time-voltage and Time-Frequency representations corresponding to the onset of the synthetic AE wave showed in **Figure 3-9**. **(a)** Data frame of 1ms displaying the onset location (at 4.4084ms, vertical orange line) of the AE wave, and showing the energetic activity of the modal frequencies after the signal arrival in the TFR. **(b)** Zoom of 100µs of the data frame depicting the appearance in the TFR of the most energetic continuous ridge (located at 263.12kHz), that indicates the onset of the AE wave.

In **Figure 4-10** and **Figure 4-11**, the resulting onset and endpoint automatic procedures for each method are depicted, using in all cases the same AE signal (and which corresponds to **Figure 3-9)**.

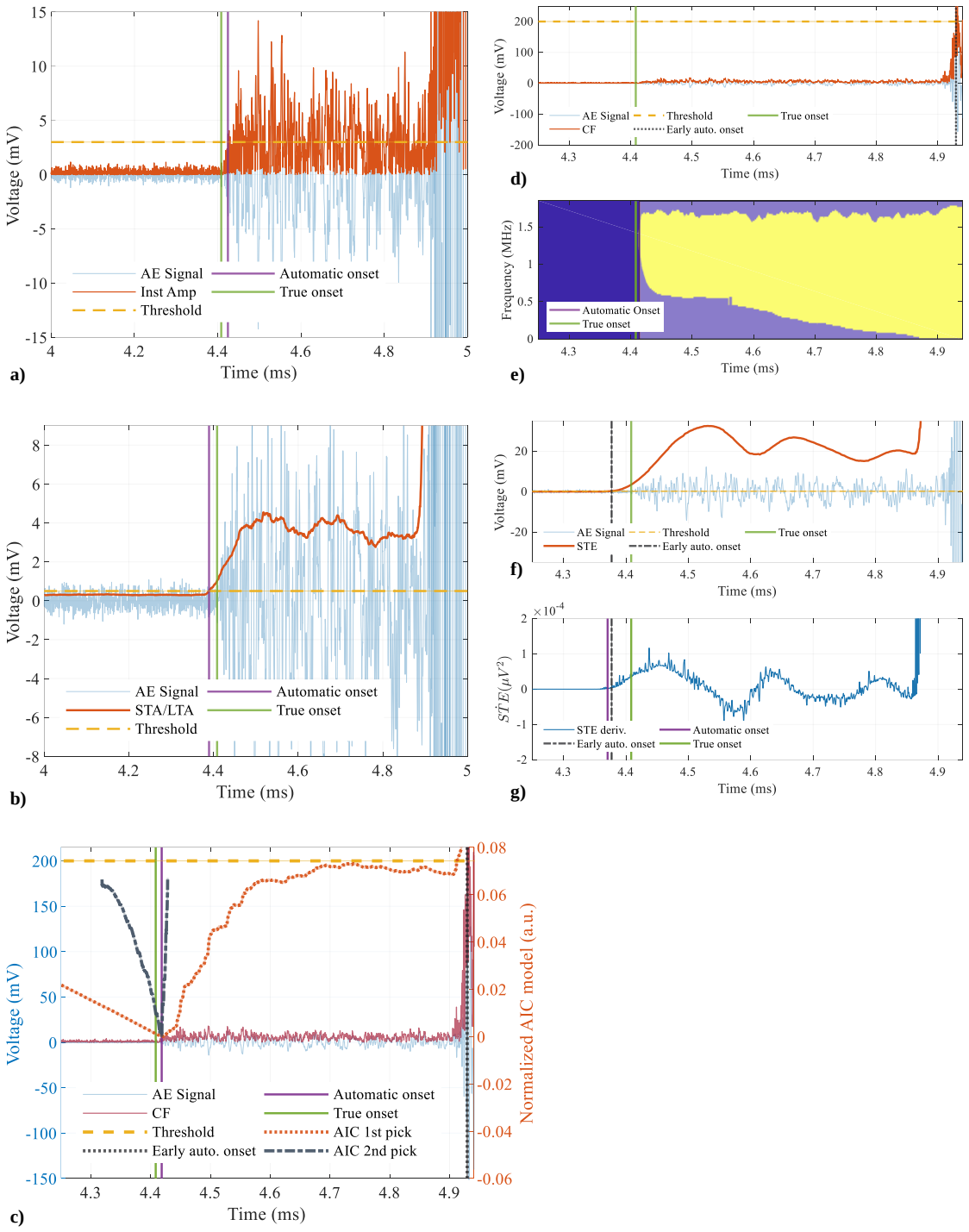

Figure 4-10. Automatic onset detection procedure of the AE wave, corresponding to the methods. **(a)** Instantaneous amplitude, **(b)** STA/STL, **(c)** two-step AIC, **(d)** CWT-Otsu (early detection), **(e)** CWT-Otsu (detection refinement), **(f)** Short-Time Energy (early detection), **(g)** Short-Time Energy derivative (detection refinement). The onset absolute error corresponding to each method is calculated with regard to the manual True onset pick of the AE wave (vertical green solid line located at 4.4084ms for this instance), and the Automatic onset pick (vertical lilac solid line) that each method identifies.

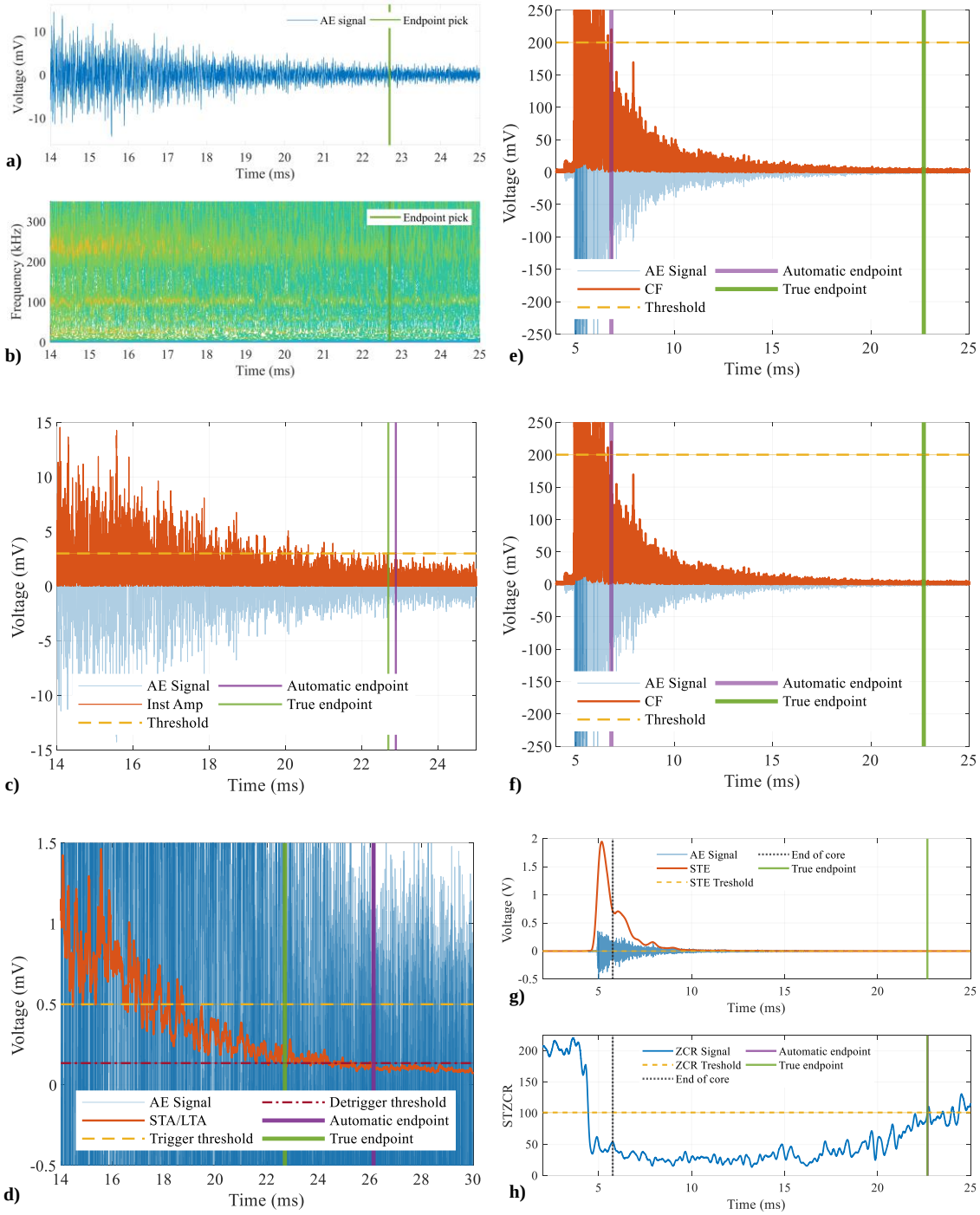

Figure 4-11. Manual endpoint pick (vertical green solid line located at 22.6973ms for this instance), and detected when the bi-dimensional manifold created by means of the most energetic ridges of the SSWT is vanished. **(a)** Time-Voltage, **(b)** Time-Frequency. Automatic endpoint detection procedures of the AE wave corresponding to the methods: **(c)** Instantaneous amplitude, **(d)** STA/STL, **(e)** two-step AIC, **(f)** CWT-Otsu, **(g)** Short-Time Energy (early endpoint detection) and **(g)** Zero-Crossing Rate (detection refinement). The endpoint absolute error corresponding to each method is calculated with regard to the true endpoint of the AE wave.

For the onset determination, in **Figure 4-10** can be observed that due to the significant difference between the amplitudes of the primary wave (4.4 - 4.9ms) and the secondary wave (from 4.9ms on) regarding to the AE artificial source, all methods deal with a challenging signal to accurately determine its onset time. This condition forces to lower down the threshold level as minimum as possible for the IA and the STA/LTA methods (increasing the chances to false-positive detections due to noise floor). For the AIC and CWT-Otsu methods, since they perform an onset refinement detection procedure, they allow to maintain a higher threshold level for the early threshold detection (with the aim of avoiding false-positive detections). In the same way, the proposed method through its onset refinement measure by means of the derivative of the STE, also allows to maintaining a higher threshold level in order to avoid trigger false-positive detections.

For the endpoint detection case, **Figure 4-11 (h)** shows that with the Zero-Crossing-Rate procedure although in order to be operative still makes use of a threshold value parameter, this measure provides a reliable indicator with which determine the conclusion of the signal. In contrast, **Figure 4-11** it also shows that the other methods by making use of a combination of a threshold level along with preset fixed timers entail to a lack of accuracy to the estimation of the end of the signal.

In **Table 4-2** the accuracy of the onset, endpoint and lifespan of the analyzed methods are quantified by means of the absolute error (from the outcomes of the analyzed methods with regard to the manually picked instants of time). In **Table 4-2,** it is also showed the accuracy results for the operational robustness in front of three induced levels of background noise on the dataset. Finally, the average required consumed time in order to process an AE event belonging to the dataset are also displayed.

For the onset detection measure, the results indicate that all methods perform relatively well, accomplishing errors less than 20μs. However, the CWT-Otsu is the method that achieved the higher accuracy, obtaining an average error of only 1.19μs, yet at expense of displaying the worst dispersion of the considered methods For the STE-ZCR case, it reached the second best results, and also can be observed that the STE-ZCR technique tend to detect the AE event before of its arrival, contrasting with the rest of the methods which are likely to determine the onset time after of the actual start of the event.

Table 4-2. Absolute error and standard deviation of the onset, endpoint and lifespan detections in regard with the Hsu-Nielsen test-bench.

Method	Onset error (µs)	Endpoint error (µs)	Lifespan error (µs)	Processing time (s)
LA (original signal)	-21.83 ± 8.26	2454 ± 1120	2476 ± 1120	2.53 ± 0.34
LA (SNR 20dB)	4271 ± 110.3	-20683 ± 1211	-24955 ± 1197	19.30 ± 2.32
LA (SNR 15dB)	4271 ± 110.4	-20504 ± 1273	-24776 ± 1263	22.94 ± 1.03
LA (SNR 10dB)	4271 ± 110.4	-20104 ± 1275	-24376 ± 1268	25.98 ± 1.59
STA/LTA (original signal)	-19.82 ± 7.92	3828 ± 1159	3848 ± 1161	1.56 ± 0.12
STA/LTA (SNR 20dB)	27.22 ± 185.44	3875 ± 1071	3848 ± 1161	1.58 ± 0.34
STA/LTA (SNR 15dB)	4256 ± 110.88	8104 ± 1174	3848 ± 1161	1.56 ± 0.11
STA/LTA (SNR 10dB)	4272 ± 110.39	8131 ± 1195	3902 ± 1197	1.60 ± 0.09
AIC (original signal)	-13.34 ± 7.00	16338 ± 1045	16352 ± 1045	2.98 ± 0.14
AIC (SNR 20dB)	-515.18 ± 7.31	18825 ± 1126	19340 ± 1126	3.09 ± 0.16
AIC (SNR 15dB)	-517.02 ± 6.96	18661 ± 1100	19178 ± 1100	3.24 ± 0.21
AIC (SNR 10dB)	2121 ± 2066	21959 ± 3108	19838 ± 1152	6.60 ± 9.92
CWT-Otsu (original signal)	-1.19 ± 97.88	17795 ± 1047	17796 ± 1039	1.57 ± 0.12
CWT-Otsu (SNR 20dB)	369.29 ± 582.2	18881 ± 1119	18447 ± 1301	1.67 ± 0.14
CWT-Otsu (SNR 15dB)	320.00 ± 647.9	18656 ± 1092	18336 ± 1309	1.85 ± 0.17
CWT-Otsu (SNR 10dB)	2425 ± 1892	21632 ± 3274	19207 ± 1763	4.52 ± 1.55
STE-ZCR (original signal)	3.29 ± 13.40	-0.63 ± 1797	3.31 ± 1800	0.013 ± 0.001
STE-ZCR (SNR 20dB)	-29.36 ± 12.13	9560 ± 2142	9589 ± 2145	0.029 ± 0.009
STE-ZCR (SNR 15dB)	-22.90 ± 193.7	11510 ± 4459	11533 ± 4467	0.027 ± 0.011
STE-ZCR (SNR 10dB)	236.5 ± 873.66	12986 ± 5788	12749 ± 5263	0.024 ± 0.009

For the endpoint detection case, results reveal that none of the comparative methods achieves a reliable measurement, yielding to absolute errors about two and four orders of magnitude with regard to the onset detection procedure. As observed in **Figure 4-11**, this lack of accuracy owes that all methods make use of the combination of threshold levels along with preset fixed timers (i.e., HDT, HLT, etc.), without considering the actual behavior of the signal. As consequence, these inaccuracies for the endpoint detection directly lead to errors to the lifespan determination. Differently, and despite of producing the result with higher dispersion and still depending on a calibration parameter, the STE-ZCR method achieved the best accuracy by considering an intrinsic indicator of the waveform.

For the results regarding to the average consumed time to process each AE event, it can be observed that the most expensive technique corresponds to the two-step AIC, since it involves the refinement of the onset measure in two sequential instances (having to modelling the signal in two occasions as consequence). For the IA technique, despite of performing the most basic approach of the considered methods, it achieved the second poorest performance on the test-bench, owing to that it is computationally expensive the searching-and-resetting scheme required to determine the endpoint time over a CF, which

exhibits a pronounced amount of rippling. The most balanced options are represented by the STA/LTA and the CWT-Otsu methods, by reducing about to half of the required processing time with regard to AIC and IA techniques. Still, for the STE-ZCR method case, since its operation is carried out on a very straightforward fashion, the results show that its performance by means of the considered software implementation greatly excels to the current methods of the state of the art, achieving a reduction about of 99% of time regarding to the comparative methods.

Finally, the results corresponding to the operational robustness in front of induced AWG background noise, show that the less resilient method is the IA technique by saturating both measurements (i.e., by leading the onset detection to the start of the data frame, and lagging the endpoint determination to the end of said frame), at the first evaluation of added noise; additionally, it also can be noticed that the required processing time considerably increases when a greater amount of rippling is present in the CF. For the STA/LTA method by being endowed with a secondary threshold (aimed to determine the end of the event), their endpoint measurements showed some regularity during for all noise evaluations, additionally, the method proved to be the most resilient for the first evaluation of added noise (due to the robustness delivered by its CF), furthermore, the required processing time was sustained for all evaluations; however, the onset measurement failed for the 15 and 10dB ratios, by showing saturation. The performance achieved by AIC technique for the onset determination revealed some regularity for the 20 and 15dB ratios, nevertheless the measurement failed for the 10dB ratio evaluation; for the endpoint measure, by only depending on the threshold-timer scheme and by maintaining a high threshold level value for the test-bench, the obtained results were closed to those generated when evaluating the original signal, still, all of these containing a high uncertainty degree; it also can be observed that as the signal contained greater presence of AWG noise, the task of modelling the AE signal becomes more difficult for the technique, impacting on the required processing time as consequence. The onset evaluation achieved by the AIC-Otsu method, was the one that showed the closest coherence with regard to the AE phenomenon development, by approaching to correctly determine the arrival of the secondary waves for the 20 and 15dB ratios, nevertheless its accuracy was lost for the 10dB ratio; for the endpoint measure, by implementing the same scheme of the AIC in order to determine the conclusion of an AE event, results are equivalent; for the analysis of the average consumed time per AE event, the technique showed a tolerable time consumption in order to analyze the three levels of induced AWGN with regard to the results obtained by analyzing the original signal. For the

case of the STE-ZCR method, owing to implement a threshold adjustment procedure based on an early estimation of noise floor, the technique proved to be the most resilient alternative for onset detection measure regarding to the considered methods, by considerably reducing the amount of error as well as never saturating its detections; for the endpoint determination and despite of been heavily biased by AWGN, the ZCR alternative measure showed coherence with regard to the AE phenomenon development; for the required average processing time, the method proved to be the most efficient alternative by practically maintain unaltered the results obtained by analyzing the original signal.

4.4.2 Uniaxial tensile test. Quality of detection statistical indicators

The objective for this second test-bench is to quantify the quality for event detection over a data frame collected from a standardized tensile test, which contains a substantial diversity of continuous AE events. In comparison with the artificial AE events produced by the Hsu-Nielsen procedure, real AE waves typically will exhibit smaller amplitudes and shorter durations (of course depending on the stage of damage of the specimen under evaluation). Therefore, for the calibration used for this test-bench (see **Table 4-3**), the time-driven parameters as well as the threshold levels have been reduced in order to increase the sensitivity (regarding to temporal and amplitude detection capabilities) of the methods.

Table 4-3. Calibration parameters values used for each method for the field data test-bench.

Parameter	Method				
	LA	*STA LTA*	*AIC*	*CWT Otsu*	*STE ZCR*
Fixed threshold level	2.25e-3	4e-3	6e-3	6e-3	55e-6
Hit Definition Time [µs]	100		100	100	
Hit Lockout Time [µs]	15		15	15	
Threshold de-trigger		3e-3			
STA window time [µs]		25			
LTA window time [µs]		10e3			
Pre-event time [µs]		1			
Post-event time [µs]		0.5			
Weighting-R constant			4	4	
End delay time window 1 [µs]			10	10	
End delay time window 2 [µs]			5		
Start delay time window 1 [µs]				75	
Start delay time window 2 [µs]			20		
CWT scales				101	
Grayscale image bit-depth				16	
Median filter pixel neighbors				50	
STA duration [µs]					15
STA window					Hamming
Overlapping window samples					1
ZCR threshold [%]					80
α-weighting STD noise					1
Early noise analysis [µs]					5

Once that all methods have processed the field data frame of 500ms length, the quality of event detection is quantified in two steps. First, by totaling the total number of detected events against the true locations (referring a total amount of 380 AE events present in the data frame), and by classifying the properly detected events (true-positive), missed events (false-negative) and the mistakenly detected events (false-positive), that each method concludes (see **Table 4-4**).

Table 4-4. Classification of the identified events regarding to 380 AE waves present in the data frame.

Count	Method				
	IA	*STA/LTA*	*AIC*	*CWT-Otsu*	*STE-ZCR*
Total detections	373	380	372	372	367
True-positive	322	324	299	299	338
False-negative	58	56	81	81	42
False-positive	51	56	73	73	29

For this field data test-bench, and from the total number of True-positive detected events, the absolute error for the onset, endpoint and lifespan are also calculated (see **Table 4-5**).

Table 4-5. Absolute error and standard deviation of the onset, endpoint and lifespan detections regarding to the field data test-bench.

Method	Onset error (µs)	Endpoint error (µs)	Lifespan error (µs)
IA	-9.69 ± 7.56	38.39 ± 101.27	48.09 ± 102.13
STA/LTA	-2.49 ± 8.63	12.07 ± 83.65	14.56 ± 84.85
AIC	-6.15 ± 10.44	19.57 ± 543.74	50.4 ± 692.6
CWT-Otsu	2.53 ± 29.45	-92.36 ± 97.4	89.82 ± 97.74
STE-ZCR	4.62 ± 53.79	-4.42 ± 114.15	-9.05 ± 102.04

From **Table 4-5**, it can be observed that despite of reducing the onset and endpoint error measures with regard to the Hsu-Nielsen test-bench (due to having to deal with less challenging AE events by exhibiting less pronounced s-waves), the order regarding to the competency of the performance of the considered methods is better aligned with the results obtained for the first round of operative robustness (SNR 20dB). All methods exhibit a sustained performance for the onset detection of the AE events by achieving an average error less than 10µs for all cases. For this experimental scenario, the STE-ZCR method accomplishes yet again the best endpoint determination and in consequence the best lifespan measure, ensuring that most of the detected events are complete in case of requiring a subsequent assessing analysis. From results of **Table 4-4**, it can be observed that despite that in average, all the comparative methods nearly detect 99% of the detection objective (i.e., 380-hits), none of them reaches more than 85% of true-positive detections. In consequence, given the quality with which these detections are performed, the reliability of the methods is

not assured. In **Figure 4-12**, a representative instance (which is derived of the test-bench and containing five different AE events) depicting this matter, as well as the different automatic detections that each method identifies, is showed.

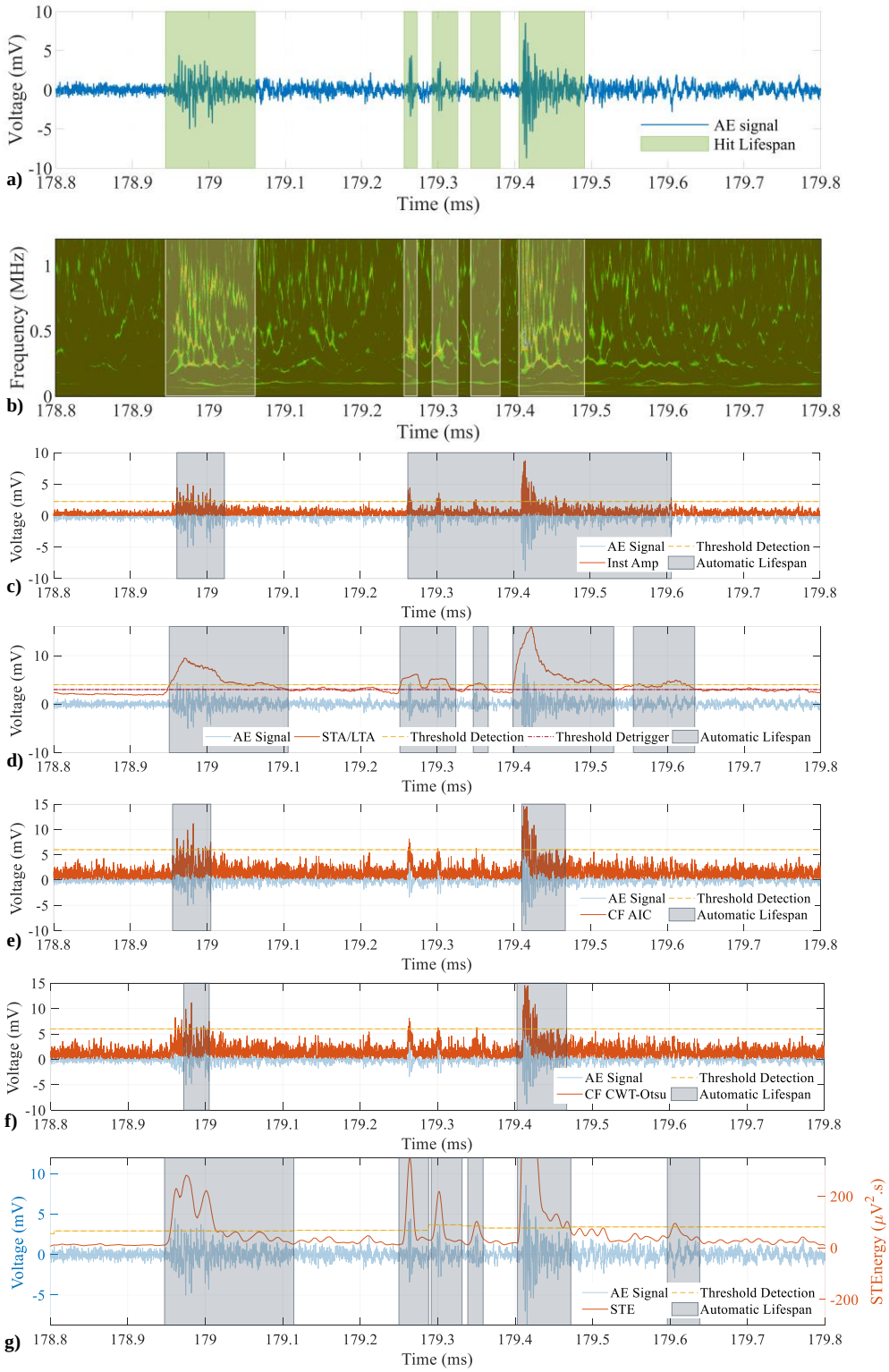

Figure 4-12. Comparison of events detected by the considered methods for an instance of 1ms (derived from the uniaxial tensile test). **(a)** Time-Voltage and **(b)** Time-Frequency manual detections. Automatic: **(c)** Instantaneous Amplitude, **(d)** STA/LTA, **(e)** AIC, **(f)** CWT-Otsu and **(g)** STE-ZCR proposed technique.

Finally, the STE-ZCR method despite of also executing the same false-positive detection as the STA/LTA technique (corresponding to the last event at 179.6ms), it can be observed that is the only method that accomplishes the detection of all existing events, besides of also achieving the most accurate lifespan measure for said events.

The last step for this test-bench comprises on the quantification of the quality of event detection of the considered methods. For this, by means of the number of classified events from **Table 4-4**, a set of statistical indicators are calculated. These are: (a) accuracy (the ratio of true-positive events to all detected and not detected events), (b) precision (the ratio of true-positive events to the amount of true and false-positive events), (c) sensitivity (the ratio of true positive events to the sum of true-positive and false-negative detections), (d) F1-score (the harmonic average between precision and sensitivity), (e) false discovery rate (the ratio of false-positive detections to all detected events), (f) false-negative rate (the ratio of false-negative detections to the sum of false-negative and true-positive events), see **Table 4-6**.

Table 4-6. Statistical metrics corresponding to the quality for event detection concerning to the data field test-bench.

	Method				
	IA	*STA/LTA*	*AIC*	*CWT Otsu*	*STE ZCR*
Accuracy (%)	74.71	74.31	66.00	66.00	82.64
Precision (%)	86.33	85.26	80.38	80.38	92.10
Sensitivity (%)	84.74	85.26	78.68	78.68	88.95
F1 score (%)	85.52	85.26	79.52	79.52	90.50
False discovery rate (%)	13.67	14.74	19.62	19.62	7.90
False negative rate (%)	15.26	14.74	21.32	21.32	11.05
Processing time (sec.)	220.49	33.54	608.56	182.92	19.6

For this test-bench, it can be observed that comparative methods perform with reasonable accuracy confidence by achieving an average score of 70%, and also can be noticed that the accuracy score is consistently aligned with the endpoint determination accuracy (i.e., the better the endpoint is detected, the higher the accuracy will score). In general terms all methods achieve better scores for the precision indicator than for the accuracy, this owes to the fact that in the dataset exists a larger amount of true AE events with regard to false events (as high-energy reflections and mechanical noises, e.g., slips). For the sensitivity metric, all methods slightly diminish their performances with regard to precision metric by being slightly prone to generate false-negative detections (mostly of them derived from spliced detections).

In the case of the STE-ZCR method, as can be observed it excels to the rest of the considered techniques about 12% for the accuracy metric, 10% for the precision metric, 7% for the sensitivity metric, 8% for the F1-score, 10% for the false discovery rate and 7% for the false negative rate case. This improvement clearly owes to performing the endpoint detection with higher accuracy. Finally, it can also be observed that the STE-ZCR technique reduces the required processing time with regard of the rest of the considered methods about 45-97%.

4.5 Discussion and conclusions

An Acoustic Emission activity detector, which allows an automatic and continuous detection of AE events, was presented in this chapter by using time domain features obtained from the waveform of the signal of interest. The proposed methodology was realized by revisiting a well-established signal processing technique from the speech processing area, and adapting it to the requirements of the AE phenomenon.

Additionally, in this chapter, two experimental scenarios were arranged to quantifying the performance of the proposed method, and with the aim of analyzing three critical aspects related to the AE event detection: the onset and endpoint accuracies, as well the quality of event detection.

Firstly, in the Hsu-Nielsen test-bench, for the case of the onset detection measure, the proposed STE-ZCR method improved the accuracy with regard to the IA method by in average, diminishing the measuring error by 18.54μs, 16.53μs for the STA/LTA and 10.05μs for the AIC method. The STE-ZCR method despite of producing a larger average error of 2.1μs with respect to the CWT-Otsu technique, it diminished the respective dispersion error by 84.48μs.

For the endpoint detection measure, by implementing an intrinsic indicator derived from the waveform of the AE signal, the STE-ZCR method surpassed the accuracy of the comparative methodologies in about four and five orders of magnitude, which in turn contributed to achieving the lowest error for the lifespan measure.

Lastly for the Hsu-Nielsen test, the STE-ZCR by implementing an adaptive threshold scheme, proved to be the most resilient method under noisy scenarios by never saturating its measurements in the corresponding test.

Secondly, for the uniaxial test-bench, besides of having verified that the obtained results for the onset and endpoint measures of the considered methods are consistent with the obtained for the Hsu-Nielsen test, it was studied the quality with that the AE events are detected.

Results showed that for a data-frame which contains 380 AE events of different durations, amplitudes and random manifestation, the STE-ZCR was the method that achieved the highest amount of true-positive detections and the lowest amount of false (both, positive and negative) identifications. Quantitatively, the STE-ZCR method excelled in average to the rest of the considered techniques in about 12% for the detection accuracy, 10% for the

precision and 7% for the sensitivity; and simultaneously reducing in average around of 10% and 7% the false discovery and the false negative rate cases respectively. Once again, this improvement over the rest of the considered methods responds to the fact of implementing a dedicated indicator with which to detect the end of the AE events.

In addition, the proposed STE-ZCR method by using a direct processing scheme, in both experimental scenarios it was the one that achieved the best processing times, by in average reducing the required search time in one up to three orders of magnitude in comparison with the others considered techniques.

It must be noted that despite of the detector has been oriented specifically on the automated detection of AE events for an application related to the characterization of metallic components, by only requiring the waveform of the AE phenomenon to be operative, its direct use for another applications and materials with similar characteristic for their waveforms could be feasible.

Finally, its straightforward scheme and the diminished consumption times, suggest a possible and efficient hardware implementation for online monitoring applications. Furthermore, and in the same line, with the aim of reducing the payload required to transmit or store the large data streams demanded by the phenomenon, by achieving an adequate identification and separation of the AE events, it could be possible to only working with the identified events.

Chapter 5. FATIGUE LIFE ASSESSMENT FOR AHSS THROUGH THE AE SPECTRUM

5.1 Introduction

High requirements are demanded on safety and reliability specifications for the design and manufacturing of metallic materials, particularly in the transportation sector, where lifetime, performance, weight and cost of structural parts are critical features. This has led to extensive scientific and technical study of the mechanical properties of metallic components [105,106]. In this regard, the use of advanced high strength steels (AHSS) for chassis and body-in-white (BIW) components has exponentially increased in the automotive industry in the last two decades with the aim of meeting said requirements [107].

AHSS are particularly suitable as lightweight crash resistant automotive components due to their superior mechanical properties combining high strength and great energy absorption capacity, which allow to reducing the total vehicle mass without compromising the safety of the passengers. For this reason, the mechanic characterization of AHSS has become one of the main issues for steelmakers and automotive components manufacturers [108].

As mentioned in Chapter 2, typically, the mechanical characterization of metallic components requires estimations of the post-yield strength, the tensile strength and the elongation of metallic specimens, which are evaluated through a standardized tensile test [109,110]. Determining the plastic strain evolution exhibited by the specimen is critical in order to estimating the seek properties of the metallic component; said evolution typically is measured by means of a strain gauge [111].

Furthermore, as is known [112,113], fatigue life of any material can be divided before and after the nucleation of (at least) a crack, thought its propagation and the eventual rupture of the material. In this sense, additionally to the traditional mechanical descriptors obtained from the test, one current interest lies on accurately determining the nucleation and growth of cracks during the assay. In this regard, the use of video extensometer-based systems has also been implemented as a supplementary measuring, thus allowing visual forensic analysis. Nevertheless, the time period capture between images is usually in the order of milliseconds, causing loss of resolution between frames; moreover, only the surface of the specimen can

be monitored, thus losing information of the internal damage process of the evaluated specimen [114]).

Accordingly, in current literature the analysis of the acoustic emission (AE) phenomenon has been included as an additional mechanical descriptor to enhance the characterization capabilities of the assay [43,115–118]. Nevertheless, in order to conduct such analysis, the appropriate detection, processing and interpretation of each AE event is essential.

As deeply analyzed in Chapter 3, the use traditional threshold detection method entails several disadvantages for the identification and the later analysis of AE events as well [119]. Nevertheless, its use further extends through the AE discipline, since a number of currently used parameter-based damage estimators are originated from this detection technique. Such as the case of the Rise Angle -RA (i.e., the tangent of the peak voltage between the required time to reach said peak), the Average Frequency -AF (i.e., the average number of crossings of the threshold level per the time of duration of the AE event), the initiation frequency -IF (i.e., the number of threshold crossings per the time of duration of the AE event), among others [120].

Additionally, for concrete related applications, there exist additional estimators, which are originated by the combination of these abovementioned damage estimators, as is the case of the combination of the AF and the RA, and which is used to classify between shear and tensile crack types [64,121–125]. Still, nowadays this RA/AF classificator is extended to metallic component applications as well [126–130].

Although the aforementioned estimators, have proven to deliver useful information about the damage evolution on the metallic components [131–136], their use implicitly add a considerable amount of uncertainty to the outcome assessment. This, by ineluctably depending of the used threshold value level. Precisely, by producing different outcomes for the same AE event, when different threshold values are used.

Hence, this drawback generates the necessity to develop methodologies that can reliably assess the evolution of the AE phenomenon without biasing their outcomes. In this sense, frequency content analysis of the generated AE events, offers a framework with the capability to glimpse the involved fracture processes during metallic destructive assays. Nevertheless, in current literature although frequency-based works remain significantly extended [13,137–146], authors come to different conclusions for the associated characteristic frequencies regarding to damage processes; i.e., some researchers suggest that crack related events are

composed of high frequency energies, while others correlate a low spectral content for these fatigue events.

An additional disadvantage, is that due to high demanding computational resources required to assess the AE phenomenon (large data streams derived from high sampling rates), it is a common practice to only evaluate a fragment of the actual AE events; or alternatively, diminishing the resolution of the time-frequency mappings (making difficult the identification of an accurate damage indicator).

As final consideration, is that despite of AE can be related to the nucleation or growth of a crack, not all the AE events are necessarily generated by fatigue, since during tensile test, the AE phenomena can be produced by further damage sources, e.g., phase transformation, sliding and leakage [41]. Therefore, in order to validate the criteria for the frequential indicators of fatigue, it is necessary the proper corroboration of the undergoing physical changes of the assayed specimen in regard to the evolution modes of the AE phenomenon.

Studies presented in this chapter, are focused on detecting the initiation and evolution of mechanical fatigue (i.e., the nucleation and growth of cracks) on AHSS components, during tensile tests by means of the evolution of AE phenomenon.

For this, a novel methodology is proposed, where firstly the AE activity is identified with higher accuracy than the traditional threshold method accomplishes [147]; to next (and differently of analyzing the pattern waveform as the traditional AE damage indicators perform), it is evaluated the energy contribution over different frequential bands of each detected AE event. This, with the aim of identifying tendency changes in the spectral content of the AE phenomenon during tensile tests with the purpose of detecting fatigue.

In order to corroborate the efficiency of the proposed AE methodology, traditional procedures presented in this work consist of metallographic analyses, Digital-Image-Correlation (DIC) technique and interpretation of load-displacement curves.

5.2 Methodology

For this work, with the objective of evaluating the occurrence and evolution of fatigue in AHSS specimens throughout a tensile test, the proposed methodology (see **Figure 5-1**), consists of initially the continuous capture of the signal generated by one sensor attached to the AHSS sample during the assay. Next, the acquired signal is processed under an offline scheme with the aim of identifying the AE activity from the continuous datastream to later separate each AE wave. Finally, in order to perform the identification of nucleation or growth of cracks using the variation of the AE spectral signature, the energy of each AE event is frequency decomposed by means of a filterbank.

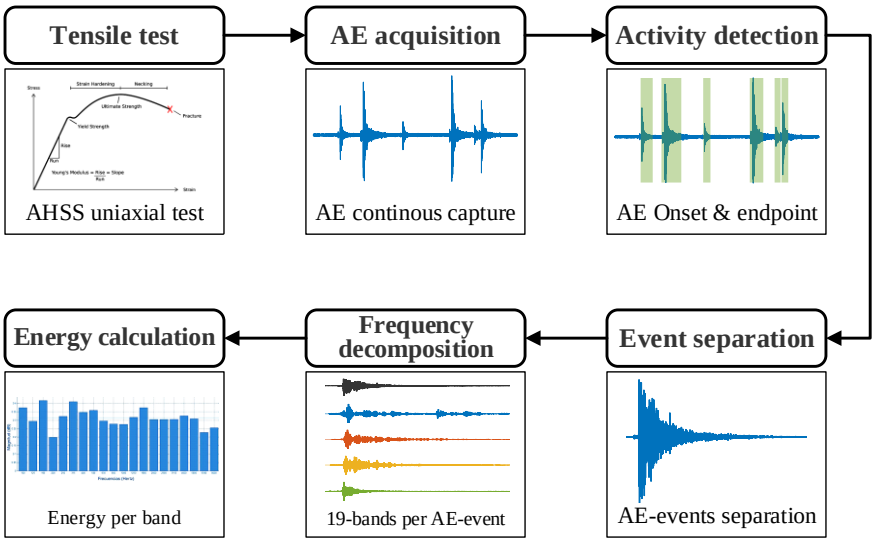

Figure 5-1. Block diagram for the related AE data processing proposed methodology based on the spectral energy evolution of the AE phenomenon.

5.2.1 Highly accurate detection of AE events

Since multiple sources of noise floor are present during assays (e.g., friction, slip, electromagnetic interferences, among others), along with the particularities of the AE phenomenon (i.e., significant randomness on the arrival, duration and amplitude of the waves), the task of detecting AE events arises as one of the most challenging in the processing chain of the AE assessment.

Thus, for any application related to AE, and as several authors point out [53,73], with the aim of achieve precise assessment outcomes, the proper identification of AE events is

critically relevant. Consequently, for the first stage of this proposed methodology, it is used a highly accurate AE activity detector previously developed by the authors of this work [147].

Unlike traditional AE event detection scheme (which is based on the crossing detection of the AE signal with regard to a preset threshold level), this AE activity detector is based on the Short-term analysis of the signal. For this, the activity detector generates two characteristic functions by means of the Short-term analysis of the Energy and the Zero-Crossing Rate respectively regarding to the acquired AE signal, in which the search work will be performed (see **Figure 5-2**).

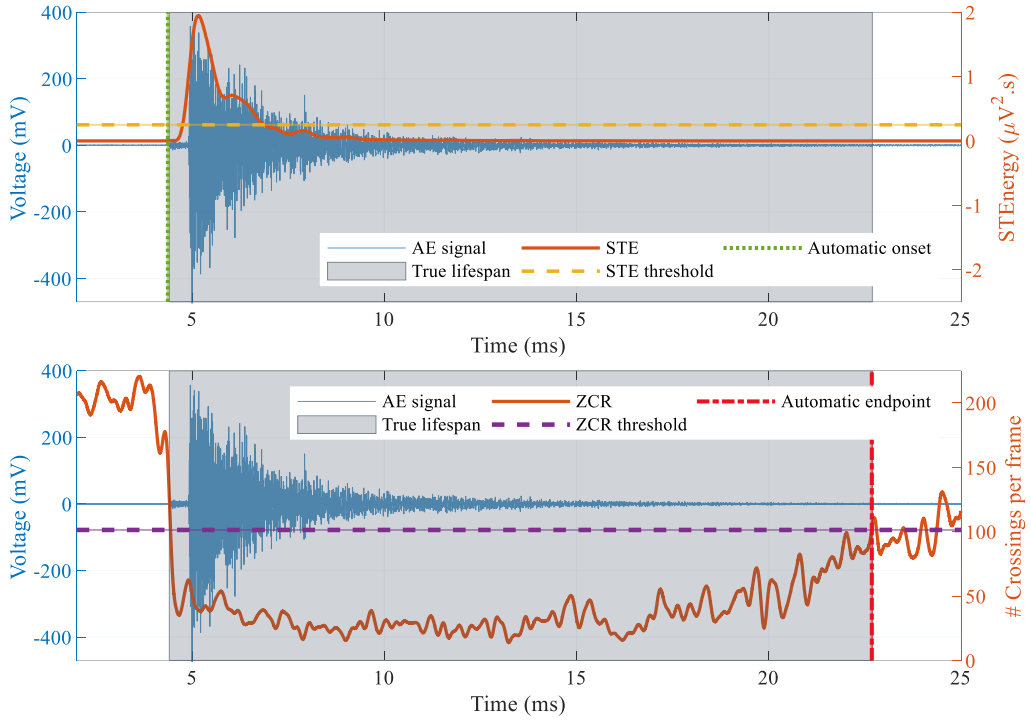

Figure 5-2. Onset and endpoint search work of an AE event, based on the short-term analysis. Disimilar to the traditional method, under this method two tresholds operate over two characteristic functions derived from the AE waveform. **(a)** Automatic onset detection using the short-time energy of the AE signal. **(b)** Endpoint detection using the short-time zero-crossing rate of the AE signal.

Regarding to current state-of-the-art AE detection techniques, in general terms, this method enhances the accuracy of the onset determination about 12%, the endpoint detection by 91%, as well as about 12% of the quality of detection accuracy (i.e., the amount of properly detected AE events).

5.2.2 Digital filterbank for the spectral analysis of AE events

Traditional spectral analysis based on the Fourier transform, allows the calculation of the corresponding energy that each frequency bin contributes to the inspected signal. Despite of being widely applied in the AE discipline, its use entails one major drawback, since in average the related duration of AE events spans about from tens to a few hundred of microseconds, and unless that the number of samples used for the Fourier analysis be equal or greater to the sampling frequency, will be generated an unavoidable loss of spectral resolution (i.e., sampling frequency per number of samples of the transformation), even if pre-processing signal techniques are used in order to mitigate this low spectral resolution (e.g., zero padding).

For the case of advanced spectral analysis techniques, particularly Time-Frequency representations (TFR), despite of its applicability has been showed for the AE area, the most prominent techniques besides of still entailing spectral resolution drawbacks, involve their own particular disadvantages. Such as the case of the time-dependent Short-Time Fourier Transform (STFT), which conveys a trade-off derived from the Heisenberg-Gabor principle of uncertainty [148], due to having to choose between spectral accuracy (disregarding the temporal information) or time accuracy (at expense of diminishing the spectral resolution). Similarly, the Continuous Wavelet Transform (CWT) regardless of improving the energy allocation in the TFR in comparison with the STFT technique, it still presents Heisenberg-Gabor type uncertainties (these become particularly evident for nonstationary signals with a higher multimodal complexity as is the case of the AE phenomenon); in addition to present an outcome heavily dependent of the selected mother wavelet (i.e., the TFR will vary in function of the chosen wavelet). In order to overcome the aforementioned uncertainty derived from the Heisenberg-Gabor principle, alternative TFR strategies have been developed. As is the case of the Wigner-Ville distribution (and their modified alternatives, e.g., Gabor-Wigner, Choi-Williams, Cohen's class, Zhao-Atlas marks, among others), despite accomplishing high resolution TFRs, their use results in additional difficulties as in the case of high computational load and artificial frequency components due to the interference between actual ones (cross-term property [149]). An additional TFR technique is the Hilbert-Huang Transform (HHT); which by means of an Empirical Mode Decomposition (EMD) of the analyzed signal, a collection of Intrinsic Mode Functions (IMFs) is obtained, which, along with the Hilbert spectral analysis, will lead to a time-frequency depiction. Although having been successfully applied in a wide range of fields due to adaptively decomposing the signal of interest, its use also brings some drawbacks, such are the cases of high computation

load, the requirement of a stopping criterion for the EMD, the difficulty for discerning separate frequency components in narrow-band signals and a mix of modal components [150,151].

An alternative spectral examination technique, consists of channeling the assessed signal throughout a bank of band-pass filters (a filterbank). This process (known as analysis) separates the energy content of the signal in different (and typically non-overlapped) spectral sub-band signals. Particularly, for the AE discipline the use of filterbanks traditionally have been implemented by means of the Discrete Wavelet Transform (DWT) theory [56,79,80,152–155].

However, and despite of having effectively demonstrated their relevance for AE applications (mainly related to noise removal and feature extraction), filterbanks based on DWT techniques feature significant limitations when the accurate quantization of spectral energy in a set of sub-bands is required.

This, owes to the fact that DWT traditional implementation methodologies (in addition of presenting significant time-shift variance and be heavily influenced by the Gibbs phenomenon [153,156]), by decomposing the original signal through iterated low-pass and high-pass filters whose limits for the frequency bands are defined by a dyadic basis (i.e., powers of the number two), be generated an extremely challenging design task in order to be able of achieving specific boundary values for the resulting filters (even with the use of more general m-ary integers construction basis; e.g., band wavelets or wavelet packets techniques).

In this sense, when precise frequency energy separation is required, due to the capability of achieving detailed control over the spectral response (i.e., rapid frequency transitions, low passband ripple and high stopband attenuation) of each of the filterbank elements, optimal filtering strategies represent a superior alternative regarding to DWT-based filters. And despite of requiring intensive modelling iterations and relatively large number of operative coefficients, nowadays their implementation is computationally feasible; nonetheless, they have not been yet completely exploded in the AE discipline. Therefore, in order to achieving the accurate frequency energy decomposition of AE events that allows depicting the spectral energy evolution trend during tensile tests of AHHS, with the aim of identifying the nucleation and growth of cracks, in this work an optimal filterbank based on the Parks-McClellan strategy [157–159], is implemented.

This procedure (based on the Remez exchange algorithm), aims to optimize a FIR Chebyshev-based low-pass prototype filter, through the minimization of the maximum error (known as minimax), between the frequency response of desired specification and the response of the prototype; by finding the narrowest passband and stopband frequency edges, (i.e., through the optimization of the extreme values corresponding to the filter function within these frequency edges) see **Figure 5-3**.

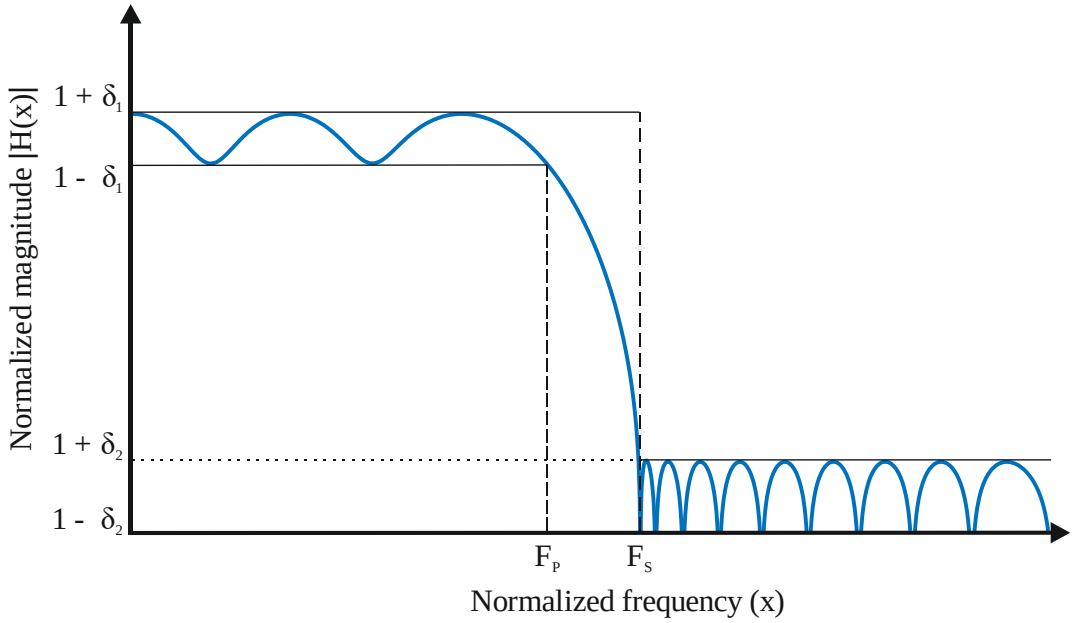

Figure 5-3. Frequency equirripple response of a prototype low-pass filter obtained with the Parks-McClellan algorithm. As is depicted, the frequency behaviour of the filter consists of three distinguishable regions. First, a ripple that extends from start frequency to pass-band frequency (F_p), which is bounded by a δ_1 pass-band edge value. Next, the transition band that comprehends from pass-band frequency (F_p) to stop-band frequency (F_s). Finally, the ripple in the stopband region (i.e., from F_s), which is bounded by the δ_2 stop-band edge value.

As aforementioned, the optimization is achieved by following the Chebyshev alternation theorem, where a closed subset F_p comprising a disjoint union of closed subsets on the real axis x is considered, and where

$$P(x) = \sum_{k=0}^{r} a_x \, x^k \qquad \textbf{(1)}$$

is treated as an r-th order polynomial. Correspondingly, $D_p(x)$ represents the desired specification response filter function (which is continuous on F_p subset), $W_p(x)$ is a positive and continuous on F_p as well, and where

$$E_p(x) = W_p(x)\big[D_p(x) - P(x)\big] \qquad \textbf{(2)}$$

is the weighted error.

The maximum error is defined as:

$$\|E_p\| = \max_{x \in F_p} |E_p(x)| \quad \textbf{(3)}$$

A required and sufficient condition so $P(x)$ is the unique r-th order polynomial that minimizes $\|E_p\|$, is that $E_p(x)$ exhibits at least $(r+2)$ alternations, i.e., there must exist at least $(r+2)$ values x_i in F_p such that $x_1 < x_2 < \cdots < x_{r+2}$, and such that $E_p(x_i) = -E_p(x_{i+1}) = \pm\|E_p\|$ for $i = 1, 2, \ldots, (r+1)$.

Filters obtained through this procedure will exhibit an equiripple behavior response; i.e., they will preserve the same maximum extreme values for their ripples within the passband and stopband frequency responses respectively. Therefore, while maintaining a reasonably fast transition band, it is ensured that passband energy never be attenuated, as well as the corresponding energy of the stopband region can never contribute to the filtered version of the signal.

Thus, under this filtering technique a straightforward yet precise frequency energy separation can be achieved in order to assessing the spectral trend behavior of the AE events generated during tensile test.

5.3 Experimental procedures

5.3.1 Material and specimen properties

Three different AHSS grades on the range of 1.4-1.16 mm thickness were investigated, one first generation AHSS cold forming grade Complex Phase (CP1000), one third generation Trip-Aided Bainitic Ferritic steel (TBF) and one hot stamped boron steel in-Press Hardened Condition, with a strength of 1500MPa (PHS1500); see **Table 5-1**.

Table 5-1. Chemical composition of investigated materials (mass %). Balance is Fe.

Steel grade	C	Si	Mn	Cr	B
CP1000	~0.1	<0.5	1.8-2.2	<0.7	<0.003
TBF	~0.2	0.5 – 1	2.2 – 2.6		
PHS1500	~0.2	~0.2	~1.2		~0.003

Previously to assays, the corresponding microstructure for each specimen was analyzed by scanning electron microscopy (SEM) means. CP1000 steel shows a homogenous matrix of bainite/tempered martensite (B/TM). TBF grade consists of a mixture of ferrite (F), bainitic ferrite (BF), bainite/tempered martensite and martensite (M), and also slightly amount of retained austenite (RA). PHS1500 is composed by a homogenous martensitic matrix, slightly auto-tempered during cooling. Geometry of specimens remain as depicted on **Figure 3-10 (b)**. Mechanical properties of specimens are shown on table

Table 5-2. Experimental specimens tensile parameters

Steel grade	t (mm)	YS (MPa)	UTS (MPa)	A80 (%)	$N_{2\text{-}4\%}$	AUTTC (MPa)
CP1000	1.4	908	1002	8.1	0.05	7825
TBF	1.5	725	1019	14.7	0.12	14045
PHS1500	1.5	1075	1552	5.2	0.08	8326

5.3.2 Mechanical testing setup

Loading is achieved by an Instron 5585H test machine, with a load cell of 250kN, and under a conventional uniaxial tensile test performed accordingly to EN-ISO6892-1 oriented at transverse orientation with regard to the rolling direction.

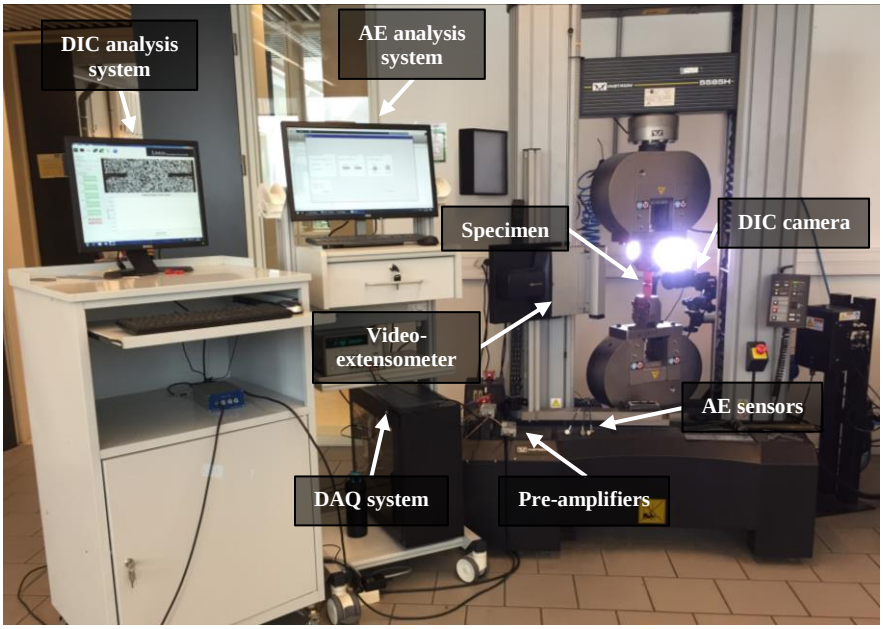

Figure 5-4. Experimental setup consisting of tensile test floor machine, AE sensors, pre-amplifiers and DAQ system, DIC camera and analysis system an a videoextensometer.

A test matrix listing the assay programs used for the validation of the proposed AE-based fatigue detection methodology is given in ***Table 5-3.*** *Assay matrix of collected AE data during tensile test***Table 5-3**. Each material is assayed at least one time under three different programs consisting of one cyclic load without breakage, and a monotonic loading scheme without breakage and with breakage.

Table 5-3. Assay matrix of collected AE data during tensile test

Specimen	Loading scheme	Breakage failure	Number of tests
CP1000	Cyclic	No	1
	Monotonic	Yes	1
	Monotonic	No	2
TBF	Cyclic	No	1
	Monotonic	Yes	2
	Monotonic	No	1
PHS1500	Cyclic	No	1
	Monotonic	Yes	1
	Monotonic	No	3

Finally, one AE sensor is attached to specimens using gel-based couplant. DIC system is also used with the aim to assist in fatigue detection. Video-extensometer system is used to record stress-strain curves.

5.3.3 AE signal processing framework

The identification of AE activity, is carried out by means of the AE detection method presented in **Chapter 4**. Calibration parameter values used by each material (resulting from a previous calibration based on the Hsu-Nielsen test), is presented in **Table 5-4**.

Table 5-4. Calibration parameters for the AE activity detection stage

Parameter	Material		
	CP1000	*TBF*	*PHS1500*
Fixed threshold level	1.5e-4	1.15e-4	1.2e-4
STA duration [μs]	15	15	30
STA window	Hamming	Hamming	Hamming
Overlapping window samples	1	1	1
ZCR threshold [%]	90	90	90
a-weighting STD noise	1	1	1
Early noise analysis [μs]	1000	1000	1000

Resulting AE events collected during tensile tests, then are identified and separated. Later, each AE event is frequency decomposed by a filterbank stage using an optimal Parks-McClellan based technique (**Figure 5-5**).

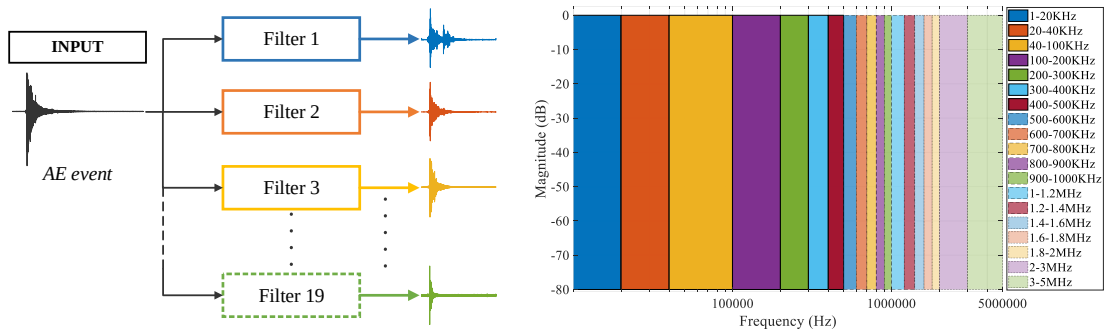

Figure 5-5. Proposed AE frequency decomposition strategy. **(a)** Cascaded frequency filterbank. **(b)** 19-frequency bands aimed to decomposing each identified AE event.

In **Table 5-5** design specifications for the filterbank are given. In **Figure 5-6**, an example of a filter element belonging to the filterbank is depicted; as can been observed and despite of requiring a considerable number of coefficients for its implementation, by using very fitted design values, the frequency and phase responses exhibited are suitable for the accurate AE frequency energy separation.

Table 5-5. Design specifications used to synthesize each element in the filterbank

Parameter	Value
Transition passband	2kHz
Transition stopband	2kHz
Passband magnitude	0dB
Stopband attenuation	-80dB
Order	12650

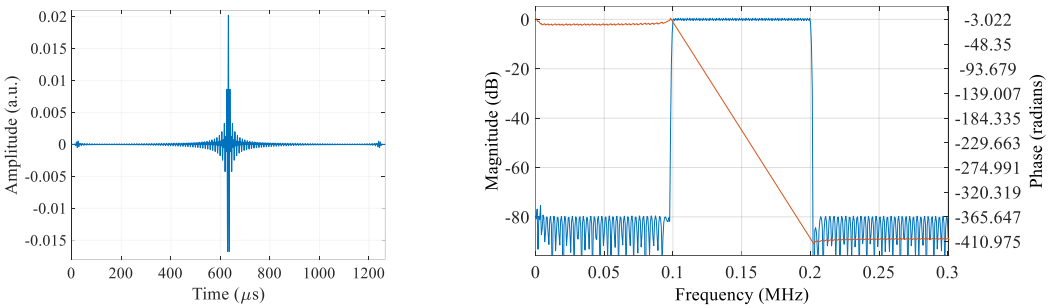

Figure 5-6. Resulting type II filter, for the fourth bankfilter element (corresponding to 100-200kHz). **(a)** Impulse response consisting of 12650 samples. **(b)** Frequency response (blue), linear phase (orange).

An additional advantage of this methodology, lies in that for achieving the required frequency decomposition, it is only necessary to convolving the AE events by the impulse responses corresponding to each element of the filterbank. Then, by following the Parseval's theorem, the resulting energy of the signal in time domain will be assured to be equal for the frequency domain; this allows a more straightforward frequency without further domain transformation techniques, diminishing the computational load.

5.4 Evaluation results

After conducting assays and process the collected signals. Evaluation results are verified.

5.4.1 Complex Phase 1000

For the cyclic assay corresponding to the CP1000 material, in **Figure 5-7** can be observed the generated AE events during the tensile test. It can be noticed the Kaiser effect since most of the AE activity is only generated when a previous load traction is equaled or surpassed.

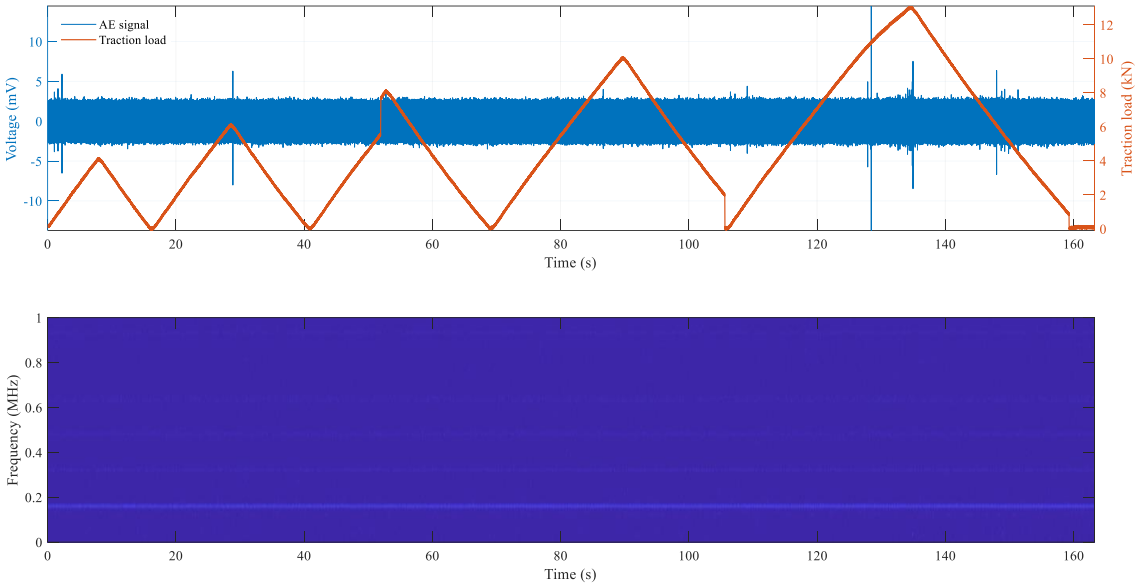

Figure 5-7. (a) Ciclic pattern load (orange) exerted on the material, and the resulting AE signal (blue). **(b)** Continous spectrogram corresponding to the AE signal.

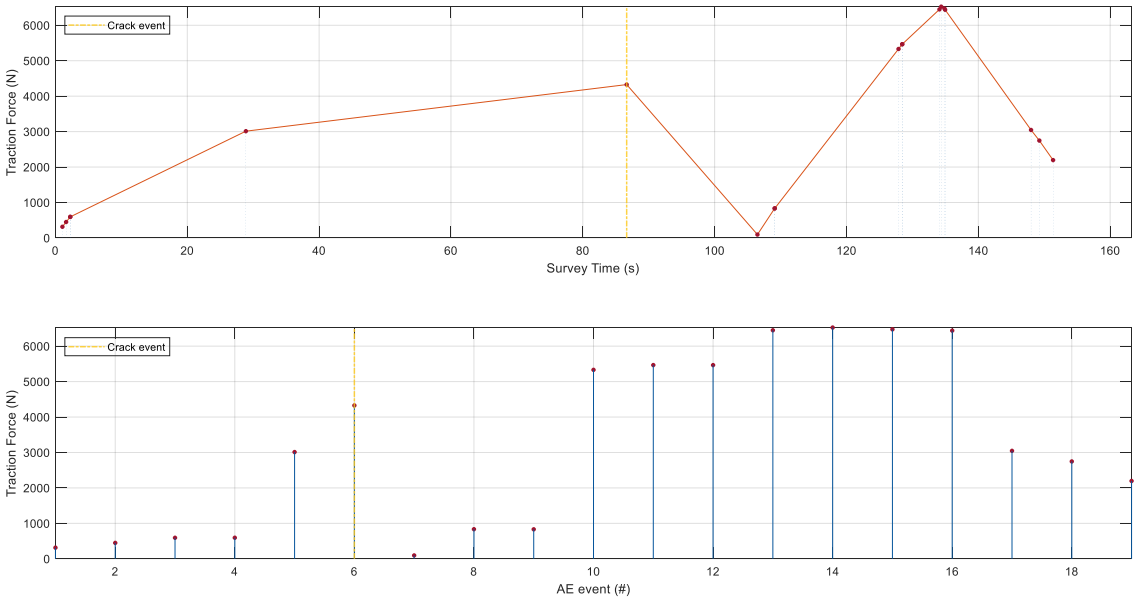

Figure 5-8. Tensile load level corresponding to each AE event. **(a)** Load per AE event during the experiment. **(b)** Load per individual AE event.

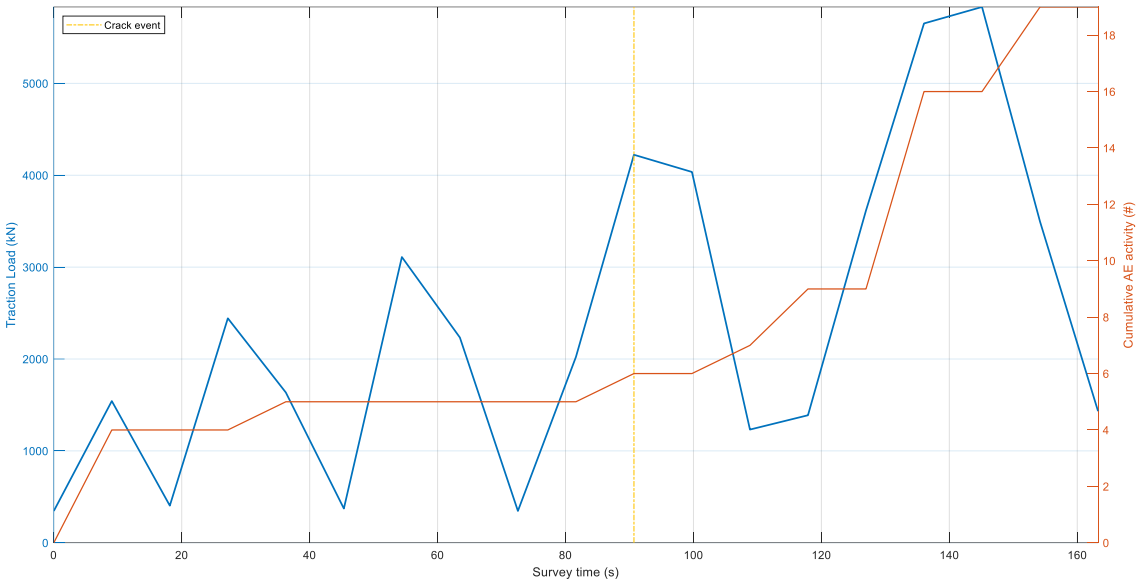

Figure 5-9. Sketch of the traction pattern (blue) vs. cumulative detected AE events (orange).

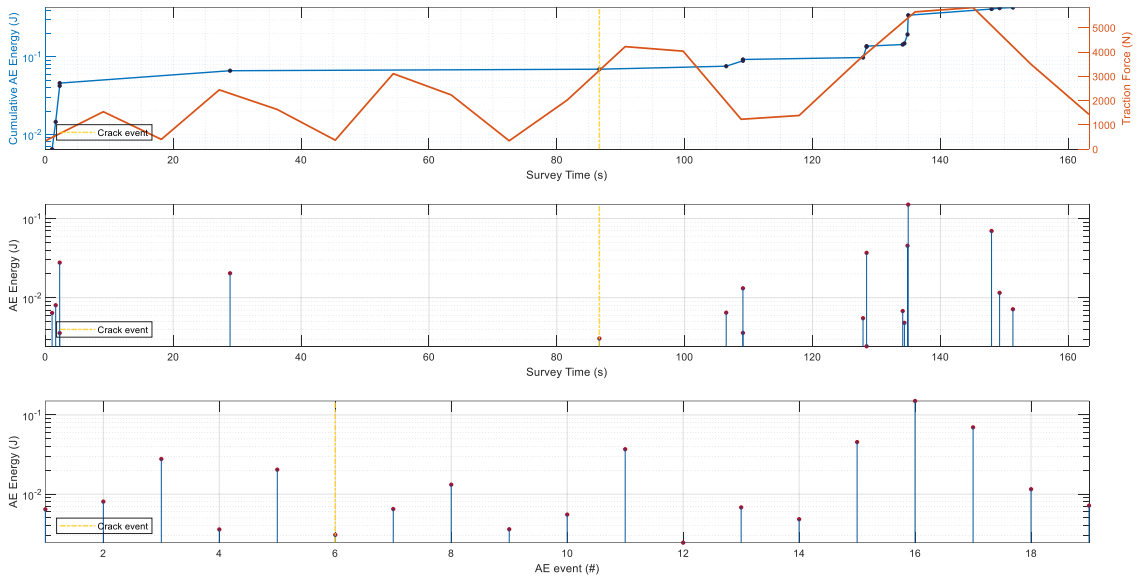

Figure 5-10. (a) Outline of the traction pattern (orange) vs Accumulated AE energy (blue). **(b)** AE energy per event during the test. **(c)** Individual energy per AE event.

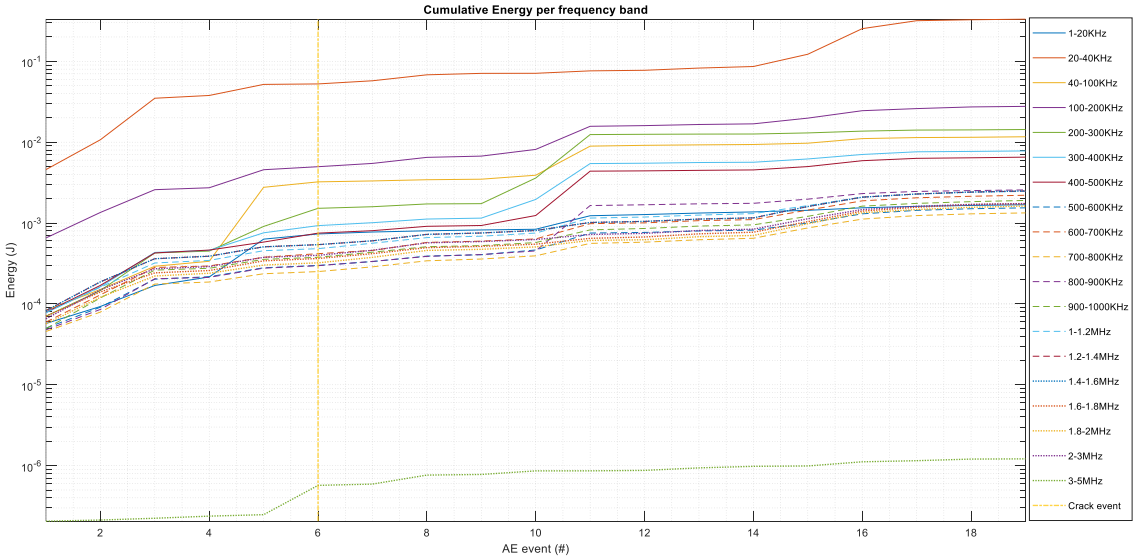

Figure 5-11. Evolution of the cumulative AE energy during the test, distributed in different frequency bands.

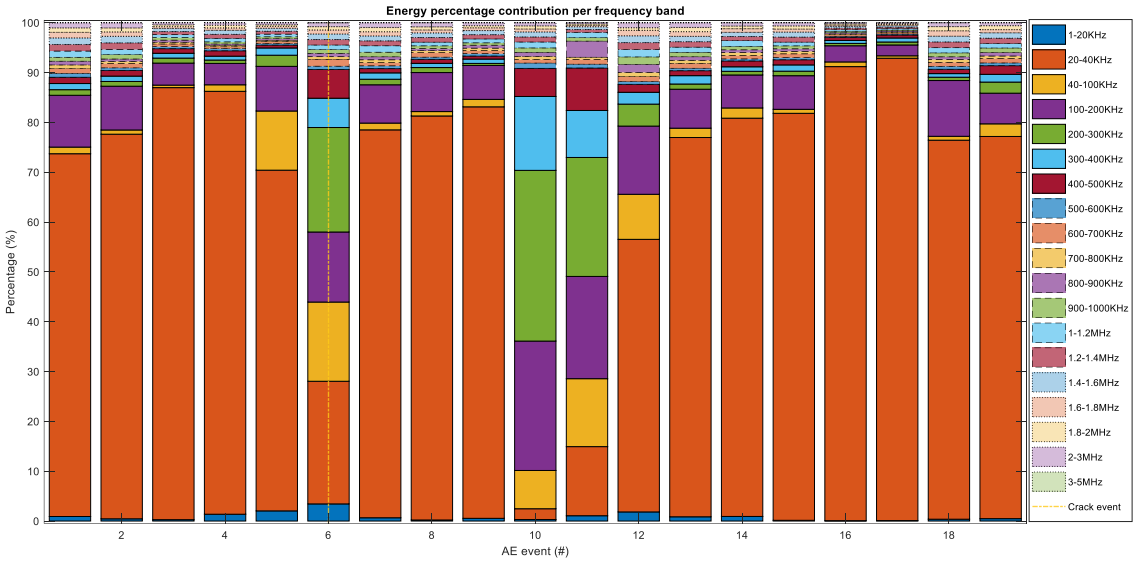

Figure 5-12. Evolution of the AE energy for different frequency bands.

As can be observed in **Figure 5-12**, trend of the frequency energy is clearly different for the AE event number six, which was generated at 4.32kN corresponding to instant of time 86.65s of the assay. Therefore, inspections were carried by SEM means in the specimen for a monotonic load below of 4kN in order to corroborate the absence of fatigue.

As can be observed a corresponding AE of the first stage of the assay (below of 4kN) is analyzed in frequency and the absence of fatigue is confirmed by metallographic inspection.

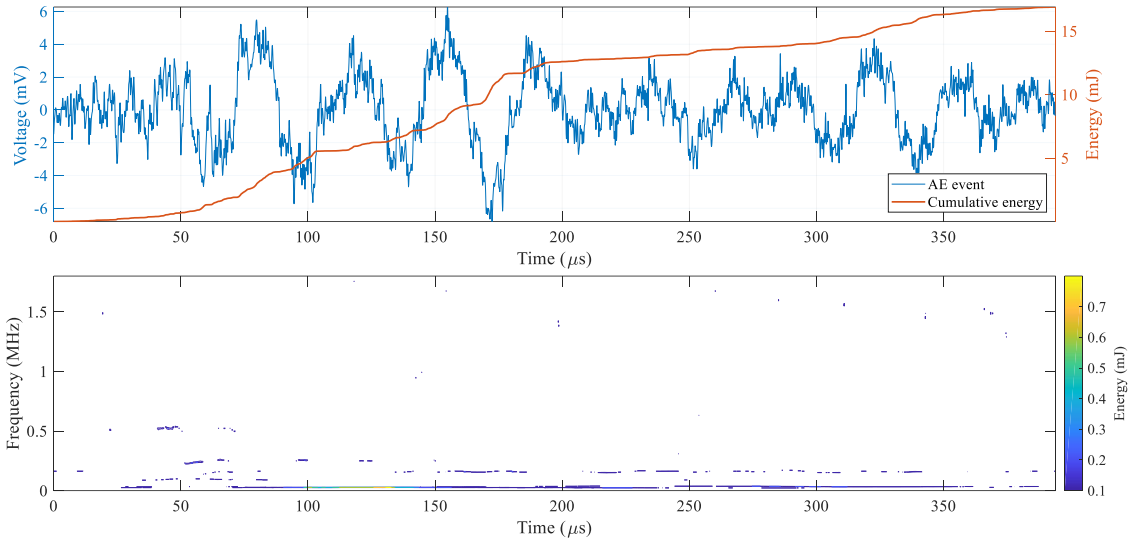

Figure 5-13. AE event presenting only low frequency energy, mainly generated by molecular slip and dislocation.

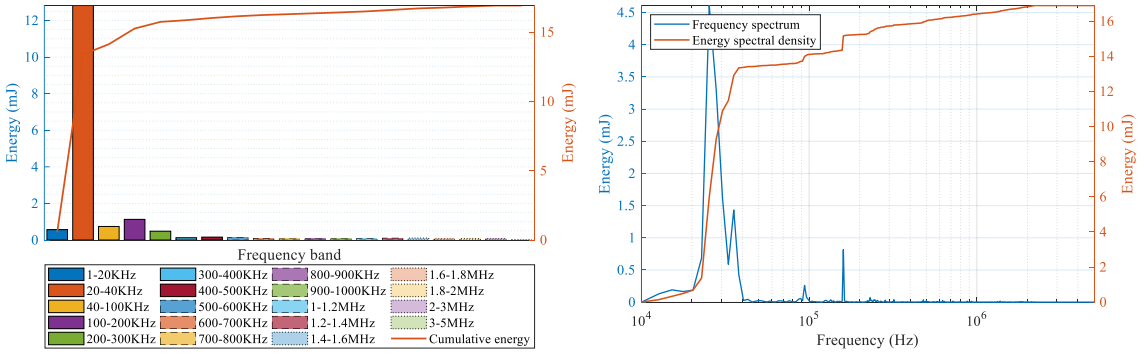

Figure 5-14. (a) Bandfrequency decomposition. **(b)** Frequency domain energy.

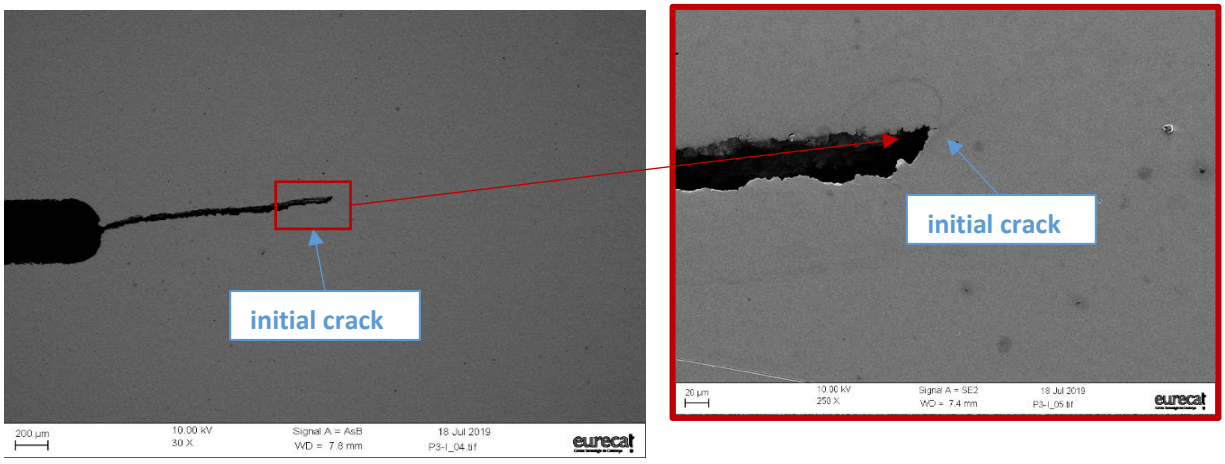

Figure 5-15. SEM inspection discarding fatigue presense.

Next, specimen is exerted under a traction load slightly above of 4.32kN. AE event is analyzed in frequency and metallographic inspection is carried out with the aim of confirming fatigue.

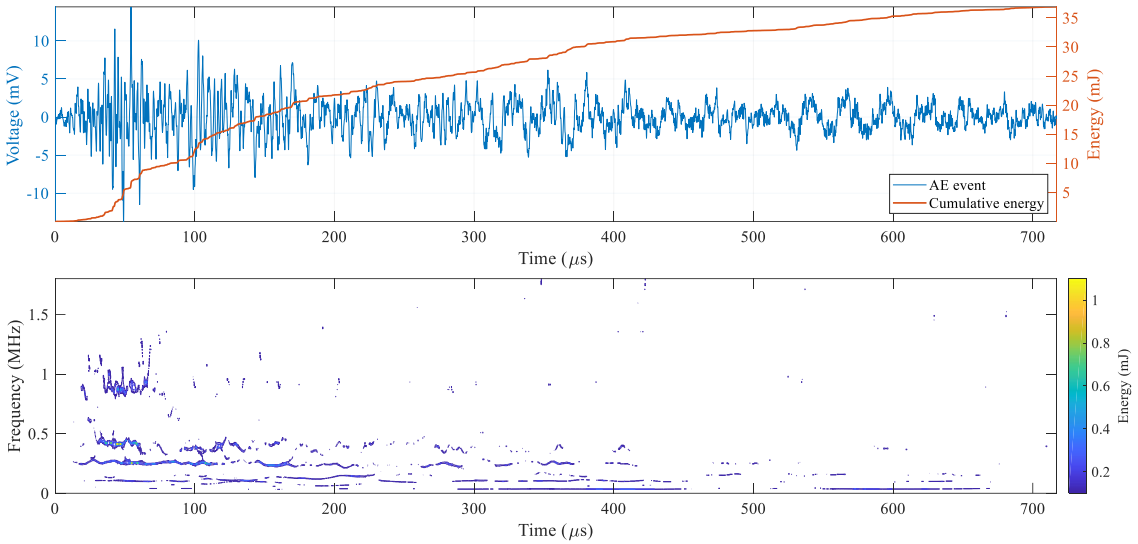

Figure 5-16. AE event mainly presenting high frequency energy. Behaviour indicates nucleation of a crack.

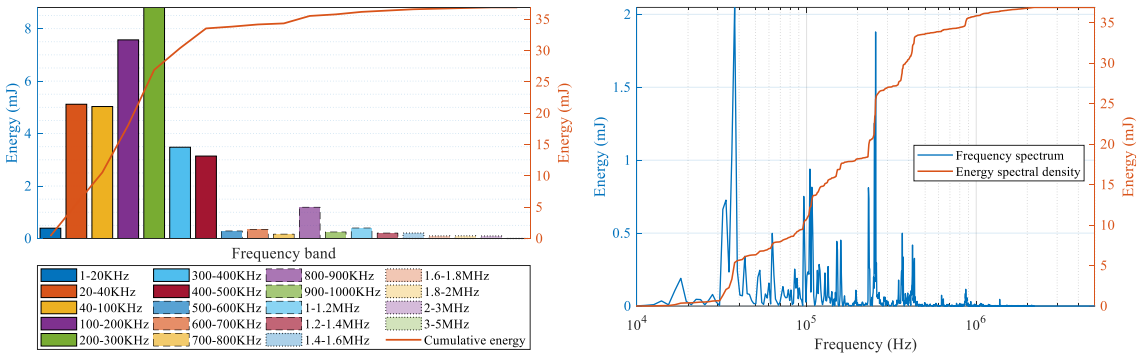

Figure 5-17. (a) Bandfrequency decomposition. **(b)** Frequency domain energy.

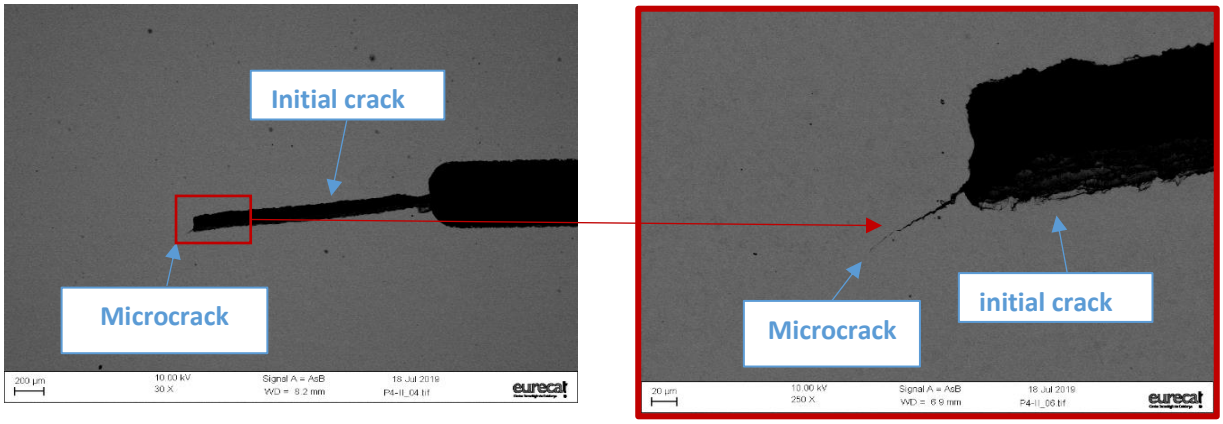

Figure 5-18. Metallographic inspection confirming a microcrack presence.

Finally, a monotonic assay is carried out in order to investigate macrocrack generation.

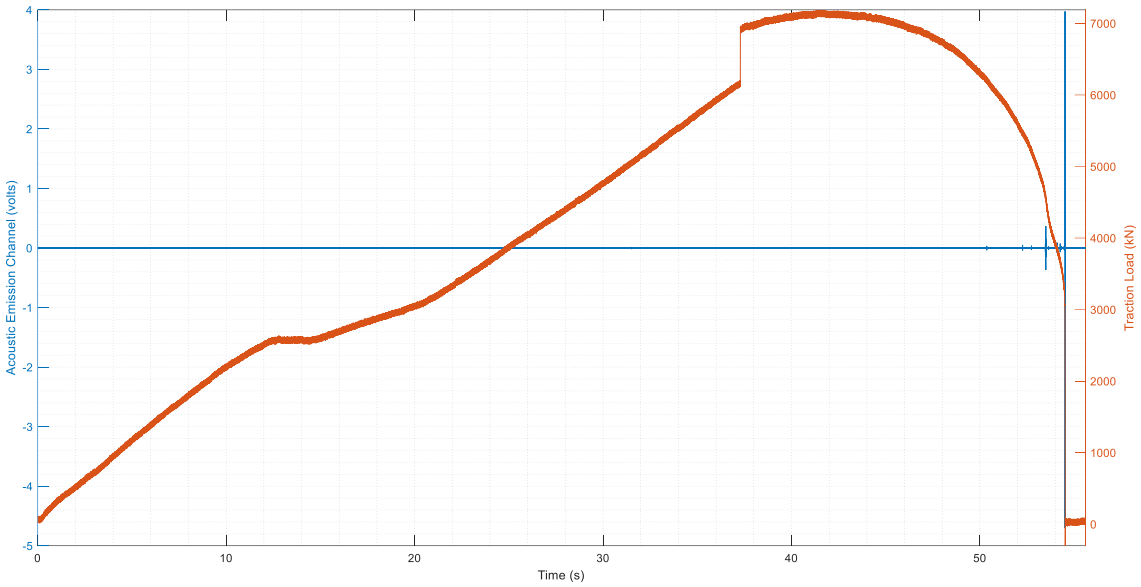

Figure 5-19. Cyclic pattern load (orange) exerted on the material, and the resulting AE signal (blue).

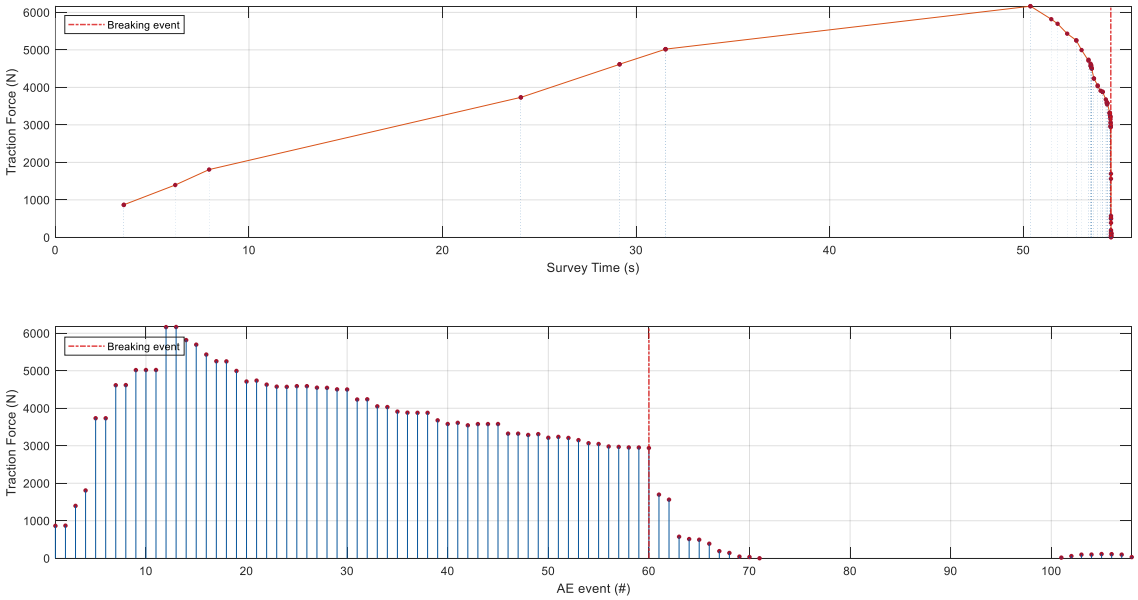

Figure 5-20. Tensile load level corresponding to each AE event. **(a)** Load per AE event during the experiment. **(b)** Load per individual AE event.

Specimen is exerted under a traction load until breakage. As it can be observed in **Figure 5-21**, the frequency energy behavior related to AE phenomenon is mainly distinguished in three zones, first, from event 1 to 10 (belonging to a microcrack propagation), next from event 14 to 60 where differently to the aforementioned cases, where only exists low

frequency and high frequency energy, for this third case the AE events are composed by high and low frequencies jointly.

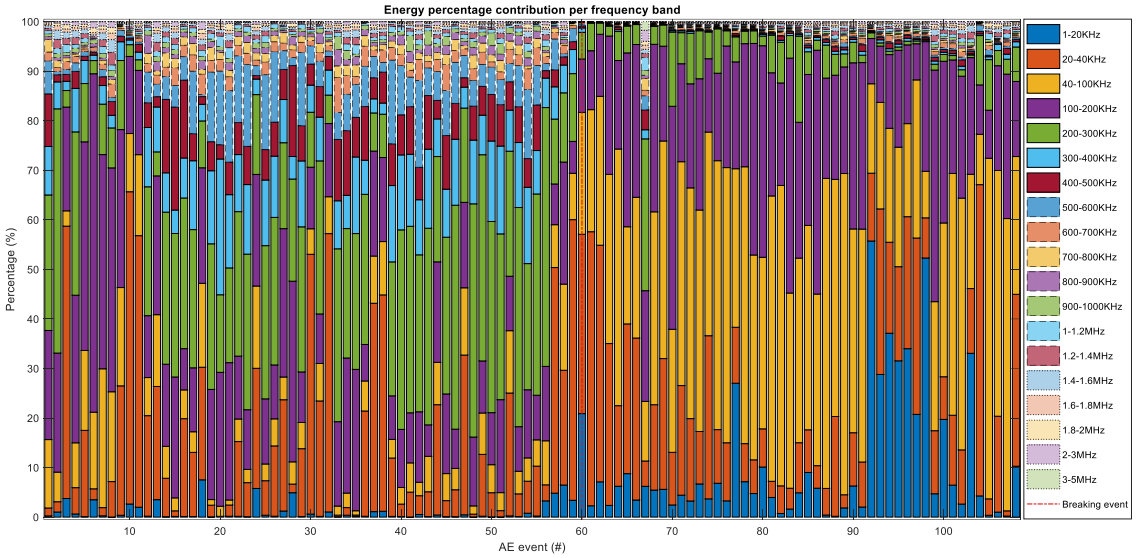

Figure 5-21. Evolution of the AE energy for different frequency bands.

In order to evaluate the specimen's state, a third metallographic inspection is carried out.

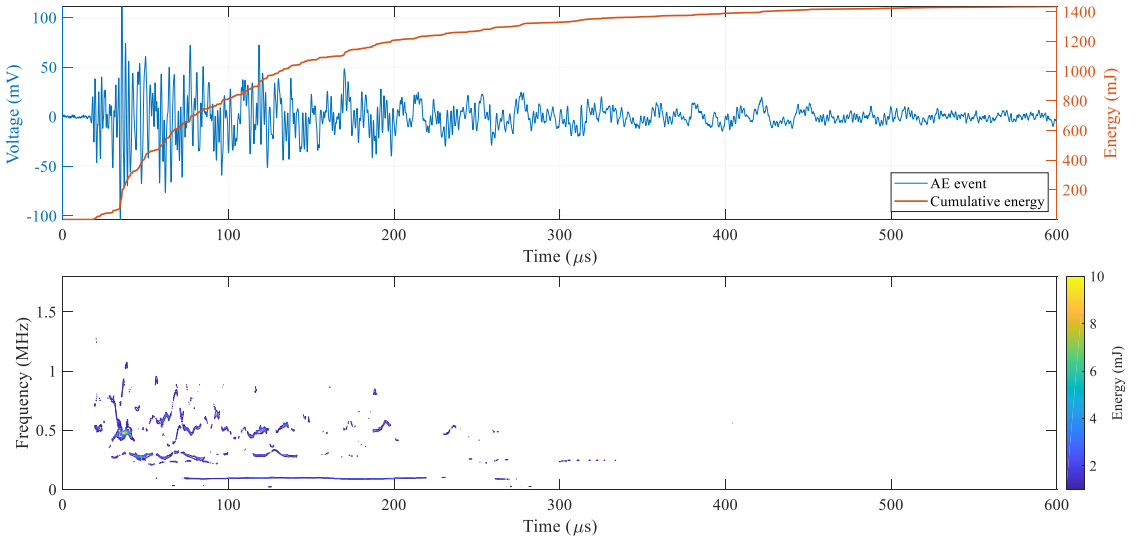

Figure 5-22. AE event belonging to the last part of the assay, composed of high and low frequencies.

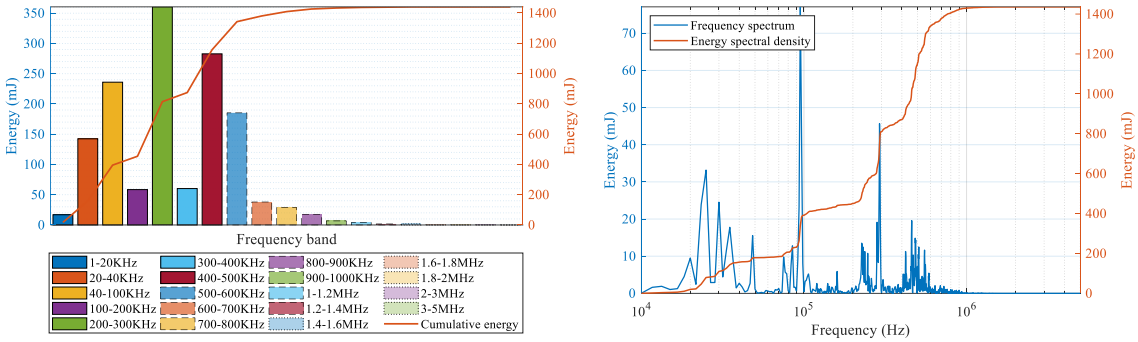

Figure 5-23. Bandfrequency decomposition. (b) Frequency domain energy.

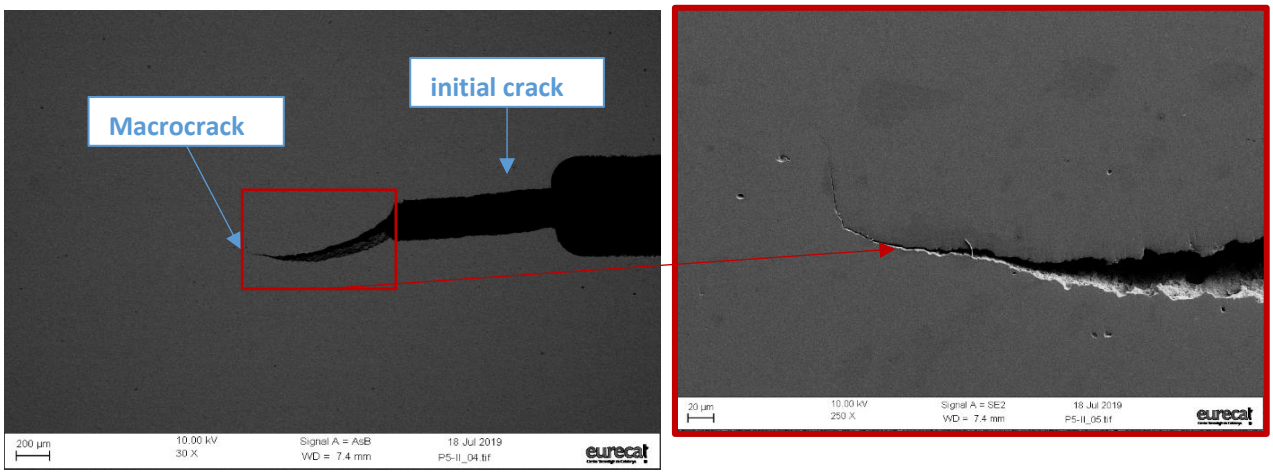

Figure 5-24. Metallographic inspection confirming a macrocrack presence.

By means of metallographic evaluation, it is confirmed that trend change presented by the AE phenomenon during the last part of the assay, which is composed of both, high and low frequencies is generated by nucleation and growth of a macrocrack.

5.5 Discussion and conclusions

As it was demonstrated, the proposed methodology is suitable of detecting fatigue in AHSS during tensile tests by means of the AE phenomenon.

Despite that the collected phenomenon represents a challenging signal to treat, when the proper identification and separation of AE events is carried out, subsequent analyses can be straightforward performed as well.

Chapter 6. CONCLUSIONS AND FUTURE WORK

6.1 General conclusions

This dissertation proposes and demonstrates a new technique for measuring and analyzing acoustic emissions in metallic components. With this, it is provided a significant advance in the understanding of fracture phenomena through acoustic emission measurements. In addition, the results of the thesis will allow the opening of a new methodology for the characterization of tensile tests on metal components.

6.2 Key contributions

By using an appropriate signal processing technique for the EA phenomenon, it has been possible to detect EA activity with high precision (by minimizing the effects of unwanted background noise). Overcoming the precision and computational performance of the advanced methods present in the literature.

By using an appropriate methodology for the spectral analysis of the phenomenon of EA, it has been possible to correlate the evolution of the phenomenon of EA with the generation and accumulation of mechanical fatigue in metal components.

Through the detection of cracking nucleation and growth, it has been possible to increase the status information of the specimens tested during mechanical uniaxial tensile tests.

6.3 Future work

While it is true that a significant improvement has been achieved compared to the current techniques present in the literature, it is still possible to achieve improvements in developments through:

• Artificial intelligence to post-process activity detection, with the aim of increasing accuracy.

• Artificial intelligence to evaluate a set of signal indicators in order to automate the fatigue evaluation process.

• Hardware implementation of the algorithms developed with the purpose of achieving a real-time detection system.

Finally, the usefulness of the developments presented in this dissertation for applications other than tensile tests could be evaluated, as would be the case for Design of semiconductors, electromechanical machinery, electrical transformers, among others

6.4 Thesis results dissemination

6.4.1 Journal publications

F. Piñal-Moctezuma, M. Delgado-Prieto and L. Romeral-Martínez, "Performance analysis of acoustic emission hit detection methods using time features" in IEEE Access. doi: 10.1109/ACCESS.2019.2919224

F. Piñal-Moctezuma, M. Delgado-Prieto and L. Romeral-Martínez, "An Acoustic Emission Activity Detection Method based on Short-Term Waveform Features: Application to Metallic Components under Uniaxial Tensile Test" in Mechanical systems and signal processing.

Under review

F. Piñal-Moctezuma, M. Delgado-Prieto and L. Romeral-Martínez, "An Acoustic Emission Activity Detection Method based on Short-Term Waveform Features: Application to Metallic Components under Uniaxial Tensile Test" in Mechanical systems and signal processing.

Submitted

6.4.2 Collaborative work

Hossam Selim, Fernando Piñal Moctezuma, Miguel Delgado Prieto, José Francisco Trull, Luis Romeral Martínez and Crina Cojocaru (April 3rd 2019). Wavelet Transform Applied to Internal Defect Detection by Means of Laser Ultrasound [Online First], IntechOpen, DOI: 10.5772/intechopen.84964. Available from: https://www.intechopen.com/online-first/wavelet-transform-applied-to-internal-defect-detection-by-means-of-laser-ultrasound

REFERENCES

[1] C.R. Farrar, K. Worden, Structural Health Monitoring: A Machine Learning Perspective, 2013. doi:10.1002/9781118443118.

[2] C.R. Farrar, K. Worden, An introduction to structural health monitoring., Philos. Trans. R. Soc. 365 (2007) 303–15. doi:10.1098/rsta.2006.1928.

[3] N.K. Kushwaha, B. Rinkesh, P. Prince, M. Hardik, Condition Based Monitoring of Rotating Machines Using Piezoelectric Material, (2014) 303–308.

[4] ASTM Standard E1316, Terminology for nondestructive examinations standard, ASTM Int. (2016) 1–72. doi:10.1520/E1316-16.

[5] M.D. Licker, Dictionary of Engineering, 2nd ed., McGraw-Hill, Chicago, 2003. doi:10.1036/0071417990.

[6] J.S. Oakland, Statistical Process Control, Fifth, Butterworth - Heinemann, Oxford, 2003.

[7] C.R. Farrar, N. a J. Lieven, Damage prognosis: the future of structural health monitoring., Philos. Trans. A. Math. Phys. Eng. Sci. 365 (2007) 623–632. doi:10.1098/rsta.2006.1927.

[8] C.R. Farrar, H. Sohn, F.M. Hemez, M.C. Anderson, M.T. Bement, P.J. Cornwell, S.W. Doebling, J.F. Schultze, N. Lieven, A.N. Robertson, LA-14051-MS Damage Prognosis: Current Status and Future Needs, Los Alamos, 2003.

[9] D.M. Frangopol, K.-Y. Lin, Estes A.C., Life-cycle cost design of deteriorating structures, J. Struct. Engng ASCE. 123 (1997) 1390–1401.

[10] M.M. Ettouney, S. Alampalli, Infrastructure Health in Civil Engineering: Applications and Management, 2011.

[11] S.A. Mohammed M.Ettouney, Infrastructure Health in Civil Engineering, Theory and components, 2012.

[12] M. Kaphle, Analysis Of Acoustic Emission Data For Accurate Damage Assesment For Structural Health Monitoring, (2012) 5–21.

[13] M. Kaphle, A. Tan, D. Thambiratnam, T. Chan, Effective Discrimination of Acoustic Emission Source Signals for Structural Health Monitoring, Adv. Struct. Eng. 15 (2012) 707–716. doi:10.1260/1369-4332.15.5.707.

[14] F. Ansari, ed., Sensing issues in civil structural health monitoring, Springer, 2005. doi:10.1007/1-4020-3661-2.

[15] J.S. Kong, D.M. Frangopol, Life-Cycle Reliability-Based Maintenance Cost Optimization of Deteriorating Structures with Emphasis on Bridges, J. Struct. Eng. 129 (2003) 818–828. doi:10.1061/(ASCE)0733-9445(2003)129:6(818).

[16] S. Djebali, S. Larbi, A. Bilek, Tenacity of Sheet Steel ST37-2 by the Essential Work of Fracture Method, Procedia Eng. 114 (2015) 306–313. doi:10.1016/j.proeng.2015.08.073.

[17] Instron Corporation, Reference Manual - Equipment: Instron Series 5500 Load Frames Including Series 5540, 5560, 5580, (2005).

[18] M.L. Maspoch, E. Franco-Urquiza, J. Gámez-Pérez, M. Sánchez-Soto, J.I. Velasco, O.O. Santana, A.B. Martínez, Application of post-yielding fracture mechanics to polymers, Rev. Latinoam. Metal. y Mater. 30 (2010) 101–118.

[19] D.R. Moore, A. Pavan, R. Brown, Fracture Mechanics Testing Methods for Polymers Adhesives and composites, 2002. doi:10.1016/S0142-9418(01)00080-0.

[20] D. Arencón, M. Antunes, A.B. Martínez, J.I. Velasco, Study of the fracture behavior of flexible polypropylene foams using the Essential Work of Fracture (EWF), Polym. Test. 31 (2012) 217–225. doi:10.1016/j.polymertesting.2011.10.013.

[21] H. Anuar, S.H. Ahmad, R. Rasid, S.N. Surip, T. Czigany, G. Romhany, Essential Work of Fracture and Acoustic Emission Study on TPNR Composites Reinforced by Kenaf Fiber, J. Compos. Mater. 41 (2007) 3035–3049. doi:10.1177/0021998307082173.

[22] S. Chaki, W. Harizi, G. Bourse, M. Ourak, Multi-technique approach for non destructive diagnostic of structural composite materials using bulk ultrasonic waves, guided waves, acoustic emission and infrared thermography, Compos. Part A Appl. Sci. Manuf. 78 (2015) 358–361. doi:10.1016/j.compositesa.2015.08.033.

[23] M. Bentahar, R. El Guerjouma, Monitoring progressive damage in polymer-based composite using nonlinear dynamics and acoustic emission, J. Acoust. Soc. Am. 125 (2009) EL39–EL44. doi:10.1121/1.2993755.

[24] D. Zhang, G. Venkatesan, A. Tewfik, M. Kaveh, Acoustic emission transient detection based on linear model residuals, in: Ninth IEEE Signal Process. Work. Stat. Signal Array Process. (Cat. No.98TH8381), IEEE, 1998: pp. 188–191. doi:10.1109/SSAP.1998.739366.

[25] H.M. Tensi, The Kaiser-Effect and Its Scientific Background, J. Acoust. Emiss. 22 (2004) 1–16. https://www.ndt.net/article/jae/papers/22-S01.pdf.

[26] J.R. Davis, Tensile testing, 2nd ed., ASM International, Ohio, USA, 2004.

[27] I. Faridmehr, M. Hanim Osman, A. Bin Adnan, A. Farokhi Nejad, R. Hodjati, M. Amin Azimi, Correlation between Engineering Stress-Strain and True Stress-Strain Curve, Am. J. Civ. Eng. Archit. 2 (2014) 53–59. doi:10.12691/ajcea-2-1-6.

[28] B. Pan, L. Tian, Advanced video extensometer for non-contact, real-time, high-accuracy strain measurement, Opt. Express. 24 (2016) 19082. doi:10.1364/OE.24.019082.

[29] J. Gamez-Perez, O. Santana, A.B. Martinez, M.L. Maspoch, Use of extensometers on essential work of fracture (EWF) tests, Polym. Test. 27 (2008) 491–497. doi:10.1016/j.polymertesting.2008.02.002.

[30] S.K. Verma, S.S. Bhadauria, A. Saleem, Review of Nondestructive Testing Methods for Condition Monitoring of Concrete Structures, J. Constr. Eng. 20113 (2013) 11. doi:10.1155/2013/834572.

[31] J.D.N. Cheeke, Fundamentals and applications of ultrasonic waves, 2012.

[32] L. Thomas, Non-Destructive Evaluation Methods, n.d.

[33] Y. Cheng, Y. Deng, J. Cao, X. Xiong, L. Bai, Z. Li, Multi-wave and hybrid imaging techniques: a new direction for nondestructive testing and structural health monitoring., 2013. doi:10.3390/s131216146.

[34] C. Niezreck, Structural Health Monitoring and Damage Detection, Volume 7, Springer, 2015. doi:10.1007/978-3-319-15230-1.

[35] A. Vary, The Acousto-Ultrasonic Approach, Acousto-Ultrasonics. (1988) 1–21. doi:10.1007/978-1-4757-1965-9.

[36] C.J. Hellier, Introduction to nondestructive testing, 2003. doi:10.1016/0308-9126(88)90483-X.

[37] R.D. Doherty, D.A. Hughes, F.J. Humphreys, J.J. Jonas, D.J. Jensen, M.E. Kassner, W.E. King, T.R. McNelley, H.J. McQueen, A.D. Rollett, Current issues in recrystallization: a review, Mater. Sci. Eng. A. 238 (1997) 219–274. doi:10.1016/S0921-5093(97)00424-3.

[38] D.R. Askeland, P.P. Fulay, W.J. Wright, The Science and Engineering of Materials, 6th ed., Cengage Learning, Stamford, CT, 2011. doi:10: 0-8400-5444-0.

[39] N.J. Carino, V.M. Malhotra, Acoustic Emission Methods, in: Handb. Nondestruct. Test. Concr., Second Edi, CRC Press, Boca Raton, 2003: p. 384.

[40] R.T. Committee, Recommendation of RILEM TC 212-ACD: acoustic emission and related NDE techniques for crack detection and damage evaluation in concrete*, Mater. Struct. 43 (2010) 1187–1189. doi:10.1617/s11527-010-9640-6.

[41] The Japanese Society for Non-Destructive Inspection, Principles of the Acoustic Emission (AE) Method and Signal Processing, in: T.J. Society for Non-Destructive Inspect (Ed.), Pract. Acoust. Emiss. Test., Springer Japan, Tokyo, 2016: p. 130. doi:10.1007/978-4-431-55072-3.

[42] W. Prosser, P.J. Shull, Acoustic Emission, in: P.J. Shull (Ed.), Nondestruct. Eval. Theory, Tech. Appl., Marcel Dekker, Inc., New York, 2002: pp. 366–443. doi:10.1201/9780203911068.ch6.

[43] E.D. Merson, P.N. Myagkikh, G. V. Klevtsov, D.L. Merson, A. Vinogradov, Effect of fracture mode on acoustic emission behavior in the hydrogen embrittled low-alloy steel, Eng. Fract. Mech. (2018) 0–1. doi:10.1016/j.engfracmech.2018.05.026.

[44] C.J. Hellier, Acoustic Emission Testing, in: Handb. Nondestruct. Eval., Second Edi, McGraw-Hill Education, New York, 2013. doi:10.1036/007177713X.ch10.

[45] ASTM International, ASTM E750-15, Standard Practice for Characterizing Acoustic Emission Instrumentation, ASTM International, West Conshohocken, PA, 2015. doi:10.1520/E0750-15.

[46] I.O. for Standardization, ISO 12716:2001, Non-destructive testing -- Acoustic emission inspection, 2017.

[47] J. Hensman, R. Mills, S.G. Pierce, K. Worden, M. Eaton, Locating acoustic emission sources in complex structures using Gaussian processes, Mech. Syst. Signal Process. 24 (2010) 211–223. doi:10.1016/j.ymssp.2009.05.018.

[48] Z. Zhou, Y. Rui, J. Zhou, L. Dong, X. Cai, Locating an Acoustic Emission Source in Multilayered Media Based on the Refraction Path Method, IEEE Access. 6 (2018). doi:10.1109/ACCESS.2018.2805384.

[49] S.A. Shevchik, B. Meylan, A. Mosaddeghi, K. Wasmer, Acoustic Emission for In Situ Monitoring of Solid Materials Pre-Weakening by Electric Discharge: A Machine Learning Approach, IEEE Access. 6 (2018) 40313–40324. doi:10.1109/ACCESS.2018.2853666.

[50] E. Dehghan Niri, A. Farhidzadeh, S. Salamone, Nonlinear Kalman Filtering for acoustic emission source localization in anisotropic panels, Ultrasonics. 54 (2014) 486–501. doi:10.1016/j.ultras.2013.07.016.

[51] P. Sedlak, Y. Hirose, M. Enoki, Acoustic emission localization in thin multi-layer plates using first-arrival determination, Mech. Syst. Signal Process. 36 (2013) 636–649. doi:10.1016/j.ymssp.2012.11.008.

[52] F. Bai, D. Gagar, P. Foote, Y. Zhao, Comparison of alternatives to amplitude thresholding for onset detection of acoustic emission signals, Mech. Syst. Signal Process. 84 (2017) 717–730. doi:10.1016/j.ymssp.2016.09.004.

[53] S.K. Al-Jumaili, M.R. Pearson, K.M. Holford, M.J. Eaton, R. Pullin, Acoustic emission source location in complex structures using full automatic delta T mapping technique, Mech. Syst. Signal Process. 72–73 (2016) 513–524. doi:10.1016/j.ymssp.2015.11.026.

[54] T.S. Eyre, M. van der Baan, Overview of moment-tensor inversion of microseismic events, Lead. Edge. 34 (2015) 882–888. doi:10.1190/tle34080882.1.

[55] T. Schumacher, D. Straub, C. Higgins, Toward a probabilistic acoustic emission source location algorithm: A Bayesian approach, J. Sound Vib. 331 (2012) 4233–4245. doi:10.1016/j.jsv.2012.04.028.

[56] X. Chiementin, D. Mba, B. Charnley, S. Lignon, J.P. Dron, Effect of the Denoising on Acoustic Emission Signals, J. Vib. Acoust. 132 (2010) 031009. doi:10.1115/1.4000789.

[57] L. Calabrese, G. Campanella, E. Proverbio, Noise removal by cluster analysis after long time AE corrosion monitoring of steel reinforcement in concrete, Constr. Build. Mater. 34 (2012) 362–371. doi:10.1016/j.conbuildmat.2012.02.046.

[58] I. Morais, Carroll F., A. Acoustic Emission Technology Corporation, Automatic Threshold Control Means And The Use Thereof, US Patent, 4,036,057, 1977.

[59] D.D. Doan, E. Ramasso, V. Placet, S. Zhang, L. Boubakar, N. Zerhouni, An unsupervised pattern recognition approach for AE data originating from fatigue tests on polymer – composite materials, Mech. Syst. Signal Process. 64–65 (2015) 465–478. doi:10.1016/j.ymssp.2015.04.011.

[60] D. Xiang, Acoustic emission detection of early stages of cracks in rotating gearbox components, AIP Conf. Proc. 1806 (2017). doi:10.1063/1.4974625.

[61] R. Unnthorsson, T.P. Runarsson, M.T. Jonsson, Acoustic emission based fatigue failure criterion for CFRP, Int. J. Fatigue. 30 (2008) 11–20. doi:10.1016/j.ijfatigue.2007.02.024.

[62] V. Barat, D. Grishin, M. Rostovtsev, Detection of AE signals against background friction, J. Acoust. Emiss. 29 (2011) 133–141.

[63] K. Ito, M. Enoki, Acquisition and Analysis of Continuous Acoustic Emission Waveform for Classification of Damage Sources in Ceramic Fiber Mat, Mater. Trans. 48 (2007) 1221–1226. doi:10.2320/matertrans.I-MRA2007850.

[64] C.U. Grosse, M. Ohtsu, Acoustic emission testing: Basics for Research-Applications in Civil Engineering, Springer, Berlin, 2008. doi:10.1007/978-3-540-69972-9.

[65] K. Nadolny, P. Sutowski, D. Herman, Analysis of aluminum oxynitride AlON (Abral®) abrasive grains during the brittle fracture process using stress-wave emission techniques, Int. J. Adv. Manuf. Technol. 81 (2015) 1961–1976. doi:10.1007/s00170-015-7338-1.

[66] R. V. Allen, Automatic earthquake recognition and timing from single traces, Bull. Seismol. Soc. Am. 68 (1978) 1521–1532. http://www.bssaonline.org/content/68/5/1521.short.

[67] H. Akaike, A new look at the statistical model identification, IEEE Trans. Automat. Contr. 19 (1974) 716–723. doi:10.1109/TAC.1974.1100705.

[68] N. Maeda, A Method for Reading and Checking Phase Time in Auto-Processing System of Seismic Wave Data, Zisin (Journal Seismol. Soc. Japan. 2nd Ser.). 38 (1985) 365–379. doi:10.4294/zisin1948.38.3_365.

[69] J.H. Kurz, C.U. Grosse, H.-W. Reinhardt, Strategies for reliable automatic onset time picking of acoustic emissions and of ultrasound signals in concrete, Ultrasonics. 43 (2005) 538–546. doi:10.1016/j.ultras.2004.12.005.

[70] C.C. Graham, S. Stanchits, I.G. Main, G. Dresen, Comparison of polarity and moment tensor inversion methods for source analysis of acoustic emission data, Int. J. Rock Mech. Min. Sci. 47 (2010) 161–169. doi:10.1016/j.ijrmms.2009.05.002.

[71] P. Sedlak, Y. Hirose, S.A. Khan, M. Enoki, J. Sikula, New automatic localization technique of acoustic emission signals in thin metal plates, Ultrasonics. 49 (2009) 254–262. doi:10.1016/j.ultras.2008.09.005.

[72] A. Ebrahimkhanlou, S. Salamone, Acoustic emission source localization in thin metallic plates: A single-sensor approach based on multimodal edge reflections, Ultrasonics. 78 (2017) 134–145. doi:10.1016/j.ultras.2017.03.006.

[73] K.M. Holford, M.J. Eaton, J.J. Hensman, R. Pullin, S.L. Evans, N. Dervilis, K. Worden, A new methodology for automating acoustic emission detection of metallic fatigue fractures in highly demanding aerospace environments: An overview, Prog. Aerosp. Sci. 90 (2017) 1–11. doi:10.1016/j.paerosci.2016.11.003.

[74] R. Unnthorsson, Hit Detection and Determination in AE Bursts, in: Acoust. Emiss. - Res. Appl., InTech, 2013: pp. 1–20. doi:10.5772/54754.

[75] D. Bianchi, E. Mayrhofer, M. Gröschl, G. Betz, A. Vernes, Wavelet packet transform for detection of single events in acoustic emission signals, Mech. Syst. Signal Process. 64–65 (2015) 441–451. doi:10.1016/j.ymssp.2015.04.014.

[76] A. Gupta, J.C. Duke, Identifying the arrival of extensional and flexural wave modes using wavelet decomposition of ultrasonic signals, Ultrasonics. 82 (2018) 261–271. doi:10.1016/j.ultras.2017.09.008.

[77] E. Pomponi, A. Vinogradov, A. Danyuk, Wavelet based approach to signal activity detection and phase picking: Application to acoustic emission, Signal Processing. 115 (2015) 110–119. doi:10.1016/j.sigpro.2015.03.016.

[78] A. Danyuk, I. Rastegaev, E. Pomponi, M. Linderov, D. Merson, Improving of acoustic emission signal detection for fatigue fracture monitoring, Procedia Eng. 176 (2017) 284–290.

doi:10.1016/j.proeng.2017.02.323.

[79] M. Kang, J. Kim, J.-M. Kim, An FPGA-Based Multicore System for Real-Time Bearing Fault Diagnosis Using Ultrasampling Rate AE Signals, IEEE Trans. Ind. Electron. 62 (2015) 2319–2329. doi:10.1109/TIE.2014.2361317.

[80] S. Wirtz, A. Cunha, M. Labusch, G. Marzun, S. Barcikowski, D. Söffker, Development of A Low-Cost FPGA-Based Measurement System for Real-Time Processing of Acoustic Emission Data: Proof of Concept Using Control of Pulsed Laser Ablation in Liquids, Sensors. 18 (2018) 1775. doi:10.3390/s18061775.

[81] Y. Hu, L. Wang, X. Huang, X. Qian, L. Gao, Y. Yan, On-line sizing of pneumatically conveyed particles through acoustic emission detection and signal analysis, IEEE Trans. Instrum. Meas. 64 (2015) 1100–1109. doi:10.1109/TIM.2014.2355653.

[82] P. Bormann, Understanding and parameter setting of STA/LTA trigger algorithm, Bormann, P.(Ur.). 1 (2011) 1–34. doi:10.2312/GFZ.NMSOP-2_IS_8.1.

[83] K. Ono, Calibration Methods of Acoustic Emission Sensors, Materials (Basel). 9 (2016) 508. doi:10.3390/ma9070508.

[84] N. Md Nor, A. Ibrahim, N. Muhamad Bunnori, H.M. Saman, S.N. Mat Saliah, S. Shahidan, Diagnostic of fatigue damage severity on reinforced concrete beam using acoustic emission technique, Eng. Fail. Anal. 41 (2014) 1–9. doi:10.1016/j.engfailanal.2013.07.015.

[85] G.C. McLaskey, D.A. Lockner, Calibrated Acoustic Emission System Records M −3.5 to M −8 Events Generated on a Saw-Cut Granite Sample, Rock Mech. Rock Eng. 49 (2016) 4527–4536. doi:10.1007/s00603-016-1082-1.

[86] D. Fettré, J. Favergeon, S. Bouvier, Detection of Breakaway for a High-Temperature Oxidation of Pure Zirconium Using Acoustic Emission Correlated to Thermogravimetry, Oxid. Met. 87 (2017) 367–379. doi:10.1007/s11085-017-9737-1.

[87] E. Dehghan-Niri, A. Farhidzadeh, S. Salamone, Determination of the probability zone for acoustic emission source location in cylindrical shell structures, Mech. Syst. Signal Process. 60–61 (2015) 971–985. doi:https://doi.org/10.1016/j.ymssp.2015.02.004.

[88] ASTM International, ASTM E976-15, Standard Guide for Determining the Reproducibility of Acoustic Emission Sensor Response, 2015. doi:10.1520/E0976-15.

[89] ASTM International, ASTM E650 / E650M-17, Standard Guide for Mounting Piezoelectric Acoustic Emission Sensors, 2017. doi:10.1520/E0650_E0650M-17.

[90] ASTM International, ASTM E2374-16, Standard Guide for Acoustic Emission System Performance Verification, 2016. doi:10.1520/E2374-16.

[91] ASTM International, ASTM E1932-12(2017), Standard Guide for Acoustic Emission Examination of Small Parts, 2017. doi:10.1520/E1932-12R17.

[92] ASTM International, ASTM E1106-12(2017), Standard Test Method for Primary Calibration of Acoustic Emission Sensors, 2017. doi:10.1520/E1106-12R17.

[93] I. Daubechies, J. Lu, H.-T. Wu, Synchrosqueezed wavelet transforms: An empirical mode decomposition-like tool, Appl. Comput. Harmon. Anal. 30 (2011) 243–261. doi:10.1016/j.acha.2010.08.002.

[94] A. Sehgal, N. Kehtarnavaz, A Convolutional Neural Network Smartphone App for Real-Time Voice Activity Detection, IEEE Access. 6 (2018) 9017–9026. doi:10.1109/ACCESS.2018.2800728.

[95] European Telecommunications Standards Institute, TS 126 194. Digital cellular telecommunications system (Phase 2+) (GSM); Universal Mobile Telecommunications System (UMTS); LTE; Speech codec speech processing functions; Adaptive Multi-Rate - Wideband (AMR-WB) speech codec; Voice Activity Detector (VAD)., 2018. https://www.etsi.org.

[96] L.R. Rabiner, M.R. Sambur, An Algorithm for Determining the Endpoints of Isolated Utterances, Bell Syst. Tech. J. 54 (1975) 297–315. doi:10.1002/j.1538-7305.1975.tb02840.x.

[97] Z. Nazarchuk, V. Skalskyi, O. Serhiyenko, Handbook of Technical Diagnostics, Springer Berlin Heidelberg, Berlin, Heidelberg, 2013. doi:10.1007/978-3-642-25850-3.

[98] R.W.B. Stephens, A.A. Pollock, Waveforms and Frequency Spectra of Acoustic Emissions, J. Acoust. Soc. Am. 50 (1971) 904–910. doi:10.1121/1.1912715.

[99] L. Bolin, A model for estimating the signal from an acoustic emission source, Ultrasonics. 17 (1979) 67–70. doi:10.1016/0041-624X(79)90098-2.

[100] C. D'Attellis, L. Pérez, D. Rubio, J. Ruzzante, A Bank of Kalman Filters for Failure Detection Using Acoustic Emission Signals, in: Non-Destructive Test. '92, Elsevier, 1992: pp. 29–33. doi:10.1016/B978-0-444-89791-6.50012-3.

[101] M.I. López Pumarega, Relation between Amplitude and Duration of Acoustic Emission Signals, in: AIP Conf. Proc., AIP, 2003: pp. 1431–1438. doi:10.1063/1.1570299.

[102] D. Wotzka, Mathematical Model and Regression Analysis of Acoustic Emission Signals Generated by Partial Discharges, Appl. Comput. Math. 3 (2014) 225. doi:10.11648/j.acm.20140305.15.

[103] D. Wotzka, T. Boczar, P. Fracz, Mathematical Model and Numerical Analysis of AE Wave Generated by Partial Discharges, Acta Phys. Pol. A. 120 (2011) 767–771. doi:10.12693/APhysPolA.120.767.

[104] U. of S.C. LAMSS, Wavescope: Dispersion curves, group velocities, and tuning for metallic structures, (2010). http://www.me.sc.edu/Research/lamss/NV/html/L_software.html.

[105] J. Hirsch, T. Al-Samman, Superior light metals by texture engineering: Optimized aluminum and magnesium alloys for automotive applications, Acta Mater. 61 (2013) 818–843. doi:10.1016/j.actamat.2012.10.044.

[106] M.K. Kulekci, Magnesium and its alloys applications in automotive industry, Int. J. Adv. Manuf. Technol. 39 (2008) 851–865. doi:10.1007/s00170-007-1279-2.

[107] The Steel Market Development Institute, 2017 Automotive Steel Industry Technology Roadmap for Sheet and Bar Products, 2017. https://www.autosteel.org/.

[108] D. Frómeta, A. Lara, S. Molas, D. Casellas, J. Rehrl, C. Suppan, P. Larour, J. Calvo, On the correlation between fracture toughness and crash resistance of advanced high strength steels, Eng. Fract. Mech. (2018) 0–1. doi:10.1016/j.engfracmech.2018.10.005.

[109] ASTM Standard E8/E8M, 2016 (1991), Standard Test Methods for Tension Testing of Metallic Materials, Am. Soc. Test. Mater. (2016) 1–27. doi:10.1520/E0008_E0008M-16A.

[110] ISO Standard 6892-1:2016, Metallic materials - Tensile testing - Part 1: Method of test at room temperature, International Organization for Standardization, Geneva, Switzerland, 2016. doi:10.3403/30268532.

[111] H.B. Motra, J. Hildebrand, A. Dimmig-Osburg, Assessment of strain measurement techniques to characterise mechanical properties of structural steel, Eng. Sci. Technol. an Int. J. 17 (2014) 260–269. doi:10.1016/j.jestch.2014.07.006.

[112] Fed, Location, location & size: defects close to surfaces dominate fatigue crack initiation, Sci. Rep. 7 (2017) 45239. doi:10.1038/srep45239.

[113] Subra Suresh, Fatigue of Materials, 1st ed., Cambridge University Press, 1998.

[114] L. Tian, L. Yu, B. Pan, Accuracy enhancement of a video extensometer by real-time error compensation, Opt. Lasers Eng. 110 (2018) 272–278. doi:10.1016/j.optlaseng.2018.06.010.

[115] F. Dahmene, S. Yaacoubi, M. El Mountassir, N. Bendaoud, C. Langlois, O. Bardoux, On the modal acoustic emission testing of composite structure, Compos. Struct. 140 (2016) 446–452. doi:10.1016/j.compstruct.2016.01.003.

[116] W. Roundi, A. El Mahi, A. El Gharad, J.-L. Rebiere, Acoustic emission monitoring of damage progression in Glass/Epoxy composites during static and fatigue tensile tests, Appl. Acoust. 132 (2018) 124–134. doi:10.1016/j.apacoust.2017.11.017.

[117] J.-Y. Wang, J.-Y. Guo, Damage investigation of ultra high performance concrete under direct tensile

test using acoustic emission techniques, Cem. Concr. Compos. 88 (2018) 17–28. doi:10.1016/j.cemconcomp.2018.01.007.

[118] G.N. Morscher, N.A. Gordon, Acoustic emission and electrical resistance in SiC-based laminate ceramic composites tested under tensile loading, J. Eur. Ceram. Soc. 37 (2017) 3861–3872. doi:10.1016/j.jeurceramsoc.2017.05.003.

[119] F. Piñal Moctezuma, M. Delgado Prieto, L. Romeral Martinez, Performance Analysis of Acoustic Emission Hit Detection Methods Using Time Features, IEEE Access. 7 (2019) 71119–71130. doi:10.1109/ACCESS.2019.2919224.

[120] M.G.R. Sause, In Situ Monitoring of Fiber-Reinforced Composites, Springer International Publishing, Cham, 2016. doi:10.1007/978-3-319-30954-5.

[121] Federation of Construction Materials Industries, Monitoring Method for Active Cracks in Concrete by Acoustic Emission JCMS-III B5706, Japan, 2003.

[122] Neha Vivek A, Crack Classification of Concrete under Uniaxial Compression using Acoustic Emission Monitoring Technique, Int. J. Eng. Res. V6 (2017). doi:10.17577/ijertv6is030177.

[123] Y. Farnam, M.R. Geiker, D. Bentz, J. Weiss, Acoustic emission waveform characterization of crack origin and mode in fractured and ASR damaged concrete, Cem. Concr. Compos. 60 (2015) 135–145. doi:10.1016/j.cemconcomp.2015.04.008.

[124] P. Rodríguez, T.B. Celestino, Application of acoustic emission monitoring and signal analysis to the qualitative and quantitative characterization of the fracturing process in rocks, Eng. Fract. Mech. 210 (2019) 54–69. doi:10.1016/j.engfracmech.2018.06.027.

[125] A. Zaki, H. Chai, D. Aggelis, N. Alver, Non-Destructive Evaluation for Corrosion Monitoring in Concrete: A Review and Capability of Acoustic Emission Technique, Sensors. 15 (2015) 19069–19101. doi:10.3390/s150819069.

[126] B. Wisner, K. Mazur, V. Perumal, K.P. Baxevanakis, L. An, G. Feng, A. Kontsos, Acoustic emission signal processing framework to identify fracture in aluminum alloys, Eng. Fract. Mech. 210 (2019) 367–380. doi:10.1016/j.engfracmech.2018.04.027.

[127] F. Du, S. Pan, D. Li, Damage evaluation and failure mechanism analysis of steel tube confined reinforced-concrete columns by acoustic emission technology, Lat. Am. J. Solids Struct. 15 (2018) 1–14. doi:10.1590/1679-78255339.

[128] E.Z. Kordatos, D.G. Aggelis, T.E. Matikas, Monitoring of fatigue damage in metal plates by acoustic emission and thermography, Smart Sens. Phenomena, Technol. Networks, Syst. 2011. 7982 (2011) 79820V. doi:10.1117/12.881021.

[129] D.G. Aggelis, E.Z. Kordatos, T.E. Matikas, Acoustic emission for fatigue damage characterization in metal plates, Mech. Res. Commun. 38 (2011) 106–110. doi:10.1016/j.mechrescom.2011.01.011.

[130] K. Shrama, S.K. Al-jumaili, R. Pullin, A. Clarke, S.L. Evans, On the Use of Acoustic Emission and Digital Image Correlation for Welded Joints Damage Characterization, J. Appl. Comput. Mech. 5 (2019) 381–389. doi:10.22055/JACM.2018.25941.1301.

[131] M.N. Babu, C.K. Mukhopadhyay, G. Sasikala, S.K. Albert, A.K. Bhaduri, T. Jayakumar, R. Kumar, Study of fatigue crack growth in RAFM steel using acoustic emission technique, J. Constr. Steel Res. 126 (2016) 107–116. doi:10.1016/j.jcsr.2016.07.007.

[132] D.G. Aggelis, T.E. Matikas, Effect of plate wave dispersion on the acoustic emission parameters in metals, Comput. Struct. 98–99 (2012) 17–22. doi:10.1016/j.compstruc.2012.01.014.

[133] A. Zaki, H.K. Chai, A. Behnia, D.G. Aggelis, J.Y. Tan, Z. Ibrahim, Monitoring fracture of steel corroded reinforced concrete members under flexure by acoustic emission technique, Constr. Build. Mater. 136 (2017) 609–618. doi:10.1016/j.conbuildmat.2016.11.079.

[134] M.N. Noorsuhada, An overview on fatigue damage assessment of reinforced concrete structures with the aid of acoustic emission technique, Constr. Build. Mater. 112 (2016) 424–439. doi:10.1016/j.conbuildmat.2016.02.206.

[135] V.I.O. P., A. Kaplan, M.P. Gomez, M.I.L. Pumarega, N. Nieva, Characterization of Metal/Ceramic Interfaces in Dental Materials by Acoustic Emission, Procedia Mater. Sci. 8 (2015) 683–692. doi:10.1016/j.mspro.2015.04.125.

[136] Á. Angulo, J. Tang, A. Khadimallah, S. Soua, C. Mares, T.-H. Gan, Acoustic Emission Monitoring of Fatigue Crack Growth in Mooring Chains, Appl. Sci. 9 (2019) 2187. doi:10.3390/app9112187.

[137] M.Y. Bhuiyan, V. Giurgiutiu, The signatures of acoustic emission waveforms from fatigue crack advancing in thin metallic plates, Smart Mater. Struct. 27 (2018) 15019. doi:10.1088/1361-665X/aa9bc2.

[138] P.A. Vanniamparambil, U. Guclu, A. Kontsos, Identification of Crack Initiation in Aluminum Alloys using Acoustic Emission, Exp. Mech. 55 (2015) 837–850. doi:10.1007/s11340-015-9984-5.

[139] J.J.G. De La Rosa, A.A. Pérez, J.C.P. Salas, J.M.S. Fernández, A novel measurement method for transient detection based in wavelets entropy and the spectral kurtosis: An application to vibrations and acoustic emission signals from termite activity, Meas. J. Int. Meas. Confed. 68 (2015) 58–69. doi:10.1016/j.measurement.2015.02.044.

[140] C.R. Ramirez-Jimenez, N. Papadakis, N. Reynolds, T.H. Gan, P. Purnell, M. Pharaoh, Identification of failure modes in glass/polypropylene composites by means of the primary frequency content of the acoustic emission event, Compos. Sci. Technol. 64 (2004) 1819–1827. doi:10.1016/j.compscitech.2004.01.008.

[141] K. Ohno, M. Ohtsu, Crack classification in concrete based on acoustic emission, Constr. Build. Mater. 24 (2010) 2339–2346. doi:10.1016/j.conbuildmat.2010.05.004.

[142] X. Zhang, N. Feng, Y. Wang, Y. Shen, Acoustic emission detection of rail defect based on wavelet transform and Shannon entropy, J. Sound Vib. 339 (2015) 419–432. doi:10.1016/j.jsv.2014.11.021.

[143] P. Antonaci, P. Bocca, D. Masera, Fatigue crack propagation monitoring by Acoustic Emission signal analysis, Eng. Fract. Mech. 81 (2012) 26–32. doi:10.1016/j.engfracmech.2011.09.017.

[144] R. Gutkin, C.J. Green, S. Vangrattanachai, S.T. Pinho, P. Robinson, P.T. Curtis, On acoustic emission for failure investigation in CFRP: Pattern recognition and peak frequency analyses, Mech. Syst. Signal Process. 25 (2011) 1393–1407. doi:10.1016/j.ymssp.2010.11.014.

[145] T. Haneef, B.B. Lahiri, S. Bagavathiappan, C.K. Mukhopadhyay, J. Philip, B.P.C. Rao, T. Jayakumar, Study of the tensile behavior of AISI type 316 stainless steel using acoustic emission and infrared thermography techniques, J. Mater. Res. Technol. 4 (2015) 241–253. doi:10.1016/j.jmrt.2014.12.008.

[146] O. Stankevych, V. Skalsky, Investigation and identification of fracture types of structural materials by means of acoustic emission analysis, Eng. Fract. Mech. 164 (2016) 24–34. doi:10.1016/j.engfracmech.2016.08.005.

[147] F. Pinal-Moctezuma, M. Delgado-Prieto, L. Romeral-Martinez, An Acoustic Emission Activity Detection Method based on Short-Term Waveform Features: Application to Metallic Components under Uniaxial Tensile Test, (2019). http://arxiv.org/abs/1906.10956.

[148] D. Gabor, THEORY OF COMMUNICATION * Part 1 . THE ANALYSIS OF INFORMATION, J. Inst. Electr. Eng. 93 (1945) 429–457. doi:http://dx.doi.org/10.1049/ji-3-2.1946.0074.

[149] R.B. Pachori, A. Nishad, Cross-terms reduction in the Wigner–Ville distribution using tunable-Q wavelet transform, Signal Processing. 120 (2016) 288–304. doi:10.1016/j.sigpro.2015.07.026.

[150] E. Delechelle, J. Lemoine, Oumar Niang, Empirical mode decomposition: an analytical approach for sifting process, IEEE Signal Process. Lett. 12 (2005) 764–767. doi:10.1109/LSP.2005.856878.

[151] Y. Huang, C.J. Yan, Q. Xu, On the difference between empirical mode decomposition and Hilbert vibration decomposition for earthquake motion records, 15th World Conf. Earthq. Eng. (2012).

[152] M. Kharrat, E. Ramasso, V. Placet, M.L. Boubakar, A signal processing approach for enhanced Acoustic Emission data analysis in high activity systems: Application to organic matrix composites, Mech. Syst. Signal Process. 70–71 (2016) 1038–1055. doi:10.1016/j.ymssp.2015.08.028.

[153] K. Jemielniak, J. Kossakowska, T. Urbański, Application of Wavelet Transform of Acoustic Emission

and Cutting Force Signals for Tool Condition Monitoring in Rough Turning of Inconel 625, Proc. Inst. Mech. Eng. Part B J. Eng. Manuf. 225 (2011) 123–129. doi:10.1243/09544054JEM2057.

[154] S. Rao, B. Subramanyam, Analysis of Acoustic Emission Signals using Wavelet Transformation Technique, Def. Sci. J. 58 (2008) 559–564. doi:10.14429/dsj.58.1677.

[155] W. Sheng, S.F. Wirtz, D. Söffker, Wavelet Packet Transform-Based Feature Extraction for Acoustic Emission Pattern Recognition, (2018) 1–8. http://www.ndt.net/?id=23302.

[156] M. Vrankic, D. Sersic, V. Sucic, Adaptive 2-D wavelet transform based on the lifting scheme with preserved vanishing moments, IEEE Trans. Image Process. 19 (2010) 1987–2004. doi:10.1109/TIP.2010.2045688.

[157] T. Parks, J. McClellan, Chebyshev Approximation for Nonrecursive Digital Filters with Linear Phase, IEEE Trans. Circuit Theory. 19 (1972) 189–194. doi:10.1109/TCT.1972.1083419.

[158] L.R. Rabiner, J.H. McClellan, T.W. Parks, FIR digital filter design techniques using weighted Chebyshev approximation, Proc. IEEE. 63 (1975) 595–610. doi:10.1109/PROC.1975.9794.

[159] A. V. Oppenheim, R.W. Schafer, Discrete-time signal processing, 3rd ed., Prentice Hall, Inc., Upper Saddle River, NJ, 2014.

[160] R. Pippan, S. Wurster, D. Kiener, Fracture mechanics of micro samples: Fundamental considerations, Mater. Des. 159 (2018) 252–267. doi:10.1016/j.matdes.2018.09.004.